ISBN 978-82-471-2988-3 (printed ver.)
ISBN 978-82-471-2989-0 (electronic ver.)
ISSN 1503-8181

Nils van der Tuuk Opedal
Doctoral Thesis

Doctoral theses at NTNU, 2011:216

Nils van der Tuuk Opedal

NMR as a tool to follow destabilization of water-in-oil emulsions

NTNU
Norwegian University of
Science and Technology

Thesis for the degree of
philosophiae doctor
Faculty of Natural Sciences and Technology
Department of Chemical Engineering

Doctoral theses at NTNU, 2011:216
NTNU

NTNU
Norwegian University of
Science and Technology

Nils van der Tuuk Opedal

NMR as a tool to follow destabilization of water-in-oil emulsions

Thesis for the degree of philosophiae doctor

Trondheim, September 2011

Norwegian University of
Science and Technology
Faculty of Natural Sciences and Technology
Department of Chemical Engineering

NTNU
Norwegian University of
Science and Technology

NTNU
Norwegian University of Science and Technology

Thesis for the degree of philosophiae doctor

Faculty of Natural Sciences and Technology
Department of Chemical Engineering

ISBN 978-82-471-2988-3 (printed ver.)
ISBN 978-82-471-2989-0 (electronic ver.)
ISSN 1503-8181

Doctoral Theses at NTNU,

Printed by Tapir Uttrykk

PREFACE

This thesis is submitted in partial fulfillment of the PhD degree at the Norwegian University of Science and Technology (NTNU), Trondheim. The work contains six papers and was performed between August 2008 and August 2011 under the supervision of Professor Johan Sjöblom. The work behind the first five papers was performed at the Ugelstad Laboratory, NTNU, Trondheim, and the work in the sixth article was performed at the University of Alberta, Edmonton, Canada.

I obtained my MSc in Chemical Engineering in June 2008 at NTNU working with the formation of metallic nano-particles at the Ugelstad Laboratory. Later that summer I was accepted as a PhD candidate by the faculty with the working title *"NMR as a tool to follow destabilization in water-in-oil emulsions"*.

The role of the author was in paper I and II to perform the measurements, analyze the data and writing of the manuscript. Paper III was written by the author, except the part regarding Multivariate Data Analysis and the experimental work on the interfacial rheology was performed by the author. In paper IV the author participated with the interpretation of the NMR measurements. Paper V was written and the experimental work done solely by the author. In paper VI the author participated with the measurements in the SFA.

ACKNOWLEDGMENTS

First I would like to acknowledge Professor Johan Sjöblom for accepting me as a PhD-student and for his supervision during the doctoral work.

I would also like to thank Dr Geir Sørland for his patience when explaining the theory behind the NMR and for answering all my NMR related questions.

Dr Sébàstïên Simon is acknowledged for his endless knowledge of the Ugelstad Laboraty equipment and helpful character.

Statoil are acknowledged for the financial support.

Friends and family, you know who you are, you know I am grateful.

Te iubesc Mihaela, you are everything for me!

ABSTRACT

Due to depletion of conventional sources and increasing demand for crude oil, the last years have shown a shift towards the exploitation of heavier and technologically more difficult feedstocks. This shift of focus means that the entire oil industry needs to update its fundamental and practical understanding of the technology, including the separation process.

To be able to more carefully study crude oil emulsion stability, one should be able to characterize the emulsion system in higher detail. By using Nuclear Magnetic Resonance (NMR) several advantages are apparent. One is able to study the entire sample, even the inside of a dark liquid. Concentrated samples can be studied and the apparatus is highly versatile. The droplet size distribution, position dependent size profiles and position dependent brine profiles can be obtained.

With the new and validated NMR methods one can study in more detail how the various stabilizing parameters and destabilizing actions affect the behavior and the overall separation of crude oil emulsions. The method to measure the droplet size distribution can give information on the emulsification process and help predict the rheological and separation characteristics of an emulsion. Knowledge on the mean, width and shape of a droplet size distribution are important to be able to fully understand the behavior.

By measuring the stability of an emulsion, either by the acquisition of iso-volumetric or iso-metric curves, one can monitor both the oil quality and the water recovery rate. This can be helpful in studying the demulsification process where a demulsifier can be selected on the basis of how fast the water recovers or how much water there is left in the oil phase. The methods can also be used in connection with theoretical modeling of emulsion stability. The measurements of droplet growth rates, thickness of concentrated emulsion layers and the sedimentation and coalescence rates can give information that can be very valuable to understand the separation process.

PUBLICATIONS

Paper I
Opedal N, Sørland G, Sjöblom J.
"Method for Droplet Size Distribution Determination of Water-in-oil Emulsions using Low-Field NMR"
Diffusion Fundamentals, **2009**, 9 (7), 1-29.

Paper II
Opedal N, Sørland G, Sjöblom J.
"Emulsion Stability Studied by Nuclear Magnetic Resonance (NMR)"
Energy & Fuels, **2010**, 24, 3628-3633.

Paper III
Opedal N, Kralova I, Lesaint C, Sjöblom J.
"Enhanced Sedimentation and Coalescence by Chemicals on Real Crude Oil Systems"
Submitted to Energy & Fuels.

Paper IV
Grimes B, Dorao C, Opedal, N, Kralova I, Sørland G, Sjöblom J.
"Population Balance Model for Batch Gravity Separation of Crude Oil and Water Emulsions. Part II: Comparisons to Experimental Crude Oil Separation Data."
Journal of Dispersion Science and Technology, **2011**, In Press.

Paper V
Opedal N, Sjöblom J.
"Emulsion stability of a SAGD produced extra heavy crude oil"
To be submitted.

Paper VI
Wang J, Opedal N, Lu Q, Sjöblom J, Xu Z, Zeng H.
"Understanding the Molecular Interactions of an Asphaltene Model Compound C5Pe in Organic Solvents Using a SFA"
Submitted to Energy & Fuels.

TABLE OF CONTENTS

Chapter 1 Introduction

The occurrence of liquid hydrocarbons has been noticed since the antiquity; there are several references to dark oil in the Herodotus ant the Bible. The earliest fields of application were in ornaments, construction and naturally as a combustible material. The modern history of petroleum started in Pennsylvania in the 1850s. The distillation of crude oils enabled the production of first-rate burning oils. After this development the exploitation of crude oil exploded, with approximately 2000 barrels being produced in 1859 and 240 000 barrels in 1874. [1] The current world wide production of crude oil has exceeded 80 million barrels a day.

The modern economy and lifestyle is heavily affected by the availability of crude oil. Perhaps the most apparent presence of refined oil is in the transportation sector. The primary source of energy used in container ships, trucks, buses and aeroplanes are derivates from an oil refinery. Another important utilization of oil is as fuel in heaters for industrial applications or households. However, a less obvious, but still very important field is the use of refined products from crude oil as raw material for plastics, fertilizers and pharmaceuticals. [2] Given the current problems of deforestation and large areas tied to food production, there are not many alternative resources of hydrocarbons. Without the availability of hydrocarbons from crude oil and with the current demand, the costs of many vital products for the modern world will increase substantially.

The properties of a crude oil vary from well to well and the exploitation, processing, transportation and upgrading of conventional crude oils are complex processes. The flowability of the oil is important in terms of cost and ease to upgrade the oil. The earliest reservoirs that were exploited contained light crude oils, making the entire process relatively easy. As more research was invested in the process heavier crude oils could be exploited and upgraded as well, albeit at a higher cost. However, most of the conventional resources have now been exploited and new findings are reservoirs of heavier and more difficult crude oils. The combination of increasing demand for crude oil derivates and an decreasing amount of available conventional crude oil has opened up for the exploitation of extra heavy oils.

Although heavy and extra heavy crude oils are found all over the planet, there are in particular two regions with a potential for extra heavy hydrocarbon exploitation, Alberta, Canada and the Orinoco river basin in Venezuela. The extra heavy crude oils are known under many synonyms; bitumen, tar sand, oil sand. The common feature of all these crude oils is the high viscosity and the difficulties to extract them. According to estimates, the amount of crude oil in Alberta was approximated to 900×10^9 barrels. [3] Although due to difficulties in exploiting the highly viscous oil the recoverable amount of the reserves is currently around 170×10^9 barrels. With further focus on development in exploitation and upgrading techniques, this number might increase.

Chapter 2 Petroleum

The word petroleum derives from Greek and consists of Petra meaning rock and Oleum meaning oil. This chapter will give a short introduction of the origin, classification and parts of the processing.

2.1 Origin

The most accepted theory regarding the origin of crude oil is that crude oil is a product of heat, compression and bacteriological action on ancient vegetation, primarily aquatic vegetation and algae. The long term effect of pressure and high temperature in a closed environment causes the hydrocarbons to slowly form kerogen; a solid-like hydrocarbon. Given enough time the kerogen split into smaller hydrocarbons which later migrate through different layers of rock until they form a reservoir. This theory gives a reasonable explanation why there are such large differences in the properties between various oilfields. Thus, reservoirs with crude oils of different properties can be explained by how long the process has progressed. There is an alternative theory for the origin of crude oil. This theory proposes that acetylene is the precursor for petroleum. The first reaction is believed to be between calcium carbonate and alkali metals to form calcium carbide, CaC_2. Whereby hydrolysis of calcium carbide yields acetylene, C_2H_2, and acetylene will merge into larger hydrocarbon molecules. [1]

In order for a reservoir to be formed, the ground, or the rocks within the ground, has to possess certain conditions. When the crude oil has obtained fluid like properties it starts to migrate through the rocks. Due to the capillary and buoyancy forces the oil moves and in order for a reservoir to be formed the migration of the oil should be stopped. The capability of rocks to form a reservoir is determined by the porosity and the permeability. The porosity is a measurement of the capacity of the rock to hold fluids, whereas the permeability is a measurement of how easily the fluids can transmit and migrate through the pores. Thus, when the migrating oil reaches a layer of rock with low permeability the movement halts and as more oil arrives the oil accumulates and displaces the other fluids. Hence, a reservoir has formed. The “trap” in which the oil is confined can be either due to the structure of the reservoir or due to stratigraphic effects. Figure 2.1 shows two examples of reservoirs formed by structural effects.

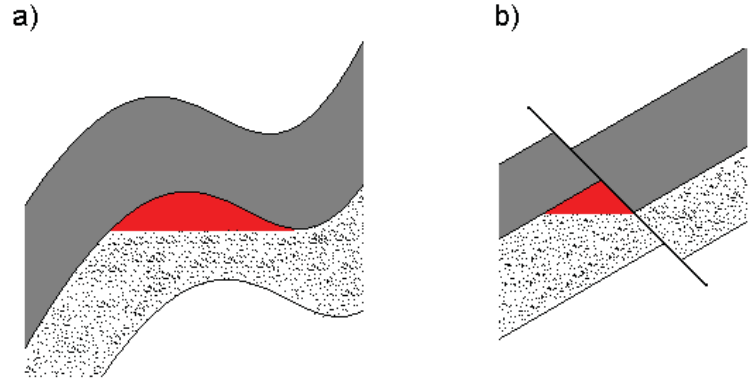

Figure 2.1 Sketch of two kinds of structural reservoir traps. a) fold. b) fault.

There are two explanations for the extreme properties of the oil sands in Alberta. One theory says that the reason for the high viscosity of the oil is the exposure the oil has experienced to the atmosphere. The long term effect of this exposure is the evaporation of most of the lighter components generally found in crude oil. Another theory says that extra heavy crude oils are still considered as a precursor to eventually becoming conventional crude oil. [3]

2.2 Composition

A crude oil is a non-uniform mixture of hydrocarbons and inorganic particles of different sizes and functionalities. To describe the composition of such a system requires some sort of simplification. The elemental composition of most crude oils can be fitted with the data shown in table 2.1. However, the elemental composition alone is not sufficient to predict and describe the behavior of the crude oil. Fractionation is another method to categorize a crude oil and fractionation can be done in several ways, for instance by molecular size, evaporation or solvency.

Table 2.1 Elemental composition of crude oil

Carbon	83 – 87 %
Hydrogen	10 – 14 %
Nitrogen	0.1 – 2.0 %
Oxygen	0.05 – 1.5 %
Sulfur	0.05 – 6.0 %
Metals (Ni, Fe and V)	<1000 ppm

The latter method is by far the most common. The SARA fractionation technique parts the oil into Saturates, Aromatics, Resins and Asphaltenes. A general schematic of the procedure is given in figure 2.2. In the presence of light alkanes such as *n*-pentane or *n*-hexane, asphaltene molecules will precipitate. Maltenes are defined as asphaltene free crude oils and the maltene fraction can then be fractionated by HPLC and the final amount of each fraction is determined gravimetrically. One should be careful with the precipitation of the asphaltenes as it has been showed that depending on which hydrocarbon one uses, e.g. *n*-pentane, *n*-hexane*, or n-heptane*, the fractionated asphaltene can exhibit different yields and properties. [4]

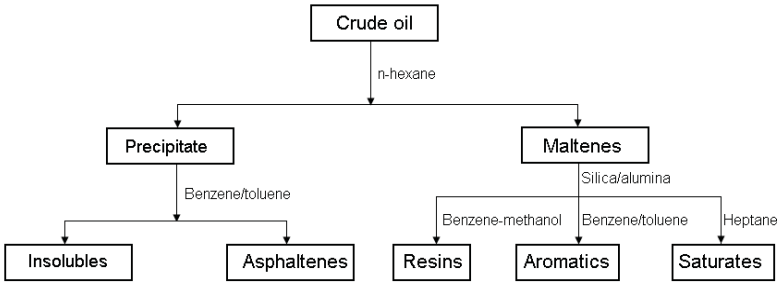

Figure 2.2 General schematic of the SARA fractionation method.

The definition of an asphaltene is *a molecule soluble in toluene, but insoluble in alkanes, such as pentane or heptane.* The main difference between asphaltenes and the other crude oil fractions is the amount of heteroatoms (S, N, O etc.) and the H/C ratio. The presence of heteroatoms opens up for different functionally groups in the molecules such as thiophenic

heterocycles (S), pyrrolic, pyrydinic and quinolinic groups (N), and hydroxylic, carbonyl, carboxylic and ether (O). [5] Compared to the entire crude oil fraction, asphaltenes have a larger amount of carbon and lower amount of hydrogen atoms. But knowledge on the elemental composition etc is still not sufficient to relate the behavior of such molecules to the macroscopic behavior of a crude oil in a process. One should also gain information on the structure of the molecules. In the literature one can find many different propositions on the molecular structure of asphaltenes. Due to the large differences between different crude oils and the broad definition of the fraction Nordgård et al [6 7 8] worked with synthetic asphaltene molecules to be able to make more general conclusions. Figure 2.3 illustrates three synthetic asphaltene molecules showed to resemble many of the properties of asphaltenes.

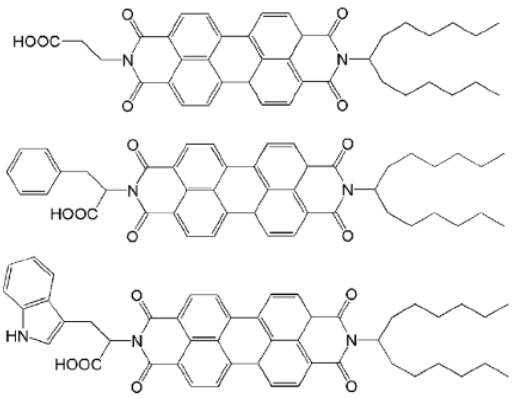

Figure 2.3 Structure of three model asphaltene molecules. [6]

The molecular weight of the asphaltenes has been under discussion since the introduction of the fraction. Asphaltenes molecules are prone to aggregate, even at very low concentration and in good solvents like toluene. The results from most of the older studies indicate that the molecular weight of asphaltene aggregates, rather than single molecules was measured. The currently accepted value of asphaltene molecular weight averages around 800 – 1000 g/mole. Since the definition of the specie is very broad, asphaltene molecules come in all kind of shapes and sizes. However, the structure of the molecule is believed to be flat or planar with an aromatic core and aliphatic chains. The combination of heteroatoms and the aromatic core opens up for intermolecular interactions, the former to H-bonding and the latter to π-bonding. These intermolecular interactions suggest that the molecule is prone to aggregate into particles or adsorb to any available interface.

The resins fraction of the crude oil consists of polar molecules with a relative high amount of heteroatoms (N, O S). The definition of resins is *the fraction soluble in light alkanes such as pentane, but insoluble in liquid propane*. Just like with asphaltenes, the presence of heteroatoms in the molecular structure opens up for functional groups. A hypothetical structure of a resin molecule is shown in figure 2.4. The aromatic fraction of the crude oil are all molecule with one or more benzene rings, whereas saturates are the non-polar compounds with no double bonds, including cycloalkanes and alkanes.

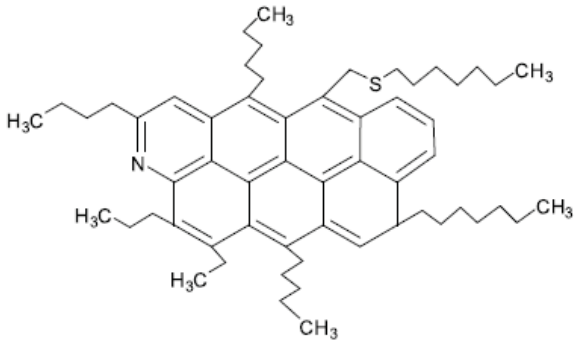

Figure 2.4 Hypothetical structure of a resin molecule. [9]

2.3 Classification

The properties of a crude oil sent to an upgrading facility in our time are different from what was upgraded in the early 1900s. Most of the feedstock sent to a modern refinery would be classified as heavy crude oil in those days. And the trend is going towards upgrading of heavier crude oils. Continuous development of exploitation techniques, methods of transportation and refining has facilitated this trend. For a crude oil to be classified as conventional it is required to flow to the surface without thermal stimulation of the reservoir. The classification of heavy and extra heavy crude oil is somewhat arbitrary. The API gravity is a measure of the density of the oil, and conventional crude oils are given an API gravity of 35 – 20 °API, heavy crude oils are found in the interval 20 – 10 °API and extra heavy crude oils are categorized below 5 °API.

However, the API gravity is not necessarily sufficient to describe the heaviest crude oils. The general trend for the heavier crudes also includes higher viscosity. Conventional crude oil has a viscosity ranging from 1 mPas to about 10 mPas. The elemental analysis illustrates the differences between conventional and heavy crudes. Heavier crude contains less hydrogen and more heteroatoms. The fractional composition for heavier crude oils also shifts towards a higher amount of asphaltenes and resins. Given the molecular size and properties of asphaltenes, there is no surprise that the extra heavy crude oil exhibit viscosities of values exceeding 1 x 10^6 mPa.s.

Many oil fields experienced processing difficulties that could not be explained by the physical properties of the crude oil like viscosity and density. One observed that the process equipment was subjected to deposits, and for some fields the separation proved to be more difficult than to other fields with similar liquid properties (viscosity and density). Research identified several other factors that should be of interest for the process engineer. The above mentioned asphaltene and resin content are important with regard to deposits and for the separation process. Waxes are found under the saturate fraction, and can at certain conditions precipitate and cause scaling, or simply form particles. The scaling cause difficulties for the process by blocking pipelines or process equipment, and the wax particles can be interfacial active and make the separation process more difficult. Acidic crude oils are another subclass of crudes that contain relatively small amounts of certain molecules that can have an accumulated effect on the process. The Total Base Number (TBN) and Total Acid Number (TAN) indicate whether there is a risk of extensive corrosion on the process equipment. Other implications with acids are ability to form deposits of naphtanic or tetrameric acids or as emulsifying

agents. [10] Solid particle content can also be important with regard to properties of the process material and with the separation.

2.4 Processing

The processing in the petroleum industry is complex and the modern process line includes almost every aspect of science and technology. The process can be categorized into four subgroups: recovery, separation, transportation and upgrading. The reservoir engineers are responsible for maximizing the recovery of available hydrocarbons located in the reservoir. In order to maximize the exploitation the behavior of the crude oil and water confined in pores should be understood. [11] The separation is the second step in the process. The stream coming from the reservoir is a multiphase flow of oil, water, gas and solids, and normally a separation is performed relatively close to the oilfield prior to transportation to the upgrading facility. The transportation to the upgrading facility is normally done via pipelines, and the pipeline engineer is engaged with ensuring the reliability of the transport. At the upgrading facility the crude oil is converted to usable products.

2.4.1 Recovery

Primary and secondary recovery

Normally the exploitation of oil is performed by making use of the high pressure in the underground reservoir. The pressure will force the oil to the surface when the drilling is completed. The method of using the pure pressure difference to obtain oil from the reservoir is called Primary Oil Recovery. The driving force of this technique is free gas or liquid expansion, or the influence of free water, or a combination of these effects. This method relies on the pressure within the reservoir as the energy source to move the oil to the surface. Therefore, the amount of oil coming from the reservoir will eventually decrease as the pressure depletes in the reservoir.

When the exploitation has progressed over a certain time the driving force of the primary oil recovery method diminishes. The primary oil recovery has a recovery rate of 20 – 30 %. There are various techniques to increase the recovery of the reservoir. One way is to maintain the pressure difference by injecting either water or gas into the reservoir. Recovery techniques in which gas or water are injected into the reservoir are called Secondary Oil Recovery Whether water or gas is used depends on many things. Firstly, the overall reservoir characteristics will influence which of the method is the most successful. Secondly, the availability of gas needs to be considered. When the reservoir has gas lying above the oil layer, as illustrated in figure 2.5, it is possible to inject gas to maintain the pressure within the reservoir. Reservoirs which can be exploited with the gas cap drive mechanism can have recovery rates of 40 – 50 %. The recovery of reservoirs which contains only water and oil can be as high as 80 %, as long as the injection of water optimized. Another way to increase the reservoir yield is to pump oil to the surface.

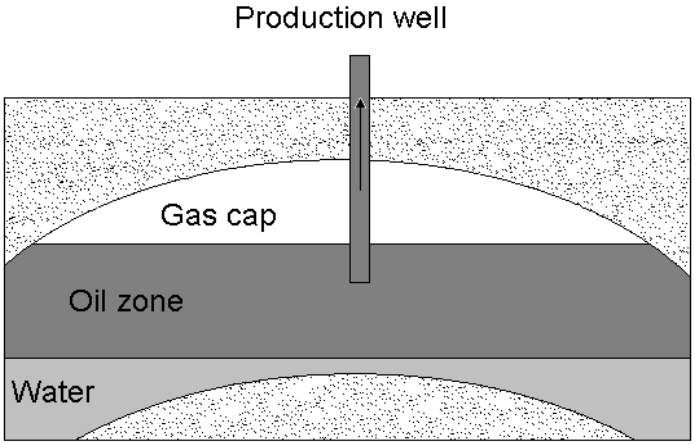

Figure 2.5 Cutaway of a reservoir with a gas cap.

Enhanced Oil Recovery
When primary and secondary recovery is no longer sufficient in terms of a viable oil production, one can initiate Enhanced Oil Recovery (EOR) techniques. The methods detailed in the previous section apply only for conventional crude oils. When the viscosity of the crude oil is too large to allow flow under normal conditions, enhanced recovery techniques are also used. The Enhanced Recovery use different approaches depending on the reservoir. For instance, heat can be used to reduce the viscosity of the oil, thereby increasing the flowability of the fluid. An important factor regarding reservoirs that have been exploited with primary recovery methods is the state of the oil in the reservoir after the primary extraction. Most of the oil is trapped within pores in the reservoir rocks, or as films along the pore wall. Surface forces between the different phases and capillary forces inside the small pores contribute to this phenomenon. It is therefore important to alter the forces in such a way that the oil de-attaches from the solid wall to increase the reservoir yield.

There are other ways to extract the oil from a well than to reduce the viscosity of the oil. Chemical methods, where surfactants, polymers and alkalines are injected into the well, are techniques that have been used to increase the yield. The mechanism of injecting polymers solutions is that it affects the mobility of the oil phase. By using viscous polymer solutions instead of just pure water, an increased area of the reservoir is swept by the polymer solution. The main motivation behind surfactant injection is to alter the interfacial properties and thus releasing the residual oil trapped in the rock pores. The mechanism of alkaline injection is somewhat similar to surfactant injection; changing the interfacial tension.

The method to use heat can broadly be divided into two parts: injection of steam and in situ combustion of the oil. Steam injection has been performed since the 1960s, and is usually performed stepwise; a sketch of the procedure is shown in figure 2.6. The first step is to inject the steam. The next step is to wait a certain period to allow the heat to be distributed in the well. The final step is to extract the oil with a reduce viscosity from the reservoir. Another method with a continuous procedure has also been used where the steam flooding has been used. With this technique the steam is injected in one well, and the oil is extracted from another well a certain distance away. There is an alternative to steam injection, the in situ combustion technique uses the hydrocarbons present in the reservoir as a heat source. To

make this technique successful air is injected into the reservoir and a part of the oil is burnt, and the heated oil of reduced viscosity is pumped to the surface.

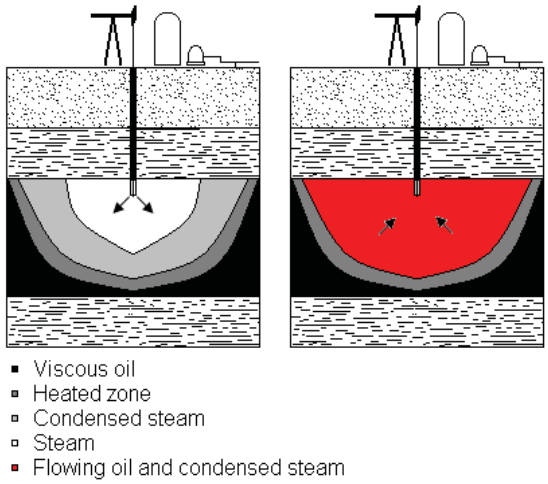

Figure 2.6 Sketch of the cyclic steam injection.

Extra Heavy Oil Recovery - Oil Mining
The oil mining method was developed in commercially since the 1960s. Certain oil fields in that region are situated just underneath the surface of the earth. The location, in addition to the fluid properties of the oil, can sometimes make oil mining a profitable technique of extraction compared to other techniques. Though, this method is viable only if the reservoir is situated at lowest 75 meters below the surface. As the names implies, sand containing oil is extracted from open mines and transported to a centralized processing plant either by vehicles, conveyor belts or as a slurry phase in pipelines. At the processing plant the mixture of oil, water and sand is treated successively to separate the hydrocarbons from the solids. A crude sketch of the process is illustrated in figure 2.7. [3]

The oil fields exploited using this technique contains on average 10 percent of hydrocarbons and about 85 percent of solid particles, clays, minerals etc. Large amounts of water are used to extract oil from the solids. As the numbers above indicate, the oil mining method does not only make an impact on the surface due to the open pit mining method, the separation also yields a substantial amount of solid waste. An optimization of the recovery will thus lead to larger output of valuable hydrocarbon resources and a reduction of the environmental effect of discharging solid waste containing hydrocarbons.

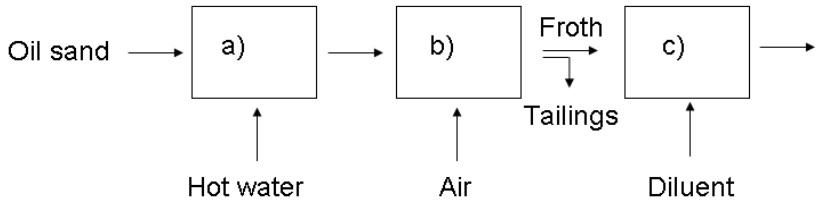

Figure 2.7 Sketch of the Hot-Water Process. a) Conditioning drum. b) Separation tank. c) Froth treatment.

There are several interfacial phenomenon that need to be considered in the process. First, the agglomerated solid particles and hydrocarbons should be separated; figure 2.8. This is done in the conditioning drum by mixing the oil sand with hot water and by adjusting the pH to 7-8 with addition of NaOH. This treatment changes the interfacial tensions and facilitates the release of oil from the solid matter which forms oil droplets dispersed in the water phase. Even though the oil has released from the larger particles, the oil droplets can still be covered by small sand grains. The presence of the sand particles can have an affect on the separation effectiveness due to the combined weight and it should be as few as possible sand particles on attached to the droplets.

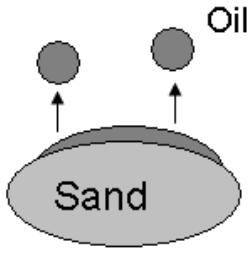

Figure 2.8 The Hot-Water Process; release of oil attached to solid particles.

In the separation tank most of the solid matter sediments and are removed as tailings. Air bubbles are introduced to the slurry to increase the velocity of the creaming oil droplets. The oil is collected at the top as froth; a mixture of oil, water, air and solid particles. It is beneficial for the process to have as low concentration of solids in the froth as possible. In order to facilitate for the release of the smaller particles the NaOH concentration is important. There is an optimum NaOH concentration in terms of obtaining the desired recovery and reducing the amount of solids in the froth. If the conditions are too lenient an insufficient number of particles will detach from the oil droplets and the froth will contain a large amount of solids. This can affect the froth treatment process with the formation of rag layers which can be difficult to break. [12 13] On the other hand, if the conditions are too harsh, i.e. high pH, the recovery of the oil decreases. Figure 2.9 can be used to illustrate the course of events. If the conditions are good the sand particles will detach from the droplet and the sand free droplet can move upwards with a faster velocity, as seen in figure 2.9 a) – c). However, at less than optimum NaOH concentration the detachment of sand particles is not sufficient and the droplet will due to the buoyancy force break into two droplets. The solids free droplet can move upwards whereas the oil droplet with solid particles still attached will not be recovered (figure 2.9 d)-e)). Another important factor regarding the recovery rate of oil sand processing is the properties of the solid phase. It has been shown that the wettability of the solids can have an impact on the recovery; where more hydrophobic solids give lower recovery and a worse froth quality. [14 15] The level of hydrophobicity for the sand particles is important with regard to how well the particles are attached to the oil droplets.

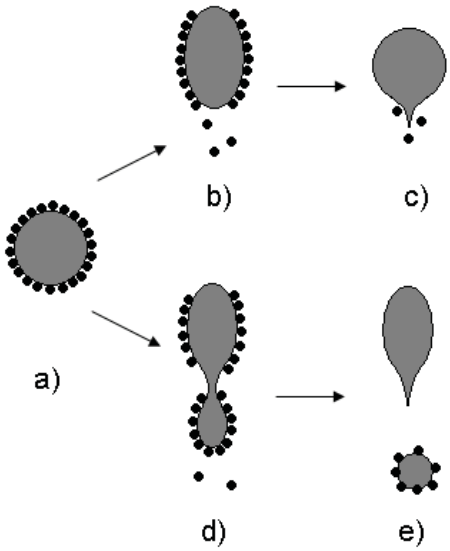

Figure 2.9 Recovery mechanisms of bitumen in the Hot-Water process and the effect of NaOH concentration. a) Oil droplet covered with sand particles. b) NaOH is added in the correct dosage and the sand particles detach from the droplet. c) The oil droplet floats. d) The NaOH dosage is not optimized and only a fraction of the sand particles detach. e) The particle free droplet breaks away and floats. [16]

The froth coming from the top of the separation tank needs to be separated before sending the oil to further upgrading. At this stage, the froth consists of 10 % by weight of fine solids, 30 % of water and 60 % of hydrocarbons. [17] The remaining water and solids are removed by diluting with naphta or paraffins (C_5-C_6) to reduce the viscosity of the oil and increase the density difference between oil and water. Centrifuges are used to further facilitate the separation. The amount of solids in the forth have caused some difficulties by accumulation at the oil-water bulk interfaces. This accumulation has been denoted as a rag layer and it consists of solid matter and water droplets. If the rag layer is not given attention there is a risk of growing a thick layer where at a certain level of accumulation there will be solids overflowing into either the oil or the water streams. [18] An impression of the complexity of the Hot-Water process can be made by considering all the different phases present; air, water, oil and a wide variety of solid particles.

Extra Heavy Oil Recovery - Non-mining methods

Different extraction techniques need to be considered if the heavy crude oil is situated lower than approximately 75 meters below the surface. Of the total resources in Alberta only 10% are found at such shallow depths, which illustrate the potential for development of non-mining techniques. Perhaps the largest obstacle for extra heavy crude oil recovery is the viscosity of the oil. The general way of performing non-mining extraction methods for extra heavy crude oils is to inject fluids to alter the flow properties of the hydrocarbons.

The previously mentioned steam process has proven to be successful for extracting heavy crude oils. However, it has been less successful for extra heavy crude oils and bitumen. The reason for this is a combination of lower permeability within the reservoir and the higher viscosity of the oils. This can be overcome by using gravity to extract the oil components. Steam Assisted Gravity Drainage (SAGD) is a process where steam is injected to the

reservoir. There are broadly two variations with regard to the process design. The steam can be injected in horizontal pipes, and the hydrocarbons are pumped via another horizontal pipeline positioned ~ 5 meters below. There is an alternative design where the steam is injected with several vertical pipelines; figure 2.10.

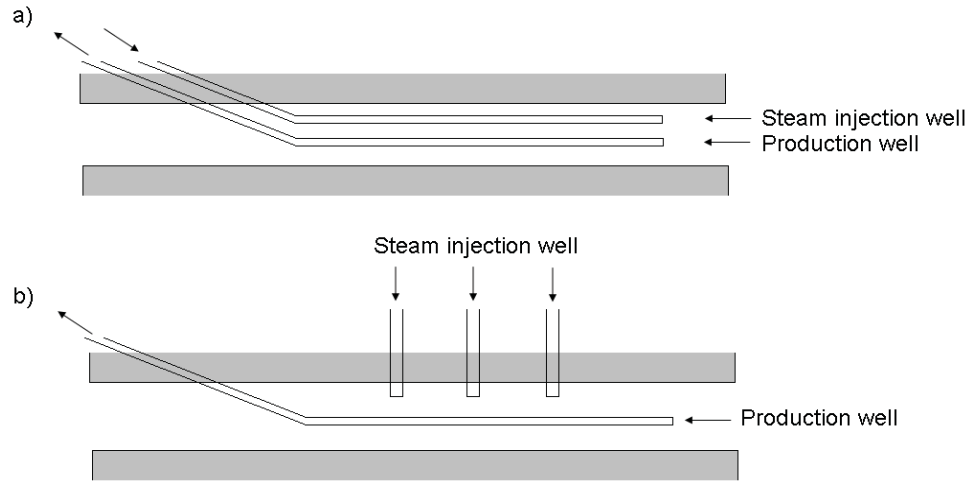

Figure 2.10 Sketch of the Steam Assisted Gravity Drainage (SAGD) method. a) Horizontal injection well. b) Vertical injection well.

The steam, and sometimes in combination with a mix of lighter hydrocarbons, will increase the flowability of the hydrocarbons. The effect of reduced viscosity and gravity will cause a downward movement for the heaviest hydrocarbons and the condensed water, whereas the lighter hydrocarbons (mostly methane) and the steam will rise. As illustrated in figure 2.11 below, two distinct regions will form. A steam chamber, consisting of steam and methane, will expand horizontally and vertically as more steam is injected. The condensed steam and liquid oil will flow downwards due to the gravity and the liquid phase of oil and water are pumped to the surface. [19]

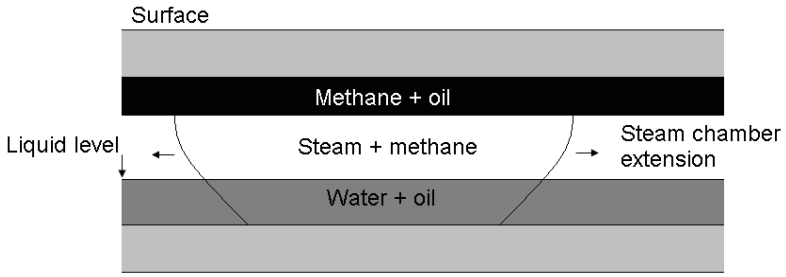

Figure 2.11 Expansion of the steam chamber in the reservoir in the SAGD process

The operation of the SAGD process can be somewhat complicated, at least compared to conventional crude oil exploitation. Not only do the reservoir properties (porosity, permeability, wettability) or oil phase properties (viscosity) have to be considered. In order to obtain a high recovery the ability to understand the heat transfer within the reservoir and to control the steam quality is also important. For this technique to operate satisfactory the volume balance within the reservoir should be maintained; the volume of oil and water

removed should be replaced. This is to ensure that the pressures of the steam chamber and the water layer are balanced. If any unbalance should occur, that can lead to breakthrough of ground water. This can be counteracted by increasing the amount of steam injected, or by reducing the pumping of the liquid, or both simultaneously.

Compared to the oil mining method, the SAGD process has a significantly reduced amount of solids in the process stream. In addition, 60 – 70 % of recovery can be obtained. Though, a large amount of thermal energy is required, making the process vulnerable to shifts in the prices of natural gas. The method will also require a large amount of water which has to be processed before being discharged or recycled. [1]

2.4.2 Transportation

Many oil fields are placed in remote areas with the necessity of transporting the raw material to the oil refinery for upgrading. There are traditionally two ways of transporting crude oil. The first one is by tanks on road, rail or ships. The second method, and the most popular, is via pipelines. Both methods have their advantages and disadvantages, which means that the engineer has to consider which method is economically optimum for each case.

The stream coming from the reservoir is a heterogeneous mixture of oil, water, gas, salt and solid particles. A certain degree of separation is important in order to minimize the volume and energy usage for pipeline transportation. Another important factor regarding the transportation via pipelines is the Flow Assurance. Within the term Flow Assurance lies several factors, such as pipeline corrosion, wall deposition and emulsion handling.

2.4.3 Separation

The goal for the process facility is to reach the specifications set by both the upgrading facility (oil quality) and the environmental regulations regarding the effluent (water quality). The incoming stream from the reservoir contains gas, oil and water and is first sent to the primary separator; figure 2.12. This vessel separates the majority of the three phases. The gas, oil and water can thereafter be transported to secondary separators for further purification if necessary. The sizing of the plant equipment, energy requirements and chemical dosages are all important parameter for the designers of a processing plant, especially for an offshore plant where space is limited. [20]

The separation section is normally one of the largest in a crude oil process facility, making this particular section interesting for size and cost reduction. Given the trend that many offshore oilfields are reaching a mature state with larger amounts of water being produced, and the exploitation of heavier crude oils, a potential for cost efficiency lies within the understanding of the primary and secondary separators. [21]

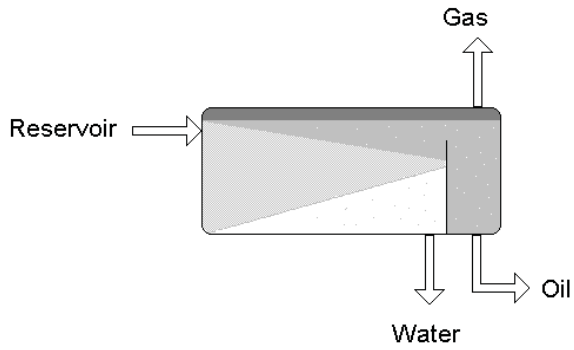

Figure 2.12 Sketch of a primary separator.

The process of separating water and oil is based on either the density difference between the two phases or the difference in dielectric constant. Gravity separators utilize the former, whereas electro-coalescers utilize the latter phenomenon. The phenomenons in the two techniques are thus somewhat different. In most cases water has a higher density than oil, meaning that a water droplet immersed in oil will move downwards, whereas an oil droplet in water will move upwards. Gravity separation can be used on water continuous and oil continuous systems. An electro-coalescer on the other hand can only be used on oil continuous systems. The method induces droplet growth by applying an electric field on the systems. The electrical field assists droplet coalescence and larger droplets sediment faster than smaller droplets. [22]

For the effluent treatment, two techniques are normally used to increase the droplet movement: hydro cyclones [20] and flotation. [23] Hydro cyclones in the oil industry increase the gravitational force to a range of 500 – 1000 g, thereby increasing the sedimentation velocity of water droplets, or increase the creaming rate for oil droplets. The flotation technique injects micrometer-sized air bubbles in the liquid to be treated. The bubbles attach to the particles/oil droplets, and their creaming rate is increased. The use of hydro cyclones is an already established technique in more or less every water treatment facility. The flotation technique is also an establish water treatment technique, and is used in particular in the separation of extra heavy crude oils.

The low density difference between extra heavy oils and water necessitate the application of a technique able to increase the vertical movement. When separating oil and water from the mining technique, the high amount of solid particles can make cyclones difficult to work without extra specification on the mechanical strength on the process equipment. Therefore the flotation technique is popular in that process. There are two important factors to keep in mind to maximize the oil recovery. Both of these are illustrated in figure 2.13. There is a risk that fine sand grains attach to air bubbles, and thereby increase the magnitude of froth formation At certain conditions, particle stabilized foams can exhibit very high stability. [24] Another issue is that the properties of solids from certain oilfields exhibit a wettability making the process to remove fine sand grains difficult. The recovery of oil from such fields can be poor because the grains attach to the oil droplet to such am extent that it will sediment rather than float. [14]

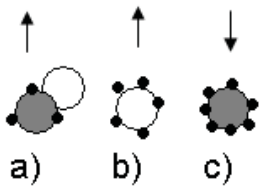

Figure 2.13 Phenomenon in the flotation technique. a) Droplet and bubble attached. b) Particles attached to bubble. c) Droplet with solids attached.

Regarding the size of the oil droplets, there is an optimum size ratio between the bubbles and the droplets in terms of obtaining high recovery. If the droplets are too small, they will not float to the top at a sufficient velocity. The smallest droplets are also more difficult to connect to the air bubbles. On the other hand, larger droplets have a tendency to break. The mechanism has been suggested to be a combination of the high buoyancy of the larger droplets together with the reduction of the interfacial tension at the oil/water interface. The combination of these two effects can stretch the droplets to an elongated shape, and finally the droplet breaks.[16]

2.4.4 Upgrading

Given the complexity of one crude oil, and the sometimes huge differences between reservoirs, the crude has to be upgraded before it can be used. In a refinery there are three different processes: physical, thermal and catalytic. The first step in a refinery is desalting and dehydration. This is performed by adding hot water which dissolves salt and other impurities.
.

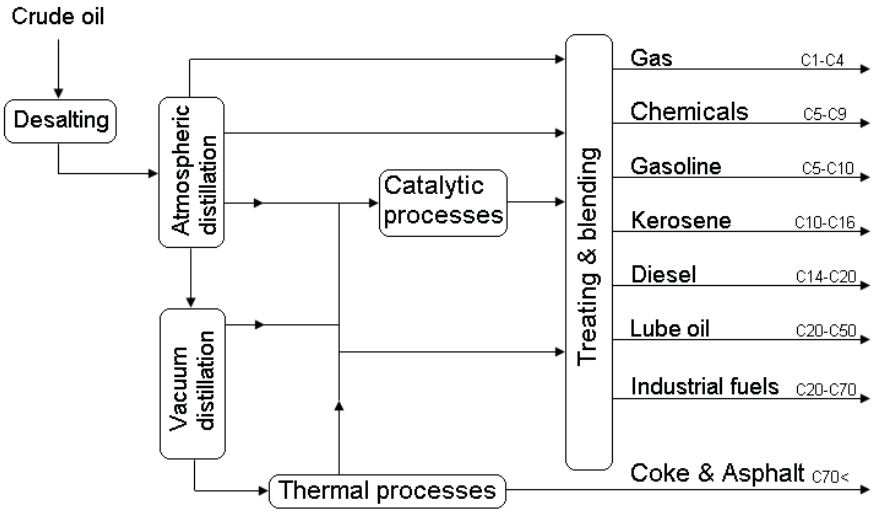

Figure 2.14 Simplified sketch of a crude oil refinery.

The second step is to separate the oil into fraction according to their volatility. At atmospheric pressure, thermal decomposition of the hydrocarbons initiates at approximately 630 K. This is undesirable due to deposition and fouling of the equipment. Thus, the fraction of hydrocarbons still in liquid form after the atmospheric distillation is distilled in the vacuum column. The non-volatile fraction after vacuum distillation is treated in a thermal process,

such as visbreaking or delayed coking. The visbreaking process is used to decrease the viscosity of the vacuum residue and maximize the output of valuable products such as gasoline and lighter products. Delayed coking is a more sever process which produces coke, in addition increases the output of lighter products.

The catalytic processes are perhaps the most important part in the refinery. The aim of these processes is to tailor make the chemical composition of the different products, for instance the octane number for gasoline and cetane number for diesel or any other products the marked might require. There are several different processes within the term catalytic processes. Catalytic cracking is a process where larger hydrocarbons are broken down to smaller molecules by acid catalysts. Hydrotreating is performed to remove heteroatoms and to hydrogenation of double bonds and aromatic rings. At more severe conditions, this process is called hydrocracking and as the name implies c-c bonds are cracked, resulting in a product of smaller hydrocarbons. Catalytic reforming is processes were the molecule structure is rearranged. And finally, alkylation is a process were small alkenes are forming larger and branched alkanes. [2]

2.5 Future

Conventional oil fields located offshore will after a certain time of production experience breakthrough of water, and as the fields get more mature the amount of water continues to increase. Figure 2.15 shows the production from one of the oldest oil fields in the Norwegian part of the North Sea, the Ekofisk field. The figure shows that the after a few years there is breakthrough of water. Injection of water to maintain the pressure in the reservoir was initiated in 1987, and as seen in the figure, the amount of water coming from the well is steadily increasing. Another important factor of mature fields is the utilization of EOR techniques by injecting various chemicals to the reservoir. Some of these chemicals can contribute to the stability of dispersed droplets. Due to increasing amounts of produced water, there might become necessary to re-design the entire separation facility to meet the specifications for some oil fields. Due to the differences in fluids from different oil reservoirs, a more field specific study on the process could lead to an economically and environmentally improved design. That means that a closer study on the separation is important.

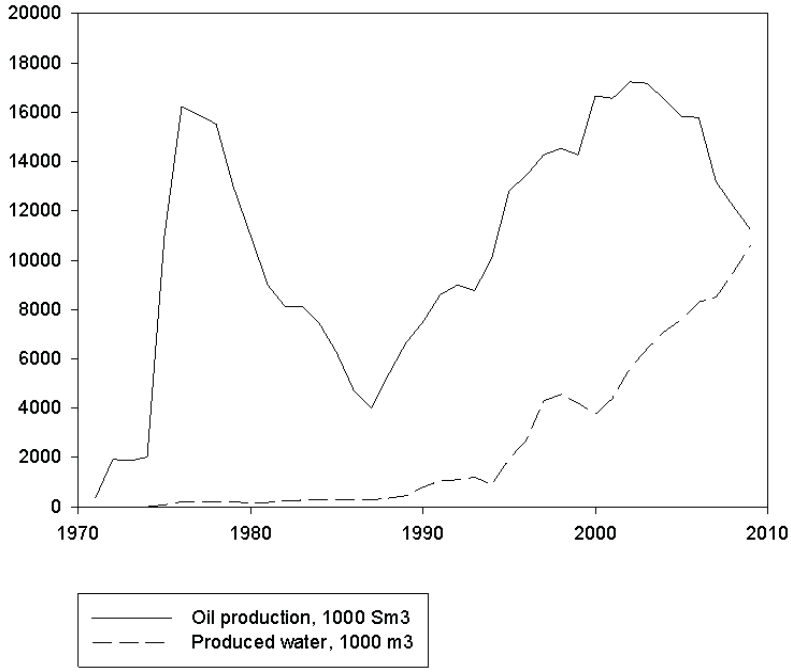

Figure 2.15 Historic production of oil and water at the Ekofisk oil field in the North Sea. [25]

The world wide demand for crude oil is increasing, and with depleting conventional resources, the decline in the availability of conventional crude oil ensures that the focus for the petroleum industry is currently changing. Estimates of the total world crude oil reserves lies in the range of 9 – 13 x 10^{12} barrels where 30 % of these are classified as conventional. Heavy crude oils are estimated to account for 15 % of the proven reserves and extra heavy oil, bitumen and oil sands for the remaining 55 %. However, the accuracy regarding crude oil reserves are somewhat low, firstly due to politically motivated manipulation of official data and secondly due to the uncertainty on how much of the heaviest crude oils that can be recovered.

The processing of heavier crude oils requires a higher investment of energy to produce the final products. This means that with a stable demand for oil products, the future price of crude oil derivatives will increase. However, there are no indications that the global importance of oil products will change. Figure 2.16 shows the daily world production of crude oil since the 1960s. Given the lack of viable and competitive replacements for energy in the transportation sector, and as a key raw material for a variety of products, there are few obstacles for the continuation of exploiting extra heavy crude oils.

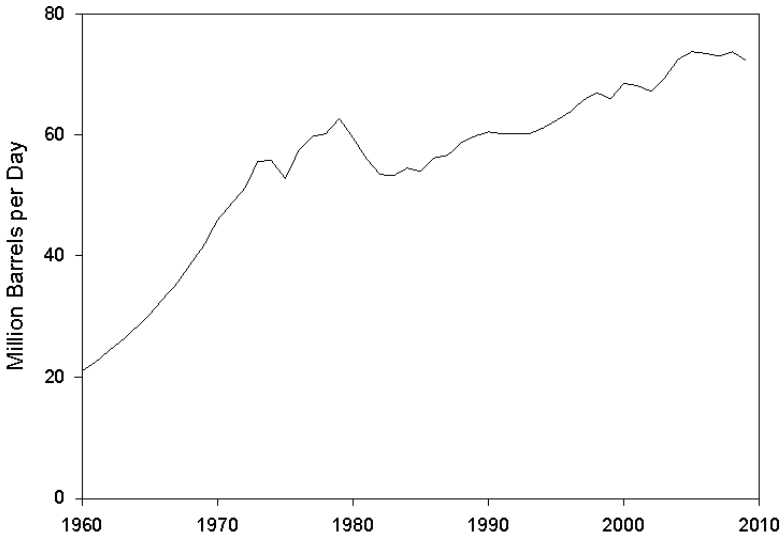

Figure 2.16 Historic total world production of crude oil. [26]

Chapter 3 Emulsions

The definition of an emulsion is a thermodynamically unstable dispersion of two immiscible liquids. Generally, emulsions are categorized in two types; oil-in-water (o/w) and water-in-oil (w/o). However, more complex double emulsions like water-in-oil-in-water (w/o/w) or oil-in-water-oil (o/w/o) do exist, but the area of application and understanding of the latter system is still in the early stages. [27] Even though emulsions are defined as unstable in thermodynamically terms, there are several emulsion systems that exhibit a lifetime of several days or months. In that sense the emulsions are kinetically stable or metastable; the droplet will sooner or later coalesce into two separate liquid phases.

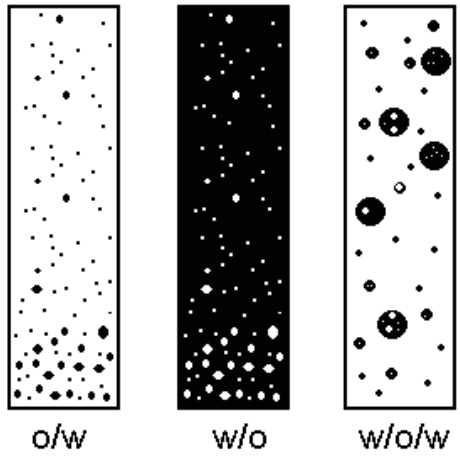

Figure 3.1 Schematics of different emulsion types. Left: oil droplets in water. Centre: Water droplets in oil. Right: Water droplets in oil droplets in water.

Emulsions are encountered in many different areas. Many of the daily life products such as food [28], cosmetics and pharmaceuticals [29 30] are emulsions. The relevance for the oil industry towards emulsions is primarily related to the processing. The stream from the reservoir in offshore oil fields, or onshore oil fields where water is used to aid the extraction of the oil, is bound to experience contact between the two liquid phases. In pipeline bends and valves the pressure drop can provide enough shear force to disperse one of the liquids into droplets.

The main technical issue with the formation of w/o emulsion is the salinity of the water causing corrosion of the pipeline and the processing equipment. Another issue is the extra energy required for the later transportation of the liquid to the upgrading facility. The increased energy requirement comes from the extra volume needed to be transported and from the increased viscosity of emulsions. And finally, the refinery plant has a minimum threshold for the water content in the crude oil. The main problem with the formation of o/w emulsion is related to environmental regulations. Even though the effluent water might contain relatively small amounts of oil (> 0.1 w%), the accumulated amount of oil from the effluent will make a tremendous effect on the environment.

One might get the impression that emulsions are something completely unwanted in the oil industry. For most of the cases, that is correct. But for the case of extra heavy crude oils, the concept of formulating o/w emulsions for transportation is rather promising. Transportation in

pipelines can be unpractical and/or financially unfeasible for such crude oils due to the high viscosity. By introducing the oil as droplets dispersed in water, the viscosity of such a system is dramatically reduced, making pipeline transportation credible. [31] [32]

3.1 Emulsification

3.1.1 Energy

Emulsions are thermodynamically unstable, meaning that they will not form spontaneously. Some kind of energy input is required to break up one of the single phase liquids into droplets. In order to have a stable emulsion, it is not necessary enough to simply form droplets. The droplets should be small enough to withstand sedimentation/flotation and coalescence within a reasonable time. This means that the deformation and subsequent break-up of the droplet is important with regard to the behavior of the emulsion. The deformation of the droplet is damped by the Laplace pressure given in equation I below:

$$P_L = \gamma\left(\frac{1}{R_1}+\frac{1}{R_2}\right) \qquad \text{(I)}$$

Where γ is the interfacial tension between the two liquids and R_1 and R_2 are the radii of the curvature of the droplet. The Laplace pressure details the difference in pressure between the concave and the convex side of a curved interface. With that, an external force is required to overcome the resistance of the curved surface to deform and break the droplet. The external force can either be due to velocity gradients, or due to pressure differences from inertial effects.

The stress on a droplet in laminar flow can be attributed to the continuous phase viscosity and the velocity gradient, and is written as $\eta_c G$. The stress is counteracted by the mentioned Laplace pressure. The ratio between these forces is called the Weber number:

$$We = \frac{\eta_C Gr}{\gamma} \qquad \text{(II)}$$

where r is the droplet radius. There is a critical Weber number, We_{cr}, indicating when a droplet will deform. At high Weber number, either due to droplet size or shear rate, and the droplet will break. This critical number depends on the ratio of the viscosity of the continuous and dispersed phase, η_d/η_c, and on the type of flow. Figure 3.2 indicates that large amounts of energy are required to disrupt droplets with a viscosity ratio higher than ~5 or lower than ~0.01. [33]

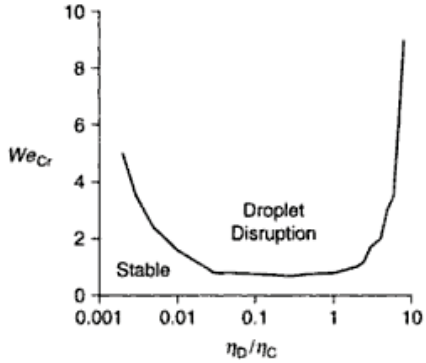

Figure 3.2 Critical Weber number for different viscosity ratios under simple shear flow conditions. [28]

During mixing the droplets are subjected to different mechanisms, as illustrated in figure 3.3. First the droplet starts to rotate. This momentum is transferred to the inside of the droplet as this liquid starts to circulate within the boundaries. At a certain circulation velocity the droplet elongates and finally the droplet has split into two separate droplets. The resistance towards droplet generation for low viscosity ratios (<0.01) can be understood by the ability to withstand high degree of elongation before the droplet is broken. For the case of higher viscosity ratio (>5), the deformation is damped by rapid and continuous reorientation due to changes in the flow field, altering of the direction of the disruptive forces. Another phenomenon partly responsible for the resistance at high viscosity ratio is the enormous power needed to initiate the circulation inside droplets of high viscosity.

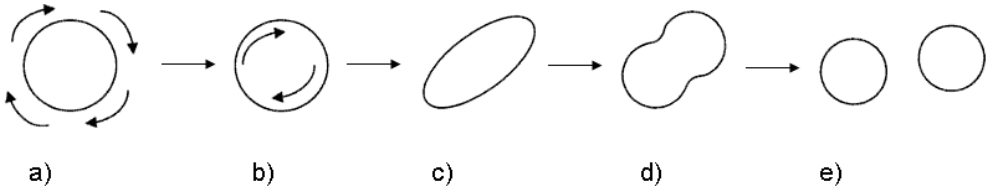

Figure 3.3 Sequences of droplet behavior in shear flow. a) rotation of the droplet. b) circulation of the liquid in the droplet. c) and d) elongation of the droplet. e) droplet disruption.

The theories mentioned above are not without assumptions. For instance, it is assumed that the liquids behave in a Newtonian manner. Any viscoelastic behavior of the liquid(s) will make the droplet break-up more complicated to explain. Another issue is that most droplets will deform and break-up several times during the mixing. Changes in the flow conditions, either elongation or shear, during the mixing can make the overall picture less trivial to explain. A third point is interfacial tension gradients. The theories apply only for droplets with uniform coverage of surfactants.

3.1.2 Interfacial tension

Another feature about equation I is that the amount of energy needed to break-up droplets decreases with decreasing interfacial tension. That means that any interfacial active compounds present during emulsification can facilitate droplet break-up. When a molecule which possesses both hydrophilic and hydrophobic domains in its structure is placed in a solution with water and oil present, it will preferably reside at the interface between the water and oil. The hydrophilic part will orient itself towards the aqueous phase and the hydrophobic part will be oriented towards the oil phase. Such molecules are generally known as surfactants; an acronym of the words surface and active. By comparing the surfactant molecule shown in figure 3.4 with the model asphaltene molecule in figure 2.3 and the resin molecule in figure 2.4, it is easy to recognize the relevance of the fundamentals of emulsion science to the petroleum separation process. The heteroatoms found in asphaltenes are often found in acidic or basic groups which will be of a hydrophilic character, whereas the long alkyl chains have a tendency to orient themselves into the oil phase. Thus, crude oil contains indigenous surfactants that can migrate and accumulate at water-oil interfaces and increase the stability of emulsion formed in the process. Additionally, there are a lot of chemicals injected into a reservoir to increase the recovery that are interfacial active and can contribute to the crude oil emulsion stability. [34]

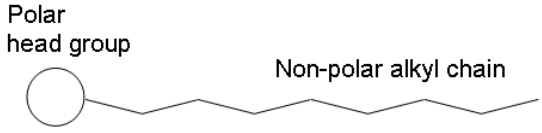

Figure 3.4 Schematic of a surfactant molecule.

Adsorption of surfactants occurs when two liquid interfaces are brought into contact. When two liquids are subjected to mixing the interface is deformed and eventually broken, in this case the interfacial area increases giving available space for more surfactant to adsorb to the interface. The role of the surfactant is to minimize the unfavorable effect of the interfacial area between the two immiscible liquids. When studying the emulsification process, it is normal to measure the interfacial tension. However, it should be stressed that measuring the tension between two static liquids is not completely comparable to the process of emulsification. The interfacial tension obtained from standard laboratory measurements is influenced mainly by diffusion of the surfactants, at least in the early stages of the measurements. The emulsification process with large velocity gradients will also include convection, not just diffusion. A normal feature observed when measuring the interfacial tension is that the tension is gradually decreasing with time until an equilibrium value has been reached. The time to achieve equilibrium interfacial tension can take anything from a few seconds, [7] to minutes, [6] or several hours. [35] The time of diffusion is normally shorter than that, which implies that the equilibrium interfacial tension is not governed by diffusion alone, but by reorganization of molecules at the interface. This reorganization can be modeled be equation III:

$$\gamma = \gamma_{eq} + (\gamma_0 - \gamma_{eq})e^{-t/\tau} \qquad \text{(III)}$$

where γ is the surface tension, γ_0 the initial tension and γ_{eq} is the equilibrium tension. The characteristic reorganizing time for the given system is given by τ. The timescale for surfactant adsorption and reorganization at crude oil-water interfaces can be understood by

the concentration and solvent properties. Generally the adsorption occurs faster at higher concentrations. But if the surfactants are solubilized in a poor solvent the surfactants can organize into flocculated particles instead of migrating to the interface. [36]

A second, and important role played by the interfacial active compounds, is the reduction of recoalescence during the mixing. An interface with adsorbed surfactants has a higher stability than an empty interface. The molecules form a barrier preventing coalescence as two droplets move closer. When a droplet has been broken into two smaller droplets, the interface is not completely covered by surfactants. In a homogenization process droplets are moving rapidly in the solution with a frequent collision rate. Depending on the rate of adsorption of surfactants to the newly formed interface, the droplets can either rapidly recoalesce or two new droplets are formed. With that said, the ability of the surfactants to adsorb and to stabilize emulsions is important for the efficiency of the energy consumption and the final droplet size distribution.

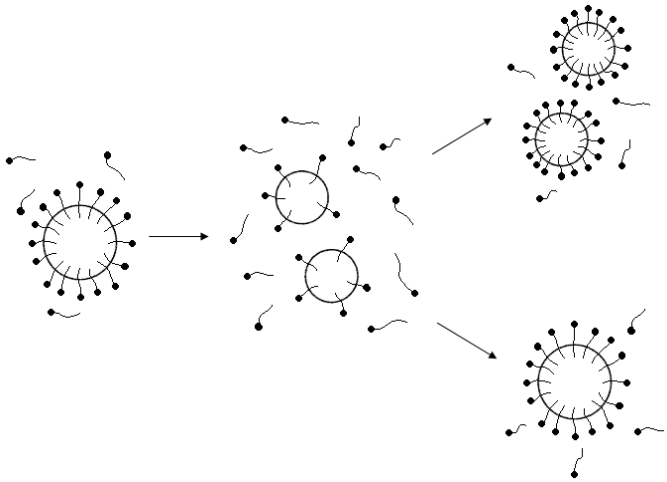

Figure 3.5 Recoalescence and adsorption of surfactants during homogenization.

The third feature of the surfactant in the emulsification process is the determination of emulsion type, whether they will be oil- or water continuous. Naturally the fraction of oil/water content is important, but the properties of the surfactants have also proven to be vital. [37] Although there are exceptions, a rule of thumb was introduced which states that the phase in which the surfactants are most soluble will be the continuous phase. This rule of thumb is known as the Bancroft's rule. To be able to more precisely predict the emulsion type the Hydrophilic-Lipophiulic Balance (HLB) was introduced. The HLB-scale is a quantification on the relative behavior in water (hydrophilic) and oil (lipophilic) and spans from values of 1 to 40 where low values indicate higher solubility in oil and high values indicates solubility in water.

3.2 Stability

The stability of an emulsion to withstand coalescence can be understood by two parameters: droplet collision frequency and collision success rate. In order to increase or decrease the stability of an emulsion one should be able to asses the importance of both parameters. The collision frequency is dependent on the number of particles and their freedom of movement,

both vertical and horizontal. In addition, the interactions between the droplet interfaces can affect the collision frequency. If the sum of the interaction forces between the interfaces has a repulsive sign a large external force is required to move the droplets together. The second parameter, the collision success rate is related to the strength of the interfaces to withstand coalescence when they are in physical contact.

3.2.1 Surfactants

The lifetime of dispersed droplets is increased when surfactants are present in the solution. As mentioned in the previous section, the surfactants adsorb to the interface and reduce the amount of collisions resulting in coalescence due to the formation of a protective layer. Another effect is the transformation of droplet interfaces with attractive forces into interfaces with repulsive forces. Two dispersed droplets of similar liquids are attracted to each other; this attraction is manifested on the low stability of emulsions formed in absence of surfactants. The reason for the attraction is the energetically unfavorable interface which reduces when the droplets coalesce into one. On the other hand, if the droplet interface has a population of surfactants of certain properties the interfaces can exhibit repulsive forces. This transformation to repulsive interfaces will reduce the droplet collision frequency. Thus, in any emulsion systems there is a presence of both repulsive and attractive forces, and the macroscopic behavior of an emulsion is affected by the sum of these forces. Figure 3.6 illustrates the different behavior depending on the sum of the forces.

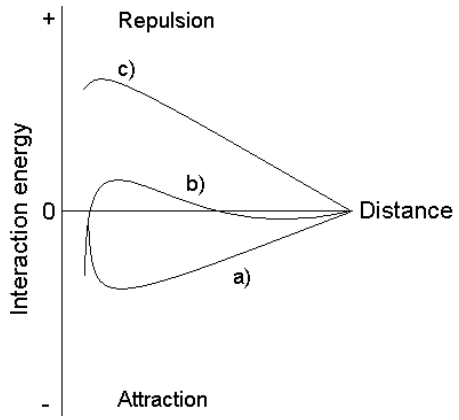

Figure 3.6 Potential energy curves for interactions between two colloidal objects at different conditions. Positive values are repulsive forces and negative values are attractive forces. a) Unstable. b) Metastable. c) Stable.

The repulsive forces are categorized into electrostatic stabilization and steric stabilization. The electrostatic stabilization occurs when the surfactants adsorbed have a charged unit, e.g. an acid or basic group. Two interfaces of similar sign will normally exhibit a net repulsion. When two interfaces of similar sign come into contact the interfaces will repel each other, as seen in plot b) in figure 3.6. Steric stabilization occurs when the interface is covered by non charged surfactant. Upon contact the solvent molecules between the close droplets will experience a decrease in the entropy, and thus there will be a flux of solvent molecules moving to increase the entropy.

3.2.2 Solids

Solid particles can increase the emulsion stability, and they are also capable of completely stabilizing emulsions without any surfactants present. The term Pickering emulsions refer to emulsions stabilized by solid particles alone. Organic particles of wax [38] [39] or asphaltenes [40], and inorganic particles of clays [41] [42] [43] have been found to be interfacial active in emulsions. Solid particles do not stabilize emulsions by reducing the interfacial tension, but their presence at the interface gives the droplet a mechanical barrier or the particles can give the interface rheological properties that reduce the coalescence rate. [44] In order for particles to counteract droplet coalescence, the wettability of the particle surface should have an intermediate value. Particles of either highly hydrophobic or hydrophilic character do not form stable emulsions since they are less interfacial active. The wettability of the particles also dictates the emulsion type of the systems. [45] The type of emulsion follows Bancroft's rule: particles that are mainly oil wet will form an oil continuous emulsion and vice versa. The particles size is also of importance when it comes to the stability of the emulsion. It has been shown that particles in the range of 5 – 30 nm can stabilize emulsions without any surfactants present. [46] However, it is not the absolute particle size which dictates the ability to stabilize emulsions but the size ratio between the particles and the dispersed droplets. In conventional crude oils the presence of solids alone has not been proven to solely stabilize emulsions, but their presence can increase the stability together with other components. However, as mentioned in section 2.4.2, the oil mining technique is heavily influenced by the amount and properties of solid particles.

3.2.3 Films

One of the main reasons why crude oil emulsions sometimes exhibit such a high resistance towards coalescence is the formation of films at the interface. The presence of a monolayer of surfactants can be sufficient to stabilize emulsions. When two monolayers approach the originally spherically shaped interfaces can be changed if the external force is sufficiently large. The change in the interfacial area that follows from the altered curvature leads to a gradient in the composition of the interface; the location on the curvature which has been stretched will have a lower concentration of surfactants and thus a higher interfacial tension (γ_2) compared to the unperturbed interface (γ_1). This concentration gradient will thus give a driving force for a migration of surfactants to the stretched area. This counteraction will prevent the droplets from coalescing and is called the Gibbs-Marangoni effect. Figure 3.7 shows a schematic presentation of this effect. The flexibility of the surfactants to move along the interface determines the ability the surfactants have to stabilize droplets, and gives the droplet interface an elastic behavior and an increased stability towards coalescence.

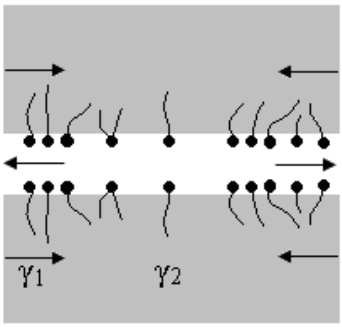

Figure 3.7 Sketch of the Gibbs-Marangoni effect

The asphaltene fraction found in crude oil has been found to have the ability to form monolayer interfaces of high compressibility and the ability to dampen the coalescence. [47] But given the complex composition and the amount of indigenous surfactants in crude oils the formation of multilayers can in some cases be more likely. By studying droplets in the micropipette technique, it has been observed that when a droplet is subjected to deflation, the interface can at certain conditions can either crumble or maintain its shape. It was observed that the interface was crumbled at low concentrations of asphaltenes, whereas at higher concentrations the interface maintained its spherical shape when deflated. To explain this phenomenon with multilayer formation at the interface seems more plausible than a monolayer. [48]

Other techniques have elaborated this behavior. By studying the interfacial rheology one can distinguish between the interfacial elasticity and the interfacial viscosity of a system. Studies have shown that the asphaltenic film strength is influenced by the aging of the film. The interfaces of asphaltenes can slowly increase their interfacial elasticity and viscosity. Whether this effect is mainly due to a slow formation of monolayer, due to rearrangements of already adsorbed molecules/aggregates or the formation of multilayers is not clear. Nonetheless, the elasticity of the film can increase two-fold the first 2-4 hours. Similar behavior is observed regarding the interfacial viscosity. After an initial rapid increase, it is normal to observe gradual changes even after 24 hours. [5]

The film strength of the oil-water interface is also dependent on the concentration of asphaltenes. In a narrow concentration range of asphaltenes the emulsion stability is markedly increased, and the observed stability coincide with an increase in the elasticity of the interface. [49] [50] The asphaltene concentration range depends on each oil phase studied, but the values typically lie around 0.1-50 g/l. At higher asphaltene concentrations the elastic and viscous modulus has been observed to pass through a maximum. [51] There are other effects of important regarding the film strength. Due to the structure of the asphaltene molecules, they are prone to aggregate into small clusters. Naturally, the degree of aggregation is dependent on the solvent of the system, but even in toluene, which is considered a good solvent for asphaltenes, formation of nano scale particles or aggregates have been observed at a concentration of 50 mg/l. [52] The presence of both single asphaltene molecules of different sizes and functionalities and asphaltene particles of different aggregation number in the systems means that it can be complicated to properly account for the changes in the film of crude oil-water interfaces.

Whether the solvent is of an aromatic or aliphatic nature can have an effect on the film properties. The mechanism of asphaltene adsorption is influenced by the solubility of the asphaltene, and higher solubility will lead to a less interfacial activity, and thus a weaker film. When the solubility of the asphaltenes is sufficiently high the driving force for adsorption to the interface is low and one will find a higher amount of asphaltene molecules as monomers. In an aliphatic solvent the asphaltene molecules will try to reduce contact to the solvent and it is energetically more favorable for them to form larger particles. The highest film strength and highest emulsion stability has been showed to be near the solubility limit of the asphaltenes. This suggests that asphaltene are at their most interfacial active state when they are in the border between solubilization and precipitation.

Figure 3.8 shows a simplified illustration of how an increase in the surfactant concentration changes the composition at the oil-water interface. At low concentrations each molecule exerts a rather large area. As the concentration increases the molecular area decreases and at a certain point multilayers can start to form. At even higher concentration the interface can change into three dimensional networks with a population of small molecular aggregates. However, the transitions shown in figure 3.8 might be accurate to describe the behavior of a simplified model system of well defined surfactants or at certain concentration ranges. As mentioned above, crude oil surfactants are not well defined and the transitions are most likely not very sharp regarding real world systems.

Another important factor to consider is the interactions between resins and asphaltenes in the system. Asphaltenes have been pinpointed as the main component in crude oil films, while studies have shown that emulsion containing both resins and asphaltenes have a different stability compared to an emulsion stabilized by asphaltenes alone. McClean and Kilpatrick observed that the stability of emulsions were at its maximum when the ratio of asphaltene:resins was at around 3:1. [53] A similar phenomenon was observed for the compressibility of the films. [54] Resins alone does not normally contribute to emulsion stability in particular way, but the resin fraction is thought to be acting as a stabilizing agent facilitating the adsorption of asphaltene aggregates. When the ratio of resins becomes larger they replace the asphaltene fraction at the interface, and due to the weaker attractions between resins molecules the film strength decreases. [55]

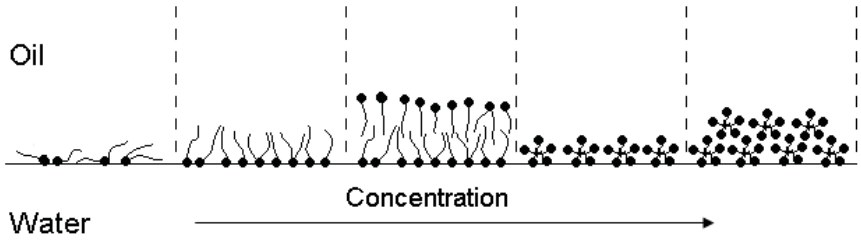

Figure 3.8 Sketch of the formation of a complex layer at the oil-water interface at increasing surfactant concentration.

So far, the parameters of importance for the properties of interfacial films have been focused on the interface alone or the oil phase. Naturally the water phase can also influence the film properties. Crude oil surfactants can contain both basic and acidic functional groups and the state of these groups and the environment in which they are confined can affect the film.

When discussing water chemistry the pH and ionic strength are important parameters to consider. The pH affects the functional groups and their protonation/dissociation and the ionic strength can screen the charged groups at the interface. [56] The relevance to a crude oil sample can be manifested in a pH dependent adsorption time or elastic properties. [35] However, it has been found that for a monolayer of asphaltenes, the interactions between the polyaromatic rings and alkyl chains are dominant forces regarding the film strength compared to the influence of the water chemistry. [57]

3.3 Destabilization

In order to destabilize an emulsion, two incidents have to occur. First, the droplets should come into contact. And secondly, the collision should result in coalescence. If one wants to increase the probability of either occurrence, there are various parameters to manipulate. The sedimentation velocity of a spherical droplet is given by the Stokes' equation: [58]

$$v_{st} = \frac{\Delta \rho g d^2}{18 \mu_c} \qquad \text{(IV)}$$

Where $\Delta\rho$ is the density difference between the dispersed and continuous phase, μ_c is the continuous phase viscosity, g is the gravity constant and d is the droplet diameter. Consequently, the liquid properties of both the dispersed and continuous phase can give an indication on the stability. A low density difference means that the fundamental driving force, gravity/buoyancy, is low. The same thing can be assumed with the continuous phase viscosity. A high continuous phase viscosity means that the movement of the droplets will be low, not just the gravitational movement in the vertical direction, but all directions. And finally, it is important to be aware of the size of the droplets in the emulsion. Smaller droplets have a lower driving force for vertical movement, and another important factor is the effect of Brownian motion of smaller droplets.

By taking equation IV into consideration, there are many different actions available for implementation to increase droplet movement and droplet collision frequency. The first and most obvious is to change the liquid properties, the density difference and the viscosity. This can be done by increasing the temperature or by diluting the oil phase. The driving force can also be manipulated by using centrifuges or cyclones to increase the gravity imposed on the system or air flotation techniques to increase the vertical velocity. [59] [13]

As mentioned above, the movement of dispersed droplets can be attributed to gravity moving the droplets vertically and the Brownian motion in any random direction. By inducing an electric current through the sample it is possible to add a third source of movement to the droplets. When water has a certain electrolyte concentration it becomes more conductive. Oils on the other hand have a lower conductivity and this can be exploited by perturbing the movement of water droplets confined in an oil phase. The use of electrostatic enhancement of w/o emulsion coalescence was first patented in 1911, and since then the technique has been developed into many different combinations and designs. Electrical methods have been used in combination with for instance chemicals, heating or centrifugation. Both alternating current (AC) and direct current (DC) have been used separately or simultaneously, all depending on the properties of the liquids to be separated. The technique exploits the difference in the dielectric constant between the two phases present, and only works if the dielectric constant of the continuous phase is lower than that of the dispersed phase. [60]

Another easy action to implement to decrease the stability of o/w emulsions is to manipulate the pH or increase the ionic strength of water phase. This can affect the electrostatic repulsions between the charged interfaces, and a reduction of the thickness of the electrical double layer. The lowering of the double layer thickness means that two droplets requires a lower momentum to be able to come into physical contact.

If the rate determining step of the separation is the frequency of collisions leading to coalescence one should start using chemical additives to change the properties of the interfaces. Numerous patents of effective emulsion breakers exist, and the roles they play have been examined in several papers. Demulsifiers can be categorized to their molecular weight, either as Low Molecular Weight (LMW) or High Molecular Weight (HMW). The molecular size of HMW demulsifiers is normally >5000 g/mol and their structure can be anything from block copolymers to poly-electrolytes. Their role is to penetrate the film at the water-oil interface and change the rheological properties of the film. The LMW demulsifiers can either be added to replace already existing entities at the interface or to change the wettability of stabilizing components at the interface, e.g. solid particles. The most efficient demulsifiers are capable of radically changing the properties of the interface in a short time scale, [61] and at a concentration in the range of 5-20 ppm. [62]

In order for a demulsifier to be effective the molecule should be able to partition into both phases. The rate of adsorption should be high and the interfacial activity should also by high to suppress the interfacial tension gradient when two interfaces are in contact. [63] When the demulsifier have reached the interface they reduce the interfacial viscosity and elasticity of the film. [61] The dosage of the demulsifier is also important; it has been found that the optimum concentration of a demulsifier can be correlated to the asphaltene concentration. At low asphaltene concentrations the demulsifiers dosage appears to be proportional to the asphaltene concentration and a critical asphaltene concentration the film seems to be saturated and the optimum demulsifier dosage is constant. [64]

3.4 Modeling

To determine the stability of an emulsion experimentally can be expensive and time consuming. In addition, given the complex connection between the various parameters involved in the topic, quantification of the contribution from each parameter to the behavior of the whole system is difficult to relate by experiments alone. By combining the experimental work with development of models, a better prediction and understanding of emulsion stability might evolve. The modeling is particularly important when the sizing of industrial scale separators is to be performed.

Simple models have already been developed to perform this, but the accuracy of these models is always under scrutiny due to the assumptions that needs to be made. For instance, the time scale of a separation can be approximated by equation IV and assuming a certain droplet size, say 100 μm diameter. This assumption might hold for a crude oil system with low amounts of surfactants. But as the exploitation of crude oils with higher amounts of “troublesome” components one should also account for the lifetime of the droplets. Another issue with the Stoke’s law is that it assumes the only force acting on the droplet is the gravity/buoyancy. At a low dispersed fraction that assumption might hold, but at increasing amount of neighboring droplets the movement will become increasingly hindered.

Hartland and Jeelani [65] used a modified Stokes' velocity to account for the dispersed phase fraction. They also included a coalescence time into the model to account for the interfacial properties of the system. The correlation with experimental data showed that it was able to follow the experimental data. [66] The Hartland model gave the time dependent location of three different interfaces, as illustrated in figure 3.9. However, the model described the system as an emulsion of mono sized droplets; another limitation of the system is that it used the continuous phase viscosity to describe the conditions. In a diluted emulsion that might not give any large errors, but in a region of droplet densely packed that can give rise to a source of error.

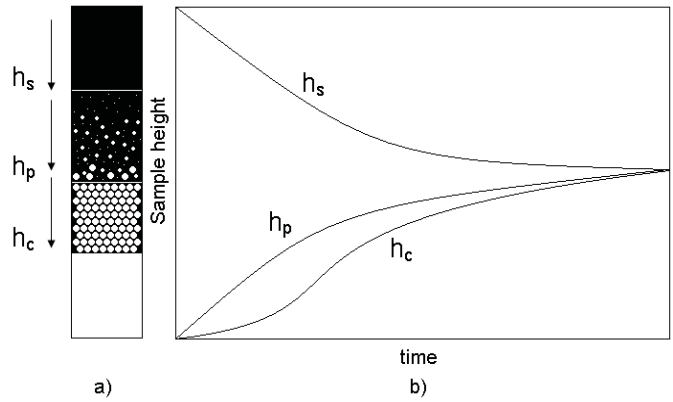

Figure 3.9 The Hartland model. a) Heights of sedimenting (h_s), dense packed layer (h_p) and coalescence heights (h_c)in an emulsion. b) Schematics of the time variation of the different fronts.

Thus in order to develop a model able to predict the separation characteristics one should be able to have a reference where one can observe if the model holds. It is not very likely to have a mono sized emulsion in a real world system, neither three well defined interfaces. For instance, it is more likely to have a many sedimentation interfaces due to several different droplet sizes. This reference should include the ability to monitor the emulsion region. To obtain the kinetics of free water formation is not particularly complicated but there are not many techniques available to monitor the sedimentation front and thickness of the dense packed layer.

Chapter 4 Experimental techniques

In order to prepare a stable emulsion or to improve the separation of a process where emulsions are present, one should characterize the system as detailed as possible. Without the correct understanding of the cause behind the stability, one might risk implementing an action without an effect or in the worst case an undesired side effect. This chapter focuses on giving a brief introduction to the different experimental techniques used during the doctoral work.

4.1 Interfaces

The study of interfacial properties might seem to be distantly related to emulsion behavior on a macroscale. However, without any further insight on the emulsion properties on a micro- or even nano-scale, the understanding of a specific emulsion system can be speculative.

4.1.1 Du Nouy ring

The De nouy ring method for measuring the interfacial tension is relatively simple and is illustrated in figure 4.1 below. A ring is connected to a force measuring device, while a vessel containing the liquid(s) moves vertically up and down. The vertical movement will measure the force experienced on the ring as the ring crosses the interface between either two liquids or liquid and air. Due to the interfacial tension, small amounts of liquid will stick to the ring as it moves upwards beyond the interface. The measured force due to this 'hanging' liquid is then correlated with the interfacial tension of the sample via equation V.

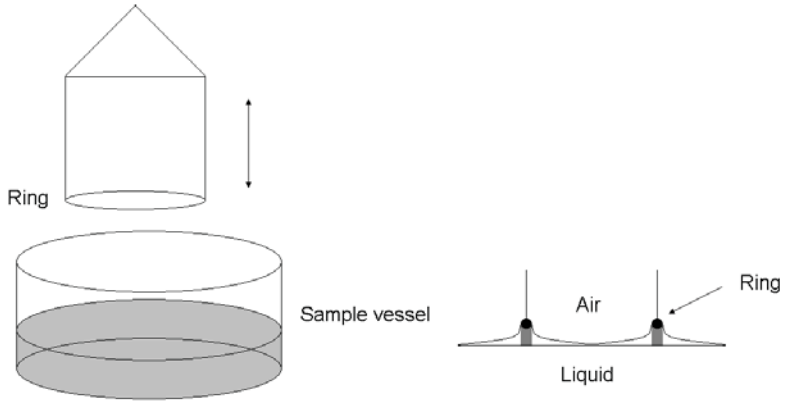

Figure 4.1 Du Nouy Ring technique for interfacial tension measurements.

The force acting on the ring is approximately equal to the interfacial tension and the perimeter of the ring. However, a correction factor is necessary to use due to the direction of the surface tension. The correction factor, β, is dependant on the ring dimension and on the density of the liquid(s).

$$F = 4\pi R\gamma\beta \qquad \text{(V)}$$

The accuracy of the Du Nouy ring method is about 0.1 mN/m. An important feature regarding the use of this technique is that the ring should be parallel to the interface. In addition, the contact angle between the ring and the liquid should be as close to zero as possible.

4.1.2 Oscillating Drop technique

A useful technique to study both liquid-liquid and liquid-gas interfacial behavior on a micro scale level is the oscillating drop, also known as the pendant drop. With this setup one of the liquids are placed in a syringe with the needle of the syringe placed in a cuvette were the second liquid is situated. The syringe is connected to a piston and the volume of the drop can be changed. A camera monitors the droplet shape, and the droplet shape is used to calculate the interfacial tension. The name 'Pendant Drop' infers that the drop is hanging. Though, for systems where the density causes the droplet to move upward, the inverse situation can also be studied. The method is then called the sessile drop. The equilibrium shape of the drop is determined by the combination of gravitational forces and interfacial forces. Gravity tries to drag and elongate the droplet, whereas the interfacial tension tries to minimize the droplet surface area.

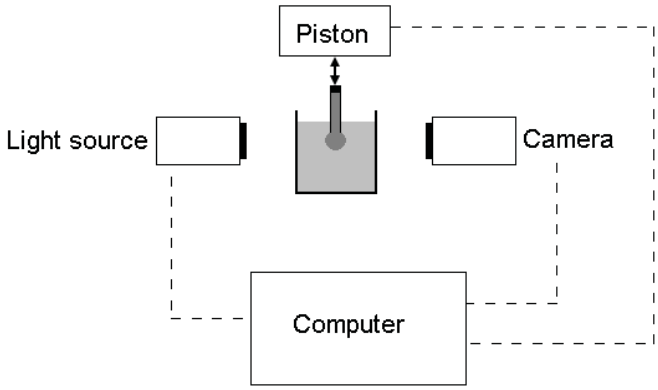

Figure 4.2 Sketch of the oscillating drop method for interfacial tension measurements.

The interfacial tension is obtained by combining equation VI and VII,

$$\Delta p = \gamma \left(\frac{1}{R_1} + \frac{1}{R_2} \right) \qquad \text{(VI)}$$

Where Δp is the pressure difference across the droplet interface, γ is the interfacial tension and R_1 and R_2 are the curvature radii. Equation 5 is known as the Young-Laplace equation, giving the correlation between surface shape, interfacial tension and pressure difference across the interface. Equation 5 gives the hydrostatic pressure,

$$\Delta p = \Delta p_0 + \Delta \rho g z \qquad \text{(VII)}$$

where Δρ is the density difference between the two phases. This means that the interfacial tension can be obtained by knowing the density difference and from drop shape calculations of the images. By using a camera and a computer, it is possible to rapidly monitor the changes of droplet shape over time. These changes can then be correlated to changes in interfacial tension due to adsorption of interfacial active molecules. However, it is important to avoid any perturbation to the drop shape. As seen in figure 4.3, air bubbles can be included in the droplet and due to the high density difference between these bubbles and the liquid the shape

of the droplet can be elongated. For a relative transparent liquid it is easy to observe whether there are bubbles inside the droplet. But for dark liquids, like crude oils, it is close to impossible to be confident that there are no extra factors affecting the droplet shape.

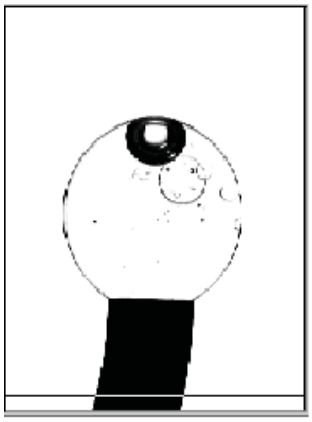

Figure 4.3 Sessile a) and pendant drop b).

Another way of using the apparatus is to oscillate the drop volume. By changing the volume of the drop, the interfacial area changes as well and the interfacial response can be studied. Periodic changes of the droplet area can be controlled with a computer controlled mechanical piston and the interfacial tension can be monitored in the manner explained above. The interfacial dilation modulus E is given as follows:

$$E = \frac{d\gamma}{d\ln A} \qquad \text{(VIII)}$$

where γ is the interfacial tension and A the interfacial area. The interfacial dilation is a complex function of the frequency of the droplet volume angular frequency of oscillation, ω.

$$E^* = E_d + i\omega\eta_d = E' + iE'' \qquad \text{(IX)}$$

Where E_d is the interfacial dilation elasticity and η_d is the referred to as the interfacial viscosity. The modulus can be written as the sum of the energy stored in the system (E') and the energy lost (E'').

A potential drawback with the pendant drop technique can be the image calibration and image quality. Another important factor is that the calculations on the interfacial tension assume that the forces acting on the droplet are given by equation VIII and IX. However, at certain conditions viscous forces can influence the response of the droplet. Freer et al [67] showed that the Capillary number is important in order to understand at which conditions the technique works satisfactorily. The Capillary number, Ca, is defined as the ratio between viscous forces and capillary forces acting on a droplet.

$$Ca = \frac{\Delta\mu\omega\Delta V}{\gamma_0 a^2} \qquad \text{(X)}$$

Where $\Delta\mu$ is the viscosity difference between the two phases, ω is the angular frequency droplet oscillation, ΔV is the volume amplitude droplet oscillation, γ_0 is the equilibrium interfacial tension and a is the radius of the capillary in which the droplet is attached. It was shown both by Freer et al and Hannisdal et al [68] that at Ca > 0.0021 the viscous forces are no longer negligible. This is important with regard to studies on crude oil, and shows that in order to study more viscous samples the frequency and capillary dimension should be optimized.

When studying the interfacial rheology it can be done either with dilational or shear rheology. Both techniques are capable of splitting the interfacial response into an elastic and viscous part, where interfacial shear elasticity and viscosity is denoted as *G'* and *G''*, respectively. On the other hand interfacial dilational rheology is denoted with an *E*, as seen in the equations above.

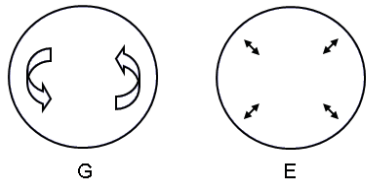

Figure 4.4 Basic principles of measurement of shear and dilational rheology.

Shear rheology is the study of an interface where the area is kept constant and the shape is changed. The principle of dilational rheology is the complete opposite where the shape of the interface is kept constant and the area is changed. Due to these differences, the comparison of results from the two techniques might not match. Comparison has shown that trends can be followed with these two techniques but the results are not quantitavely comparable. [56]

Surface Force Apparatus 2000

The Surface Forces Apparatus (SFA) 2000 is a technique used to perform measurements of forces acting between surfaces. The apparatus is using the optical properties of thin silver layers to measure the movement of surfaces down to nano meter scale. The forces are measured by moving the surfaces slowly together and apart and by monitoring the actual movement of the surfaces using optical (FECO) fringes. The FECO fringes appear on the concave mirror due to the optical properties of thin layers of silver. [69]

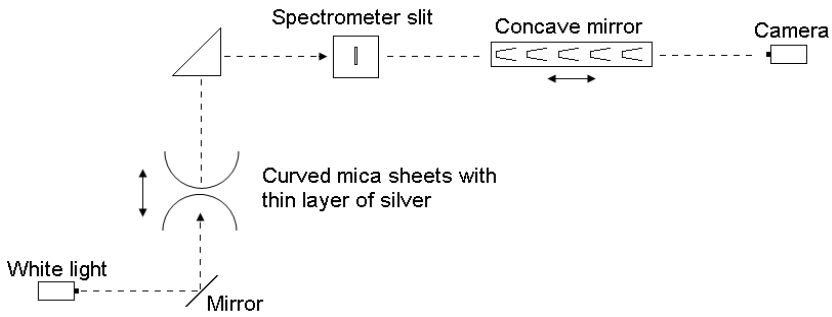

Figure 4.5 Basic schematics of the SFA 2000.

White light is directed perpendicular to two mica sheets in a cross cylindrical configuration. The configuration is mimicking the point-point contact of two spheres coming in contact. When the silver layer is sufficiently thin, only selected wavelengths of the white light is permitted through. The remaining light is then directed through a slit where the wavelengths are split into fringes on the concave mirror. As the two surfaces are moving, their actual displacement can be observed via the movement of the fringes. With that, the location and velocity of movement can be monitored. The apparatus is very important in terms of studying the forces between surfaces of various surfactants, polymers and solvents. [70] [71] [72]

4.2 Emulsions

4.2.1. Bottle test

The bottle test is perhaps the most well known and easy method to study emulsion stability. The simplicity is both the main advantages and disadvantage of the method. With this method the emulsions are prepared and left in bottles/cylinders and after a certain elapsed time the height or thickness of either the water or oil phase are recorded or a small amount of the emulsion is taken out and analyzed in a separate apparatus. The advantage is the simplicity and lack of calibration and sensitive tools. Another advantage from the lack of any complicated tools is that it is easy to scale up the tests. The disadvantage is the lack of data and the time needed to obtain kinetic data of the emulsion separation.

4.2.2 E-critical Cell

The E_{Crit} cell measures the current transmitted through a sample. A w/o emulsion will behave differently when subjected to an electric field compared to a o/w emulsion due to the difference in conductivity. An oil phase has normally a low conductivity, whereas an electrolyte solution will have a comparably larger conductivity. This can be exploited by applying an electric field to the w/o emulsion. By increasing the field strength in a stepwise manner, the water droplets will move away from their random position and align along the pathway of the current, as seen in figure 4.6. At a certain field strength a bridge of continuous water has formed and the measured current rises dramatically. The field strength in which the measured current becomes markedly higher is denoted the E_{Crit} value and is a qualitatively measure of the emulsion stability. As mentioned, the technique only works for w/o emulsions since inducing an electric field on a water continuous liquid will short circuit the system immediately.

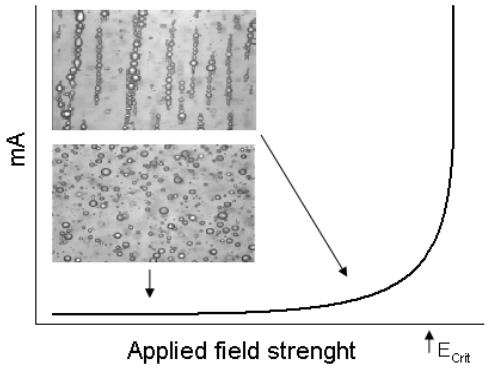

Figure 4.6 Measurements and behavior of emulsion stability in the E-Critical cell. [73]

Another method to utilize the E_{Crit} method is to measure the current with a constant field strength and monitor the time needed to increase the measured current. However, this protocol can be less accurate due to gravity induced sedimentation and/or natural coalescence of the emulsion within the timescale of the measurements. The apparatus is relatively small with a sample container radius of ~5 mm, and the emulsion is placed between two brass plates. The advantage with the technique is that it is fast and simple to perform the measurements. The downside is that the measured stability is only qualitatively; there is no information on the amount of separated water. [74]

4.2.3 Microscope

The conventional optical microscope has been used for many years within the colloid and surface chemistry. The technique is relatively simple, with a specimen being illuminated by a light source and a lens is magnifying the sample. The resolution limit is for most practical purposes around 1 μm. It can be difficult to obtain clear images of smaller droplets due to Brownian motion of droplets/particles makes the images blurred.

The technique is used to measure the droplet size distribution of both o/w [75] and w/o [76] emulsions. It is also used to measure precipitation phenomenon. [77] The microscope is an important technique for analyzing an emulsion. As seen in figure 4.67, the direct visualization of the sample can give information on the behavior of the emulsion which is difficult to obtain with other techniques. The left images shows the droplets of a crude oil emulsion, and the right images shows the droplets of a model oil emulsion stabilized by a single commercial surfactant. As seen in the figure the droplets in the two emulsions behave radically different where the droplets stabilized by the crude oil surfactants appear to be indifferent to each other. On the other hand, the droplets stabilized by the synthetic surfactant show a great tendency to coagulate/aggregate. There are no other methods capable of distinguish between coagulation, flocculation or coalescence as with a direct visualization in a microscope.

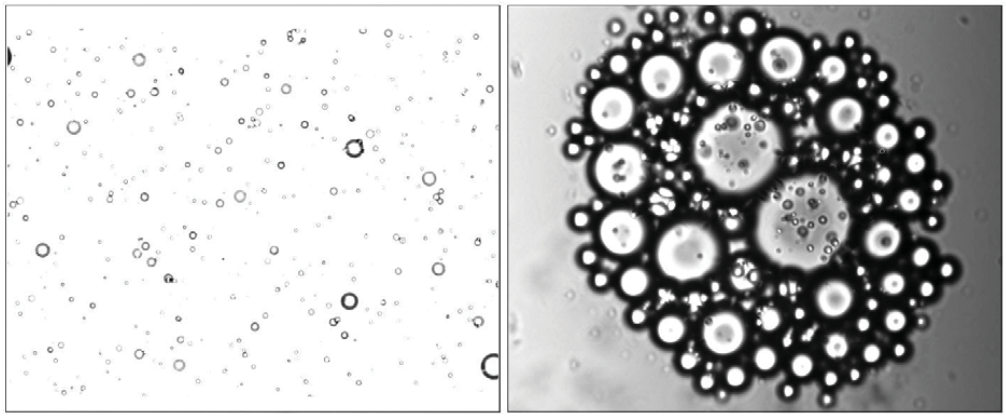

Figure 4.7 Emulsion behavior studied in microscope. Both images are captured with the same magnification.

To obtain the droplet size distribution can be time consuming when one has to manually measure and count each droplet. However, the newest microscopes can be attached to a camera and there are softwares available that can automatically detect and size darker areas on an image.

4.2.4 Optical methods

A more developed method for measuring the coalescence rate is the use of a light source and detectors. There are different setups for this technique, either the amount of backscattered or the transmitted light is recording from a sample. Although both setups can be used, care should be used when using scattered light since this can be value is dependent on the size of the droplets. [78] The principle of the commercial Turbiscan is illustrated in figure 4.8. The light source is moving vertically, whereas the transmitted and scattered light is recorded simultaneously. The information gathered from the light scattering can be difficult to interpret for some systems. But the transmitted light is indicative of the formation of free water. In addition, the degree of clarity of the free water can be qualitatively compared by recording the amount of transmitted light.

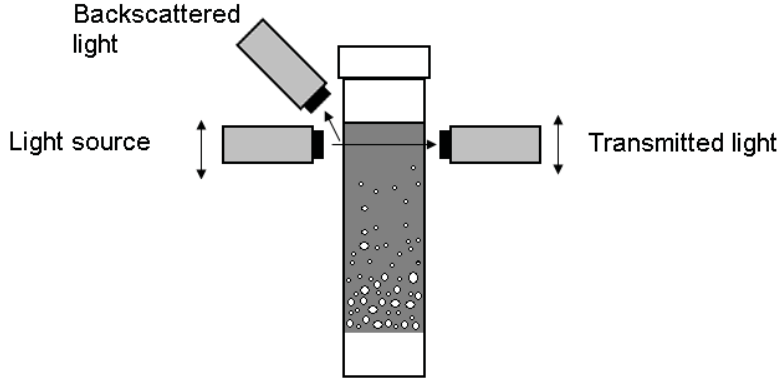

Figure 4.8 Sketch of the basic principles of Turbiscan measurements for emulsion stability.

The main advantages of the use of turbidity measurements is that the automated data recording will not be influenced by possible man-determined errors in the height of free water. The disadvantage is that it requires a liquid phase permitting transmission of light.

4.2.5 Nuclear Magnetic Resonance (NMR)

Since the discovery in 1946 of the behavior of certain nuclei in a magnetic field, NMR has proved its versatility in many different aspects of physics, chemistry, biochemistry and medicine. [79] The development of low field NMR for studying fluids has accelerated the last 15 years. A low field NMR is not bigger than a 1990s desktop computer and can be used to measure diffusion coefficients [80] [81], determine droplet size distributions of o/w [82] and w/o [83] emulsions and study the stability of emulsions. [12] The biggest advantage with the technique is the non-invasive manner in witch the data is obtained and that the entire sample is considered.

The technique makes use of the behavior of nuclei with an odd number of protons, like ^1H. When such nuclei are subjected to a magnetic field they exhibit a magnetic moment. Radio frequency pulses can excite the nuclei into a higher energy level and the relaxation back to equilibrium can be measured. The relaxation is generally determined by the ease at which protons can exchange energy. This again is governed by the molecular mobility within the liquid. A molecule confined within a liquid with high viscosity will exchange energy faster, leading to quicker energy dissipation. The relaxation for ^1H nuclei found in water molecules will thus be slower than ^1H nuclei found in hydrocarbons, making it possible to separate the signal between water and oil phase. The relaxation can be measured in the transverse direction (T_2), or in the longitude direction (T_1).

Figure 4.9 can be used to illustrate the concept. The three lines drawn there shows the T_2 distribution of three different liquids, a heavy oil, medium oil and bulk water. The T_2 distribution is the transverse relaxation time and can be measured with a CPMG measurement. . [84] [85] As the figure shows, more viscous liquids will have a shorter relaxation time. It is therefore possible to separate the signal between the oil and the water. By combining the relaxation measurements with measurements of the diffusion coefficient of the dispersed phase, it is possible to obtain the droplet size distribution.

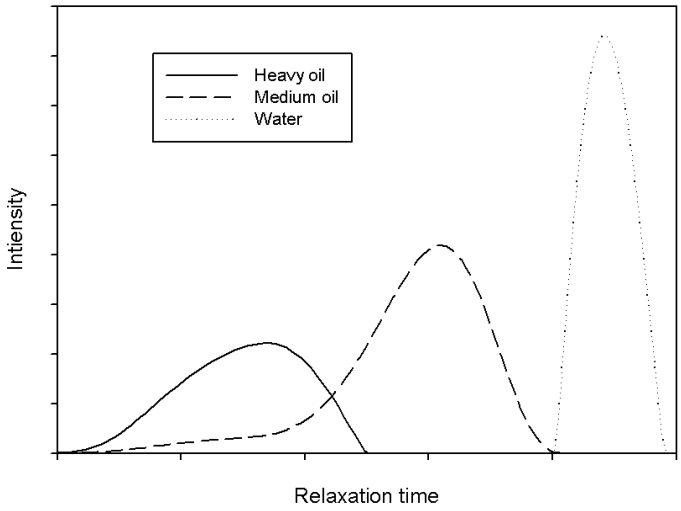

Figure 4.9 T_2 distribution of crude oils and water.

The older models for droplet size determination needed to make assumptions on the distribution shape, and normally that would give negligible difference on the final result. However, for some cases it might not explain the droplet size distribution satisfactory. Some of the newest methods are capable of determining droplet size distributions without making any distribution shape assumptions. Also, some of the sequences require long acquisition time. With regard to the acquisition time, methods have been developed enabling to determine the droplet size distribution within 3-10 seconds. [86]

The measurements of a droplet size distribution from NMR can be understood by equation XI:

$$T_2 \approx \frac{V}{S\rho} \qquad \text{(XI)}$$

Where T_2 is the transverse relaxation time, ρ is the surface relaxivity and S/V is the surface to volume ratio. The average surface to volume ratio can be obtained by measuring the diffusion of water molecules confined within the droplets. This can be done in two ways depending on the droplet sizes. If the droplets are sufficiently large only a small fraction of the water molecules are probing the interface and the restricted diffusion coefficient can be written as:

$$\frac{D(t)}{D_0} = 1 - \frac{4}{9\sqrt{\pi}}\sqrt{D_0 t}\,\frac{S}{V} + \varphi(\rho, R, t) \qquad \text{(XII)}$$

Where D is the time dependent diffusion coefficient, D_0 is the unrestricted diffusion coefficient, S/V is the surface to volume ratio and the term φ includes deviations originating from the surface relaxivity and the surface curvature. At short observation times the last term can be neglected and thus measuring the diffusion coefficient returns an average surface to volume ratio. The surface to volume ratio can then be combined with an average T_2 value of the dispersed phase and a value of the surface relaxivity can be calculated from equation XI.

When the droplet sizes are relatively small the water molecules cover a mean length larger than the cavity dimensions. In this situation the signal of the diffusion measurements in performed in the NMR can be simplified to:

$$\frac{I}{I_0} \approx \exp\left[\frac{1}{5}\gamma^2\delta^2G^2R^2\right] \qquad \text{(XIII)}$$

Where γ is the gyromagnetic ratio, δ is the gradient pulse length, G is the applied gradient strength and R is the droplet radius. By measuring the decrease in the diffusion signal from the NMR as a function of signal strength can then give the average radius of the dispersed water droplets. The radius can be converted into an average surface to volume ratio and by using equation XI the surface relaxivity can be calculated.

By assuming that the surface relaxivity is independent of the droplet size, a CPMG measurement obtains a T_2 distribution of the dispersed phase and by combining with the surface relaxivity calculated from the diffusion measurements a droplet size distribution is obtained.

Emulsion stability can be probed by the NMR as well. A position dependent signal intensity can calculated, and by accumulating these intensity profiles, the emulsions stability can be measured. With this method the movement of the entire water fraction can be monitored and sedimentation rates and the free water recovery rate can be obtained. [12]

The disadvantage with the NMR technique is related to the ability to distinguish oil and water relaxation signal. If the viscosities of the two phases are too close in magnitude it can be troublesome to separate the signal. In addition, the technique for droplet size determination is sensitive to the presence of free water. If free water is present in the sample tube, this water can be perceived as large droplets, and the distribution can be skewed.

Chapter 5 Main Results

In this section a brief summary of the most important results and the conclusions of the work will be presented. The full papers are given in the appendixes.

5.1 Paper I

"Method for Droplet Size Distribution Determination of Water-in-oil Emulsions using Low-Field NMR".

In the first paper the objective was to validate a new method for rapid determination of the droplet size distribution of water-in-oil emulsions. The validation was performed with the microscope as a reference technique. Three crude oils of different classification were studied; one conventional, one heavy and one classified as extra heavy. Emulsions with water cuts ranging from 10 to 40 % were studied. The results showed that there was a good agreement between the two techniques.

Other NMR techniques have suffered of long acquisition methods. The sequence used in this study can obtain a droplet size distribution within approximately one minute with no assumptions on the distribution shape. Figure 5.1 shows the droplet size distribution of a heavy crude oil emulsion with 20 % water cut obtained from the microscope and the NMR. The modes of the distributions obtained from the two techniques appear to be of a similar value. The distribution shape is also relatively similar. Given the timescale of how long it takes to obtain a statistically representative size distribution from the microscope the new NMR method shows its strength as a lab tool for emulsion studies.

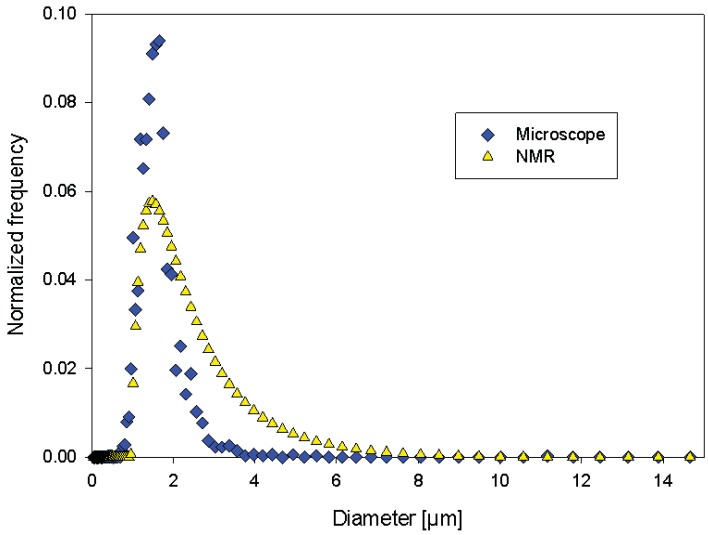

Figure 5.1 Comparison of the emulsion droplet size distributions of a crude oil studied in microscope and NMR; 20 % water cut.

Another limitation of many of the older NMR methods is the assumptions made with regard to the distribution shape. This can in some cases lead to a less accurate description of the emulsions size distribution. Figure 5.2 shows the droplet size distribution of an extra heavy crude oil emulsion of an extra heavy crude oil at two different water cuts. By comparing these size distribution with the one seen in figure 5.1 one can observe the different shape of the distributions. The distributions shown have been obtained by the NMR, and the bimodal distribution of the emulsion containing 10% of water can be recognized. The shape of the distribution of the 40 % water cut emulsion can also be seen to deviate from the standard log-normal shape by the tail of smaller droplets.

The limitation for the NMR technique is that it requires a stable emulsion. The presence of free (bulk) water will be perceived as large droplets, and will skew the mean size and shape of the size distribution. Another limitation for the technique is the oil phase viscosity. The oil phase had to have a viscosity of at least ~20 mPas. The technique exploits the difference in relaxation of the two phases, and the relaxation rate is governed by the molecular mobility. A low viscosity liquid, like water, will have a relative large molecular mobility resulting in slow dissipation of the energy of the protons. In a high viscosity liquid, the molecules cannot move as easily. This leads to an increase in exchange of energy between the protons and a shorter relaxation time.

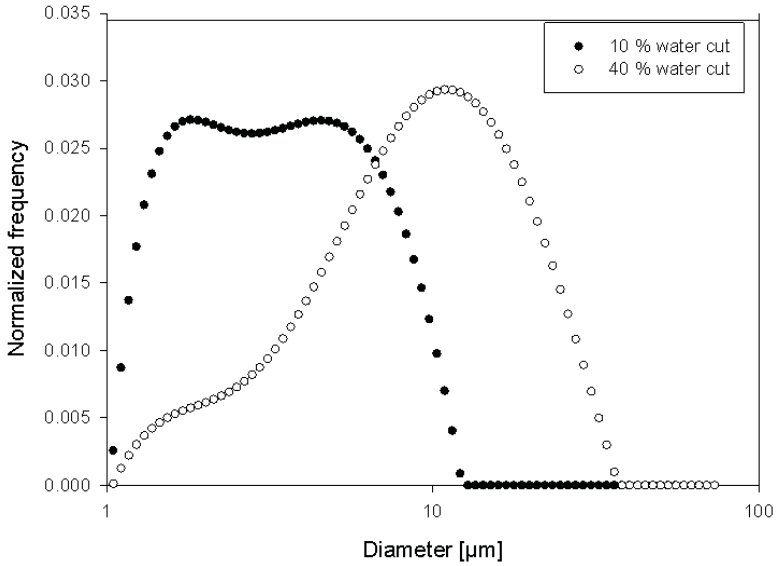

Figure 5.2 Emulsion of a crude oil with a bimodal droplet size distribution

Paper I shows the validation of a new NMR method for rapid determination of w/o emulsion droplet size distributions. The comparison with the reference technique was good and compared to many other techniques, the advantage of the NMR is the possibility of non-perturbing sample analysis. In addition, the technique considers the entire sample, and concentrated and opaque samples can be analyzed.

5.2 Paper II

"Emulsion Stability Studied by Nuclear Magnetic Resonance (NMR)"

In the second paper the field of application of the NMR was extended. In addition to studying the droplet sizes, the use of NMR to directly study the separation of emulsions was examined. The study of separation of dark sample, such as crude oil emulsions, is not performed easily. The goal of paper II was to examine the NMR method for studying the movement of the entire water fraction in an emulsion, even at high local water cuts. The method was validated by forming emulsions and studying the separation in parallel with light transmission measurements in a commercial apparatus.

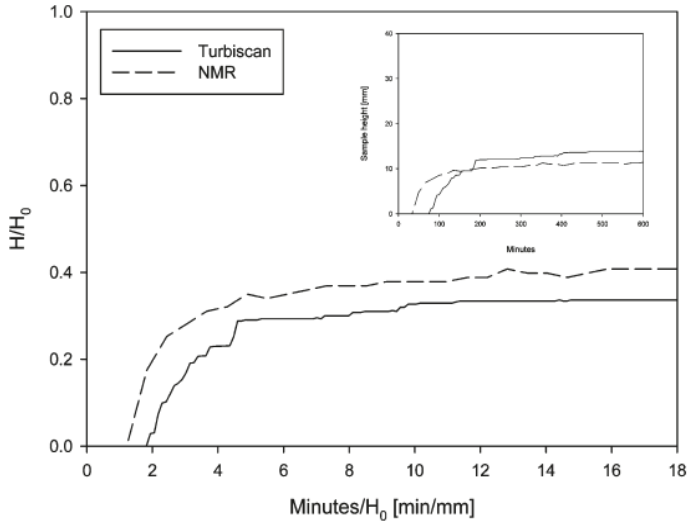

Figure 5.3 Comparison of free water formation between NMR and Turbiscan. The inset graph shows the raw data.

The comparison between the two techniques indicated a qualitatively similar behavior but quantitatively there were differences. As seen in figure 5.3, neither did the time of appearance of free water match entirely, nor the amount of separated water at the end of the separation. The reason for the quantitatively differences can be attributed to the difference in sample tubes. The NMR requires a height of about 20 mm which corresponds to 3.75 mL of sample. The Turbiscan on the other hand has a sample tube height of 40 mm. Another possible explanation for the observed difference is the measurement technique itself. The interface between water and the oil can be curved, and there can be a layer of droplets right at the interface. A dense packed layer of droplets can be interpreted as water by the NMR whereas the light transmission measurement can interpret the same area as oil.

By measuring the free water formation alone a lot of information on the emulsion behavior is still not elucidated. For instance, the shape of the sedimentation curves can be interesting information for a study on demulsification. Moreover, the amount of water in the emulsion phase can also be quantified. The importance of the fact that the entire sample is considered is illustrated in figure 5.4. In this figure five iso-volumetric curves of a crude oil emulsion containing 50 v% of water are shown. The iso-volumetric curves of 0, 25 and 40 % of water

can be considered to represent the sedimentation velocity of different fractions of the water droplets. As seen in the figure to describe the separation or the stability of an emulsion with a single sedimentation rate can be misleading. Instead, an emulsion is more likely to display a distribution of sedimentation rates just like it has a distribution of droplet sizes. One can also observe that some of the sedimentation curves are non-linear. The 90 % iso-volumetric curve can be considered as the height of free water and the area between the 60 % and 90 % curve can be considered to show the accumulation of a more densely packed layer of droplets. The formation of such layer can give more information on the coalescence rate of the droplets.

The combination of experimental data on sedimentation rates and interfacial coalescence rates can also be combined with the method shown in paper I. A more detail mapping of the macroscopic appearance of the emulsion can be combined with theoretical models. Theoretical models on emulsion stability, regardless of its complexity, are bound to contain assumptions on certain phenomenon or constants. With the ability to have real life data one can compare the results of the modeling to examine how close these assumptions are to reality.

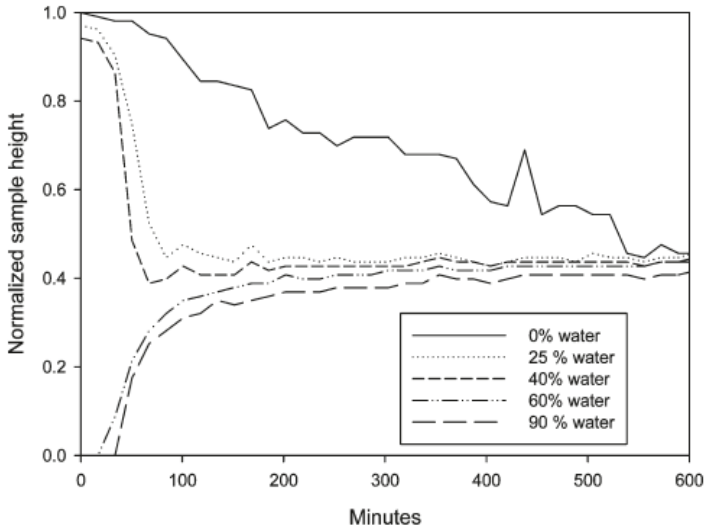

Figure 5.4 Separation of a crude oil emulsion studies with the NMR.

In summary, paper II shows the comparison between a new NMR method for directly studying emulsion stability by obtaining sedimentation rates and water recovery rates of opaque and concentrated emulsions. The comparison was done with the commercial Turbiscan apparatus and gave qualitatively good results. In addition the paper shows how emulsion stability can be studied with the acquisition of iso-volumetric curves of the emulsion separation. By combining the droplet size distribution method showed in paper I the NMR has proven its versatility and importance when studying emulsions.

5.3 Paper III

"Enhanced Sedimentation and Coalescence by Chemicals on Real Crude Oil Systems"

The fourth paper focused on chemical destabilization of heavy crude oil emulsions. The objective of the study was to include macroscale behavior of the demulsifiers in the Ecrit cell and in the NMR with the microscale response of the demulsifiers by dilational rheology in the Sinterface. Nine different demulsifiers were obtained from three different vendors, and they were screened in the Ecrit cell. A collection of the most promising demulsifiers were then studied in NMR to compare the sedimentation and free water recovery rates and in the Sinterface to study the interfacial response of the demulsifiers.

The screening performed in the Ecrit cell showed that the demulsifiers varied in their efficiency. Figure 5.5 show that the most efficient chemicals decreased the emulsion stability substantially even at a very low concentration. A dosage of 30 ppm was sufficient to reduce the stability and further increase in the concentration does not affect the stability in any particular way. Another finding from the Ecrit method is that dosages higher than 150 ppm do not affect the demulsifier effectiveness.

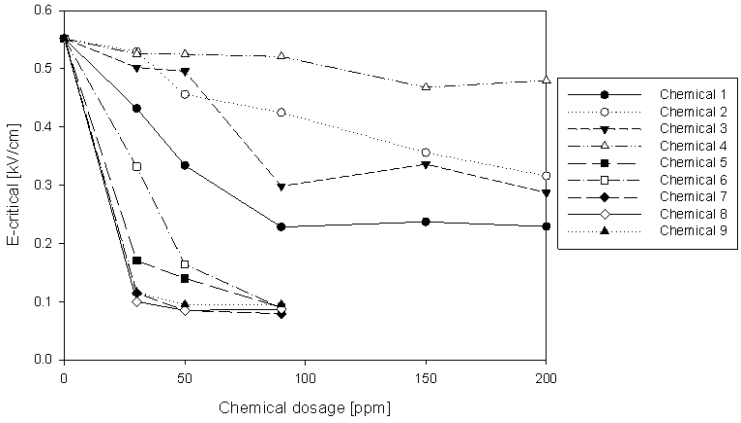

Figure 5.5 Demulsifier screening in Ecrit cell.

A selection of the demulsifiers was also investigated for their effectiveness in the NMR. The Ecrit method does not give any quantification on the emulsion stability; no indications on the extent on the separation are given. As shown in paper I and II the NMR can offer more information on the timescale of the separation and amount and quality on the separated phases. Figure 5.8 shows how the different dosages for two of the most effective demulsifiers affect the sedimentation and free water recovery. The figures are made by plotting the iso-volumetric curves of 20 % and 90 % water. The 20% curve can be considered as a representation on the sedimentation rate and the 90 % curve as the location of bulk water – emulsion interface.

The demulsifiers shown in figure 5.6 were two of the most effective in the Ecrit cell, as one can see in figure 5.5. It was shown that both these demulsifiers were increasing the sedimentation velocity in a monotone manner. The difference in the sedimentation velocity

was not very large, but the NMR showed that the amount of water left in the oil phase was slightly lower for demulsifier 5. Another difference between the two chemicals can be seen in the water recovery rates. While demulsifier 7 shows a monotone dependency on the increasing free water formation with increasing demulsifier concentration, a concentration higher than 30 ppm of demulsifier 5 did not affect the initial slope of water recovery.

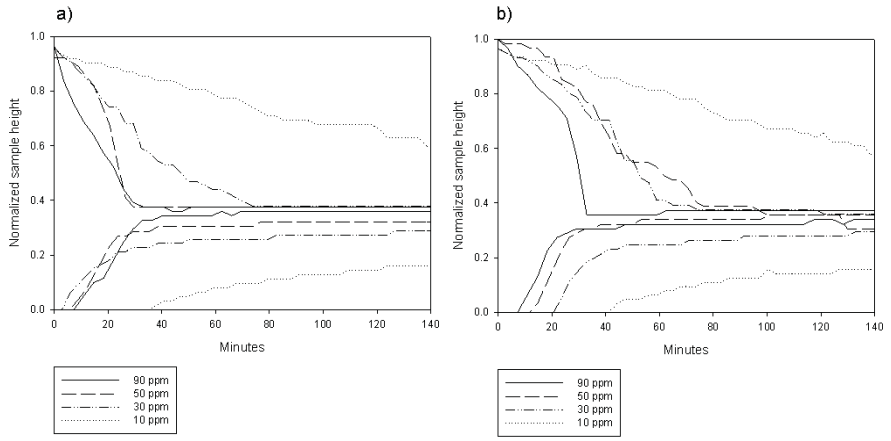

Figure 5.6 Sedimentation and free water recovery rates for emulsions with a) demulsifier 5. b) demulsifier 7.

The role of the demulsifiers was also studied with interfacial rheology. Three of the chemicals were studied in the oscillating drop method to observe how the concentration of the chemicals is affecting the interfacial response. The demulsifiers were the two most efficient, 5 and 7 and a medium effective demulsifier, chemical 4 was used. The results showed that the demulsifiers were interfacial active and that the chemicals with the fastest adsorption kinetics were the most efficient in terms of breaking the emulsions.

The same concentration range was used in both the stability and interfacial measurements. The interfacial response indicated that the demulsifiers reduced the interfacial elasticity and viscosity and increased the interfacial elasticity at higher demulsifier concentration. This trend does not seem reasonable when comparing with the separation data. However, it is not solely the concentration that matters, but the ratio between the total interfacial area and the demulsifier concentration. In the separation study the total interfacial area is much larger than in the interfacial study and a direct comparison between the concentrations might not correctly reflect the behavior.

The demulsification in the Ecrit cell was performed to screen various commercial chemicals. To obtain further information some of the chemicals were studied in NMR to see how they affected the quality of the separated phases and the timescale of separation. Additionally the interfacial response was studied and it was found that the most efficient demulsifiers decrease the interfacial viscosity and elasticity.

5.4 Paper IV

"Population Balance Model for Batch Gravity Separation of Crude Oil and Water Emulsions. Part II: Comparison to Experimental Crude Oil Separation Data"

A new theoretical model for batch gravity separation had been developed and the goal of the study was to examine how capable the model was at mimicking the separation timescale and characteristics of a real system. The model uses experimentally measured parameters, such as the initial droplet size distribution, equilibrium interfacial tension, density difference and viscosity as input and returns the amount of water as a function of time and position. Some of the separation data shown in paper IV for crude oil emulsions destabilized by various commercial demulsifiers were in paper III compared to the data obtained by the theoretical model.

There are many different theoretical models developed to account for the separation of sedimenting/creaming dispersion. However, due to the complex nature of such processes, the models are forced to make assumption on some of the phenomenon. These assumptions can make an impact on how accurate the model is and any theoretical model is ultimately judged on how capable it is at reproducing the characteristics of a real system.

Figure 5.7 shows the iso-volumetric contour plots of a real world crude oil emulsion studied in the NMR and the simulated emulsion from the model. The comparison of the two methods was good, but there were variations between the different iso-volumetric curves. The model prediction for the 1 % and 100 % curves was very good, whereas for the 10% curve the agreement was not so good. The initial prediction of the dense packed layer was also good, but after a certain elapsed time differences between the model and the experimental results appeared.

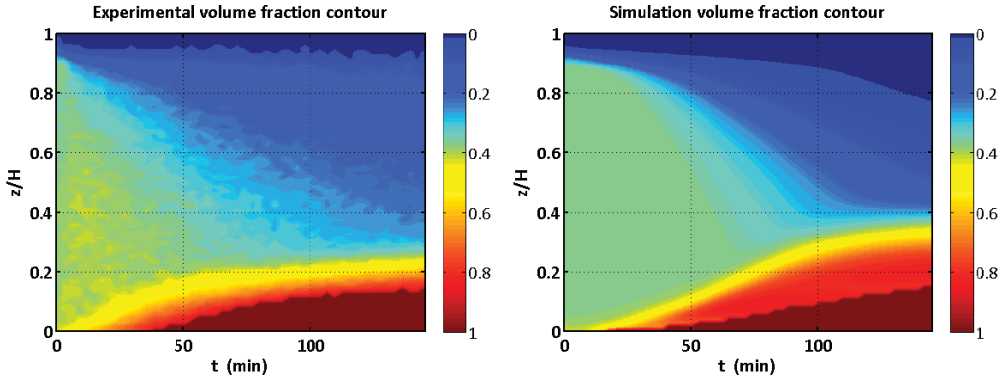

Figure 5.7 Iso-volumetric separation plots of a crude oil emulsion. Left: experimental data obtained from the NMR. Right: theoretical data from the model.

The model also predicts the development of the droplet sizes as a function of time and position. Figure 5.8 shows the results of the simulation for the same system as shown in figure 5.7. From the droplet growth rate simulation in the top right corner one can see that the droplets are growing at the fastest rate when the standard deviation of the droplet radius is at its largest (bottom left corner). This indicates that more droplets are colliding and

experiencing binary coalescence when the droplet size distribution is at its most polydisperse. The degree of binary coalescence can also be seen in the separation plots in figure todo where an increased sedimentation rate is observed at the same time as the droplets are growing at its fastest.

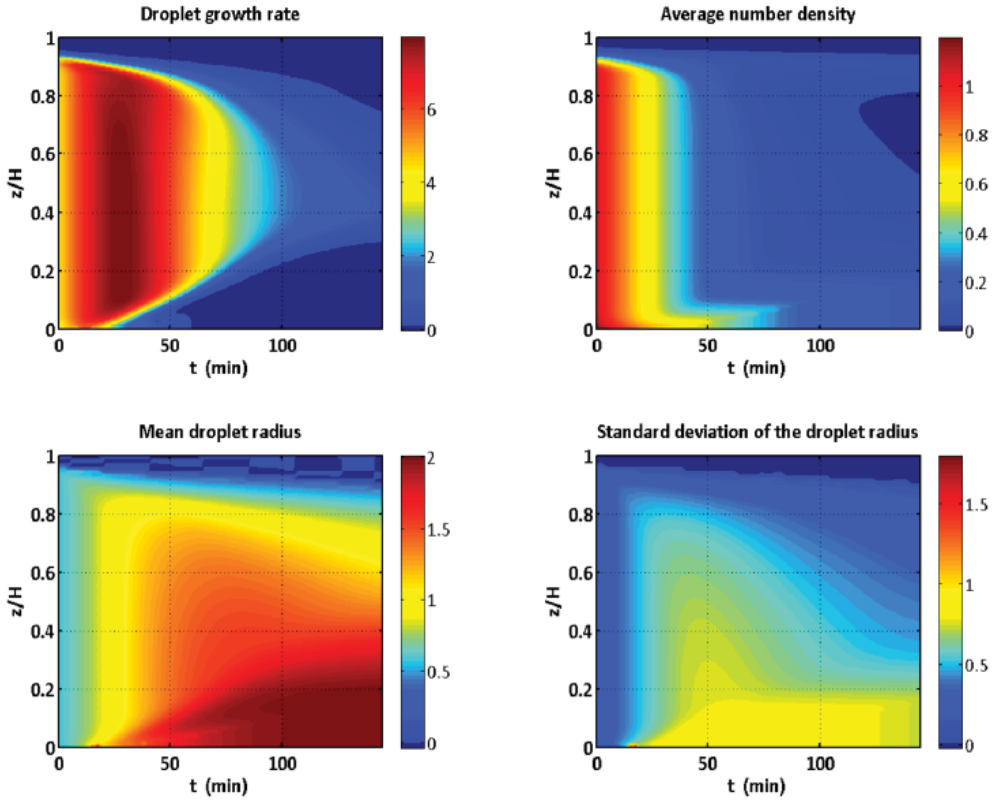

Figure 5.8 Droplet growth rate, average number density, mean droplet radius and standard deviation of the droplet radius for the separation of crude oil treated with 10 ppm of chemical 7.

Paper IV compared the predictions of a mathematical model with the experimentally obtained separation of a heavy crude oil emulsion. The methods were directly compared by the acquisition of data from both techniques on the amount of water as a function of time and position. Given the assumption made on the coalescence efficiency and the sedimentation rate constant, there was a good agreement between the two methods. The largest discrepancy occurred due to the model for hindered sedimentation which was not properly aligned with the poly dispersity of the system

5.5 Paper V

"Emulsion stability of a SAGD produced extra heavy crude oil**"**

Paper I and II introduced new NMR methods relevant for studying the w/o emulsion stability of crude oil emulsions. In paper V these methods were implemented to study the emulsions of a diluted extra heavy crude oil. The objective of the work was to prepare emulsions at different mixing intensities and oil phase viscosities and to study how this affected the initial droplet size distribution and emulsion stability. The second part of paper V was to study the oil-in-water emulsion stability of the same extra heavy crude oils at bench scale and small scale. The objective of the second part was to examine how the ion concentration and dilution affected the oil droplet stability.

By preparing emulsions with different mixing velocity different initial droplet size distributions can be formed. This is illustrated in figure 5.9 where the size distributions of four emulsions of the same liquids are prepared with a mixing velocity ranging from 750 rpm to 2000 rpm. The mode, width and shape of the droplet size distribution can have an effect on the behavior of the emulsion; the rheological properties can be changed, and perhaps more interesting for the petroleum industry, the timescale of the separation can vary greatly depending on the droplet size.

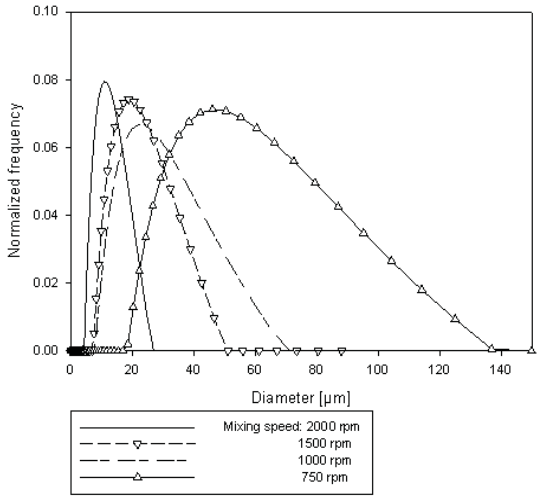

Figure 5.9 Initial droplet size distributions for a diluted crude oil emulsion prepared at different mixing intensity.

The versatility of the NMR technique was further extended in the third paper where measurements of position dependent droplet sizes were included on the separation study. By using the method to obtain the droplet size distribution presented in the first article and the brine profiles presented in the second paper, a lot of information can be gathered on the separation of emulsions. Knowledge on the initial droplet size distribution enables one to make an approximation on the stability of an emulsion. The stability can be confirmed by studying the sedimentation and free water recovery rates from the brine profiles. By being able to observe whether the droplets grow at the bulk water-emulsion interface or in the

emulsion region, as one can with the size profiles, can be even more helpful to understand the stability.

Figure 5.10 a) shows the iso-volumetric separation curve of an emulsion prepared in the study. All of the emulsions studied in the third papers exhibited non-linear sedimentation rates. Within the first ~100 minutes of the emulsion lifetime the sedimentation velocity appears to be very slow. Then after ~150 minutes an increased velocity can be observed from some of the iso-volumetric curves. The non-linear behavior can be attributed to binary coalescence or droplet aggregation. The size profile of the same emulsion system can be seen in figure 5.6 b), and the slow increase in the droplet sizes in the entire emulsion region can be observed.

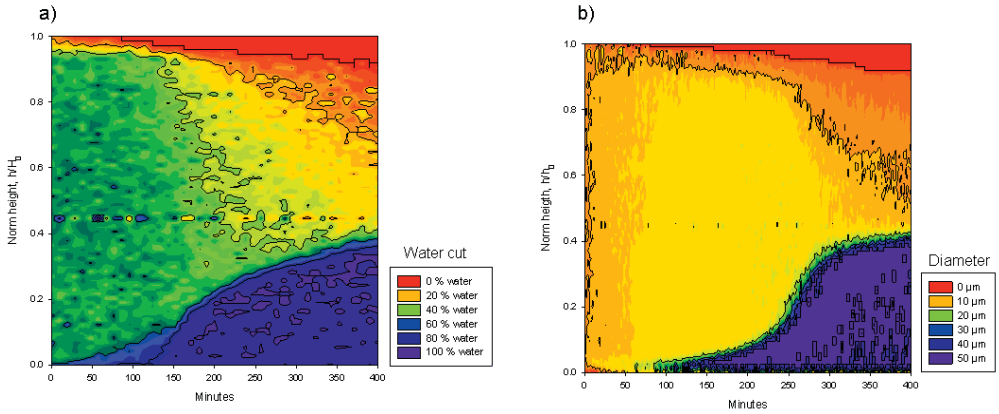

Figure 5.10 Separation plots from the NMR of an emulsion with 50 v% water cut and at a mixing intensity of 2000 rpm. a) iso-volumetric brine profile contour plots. b) iso-metric size profile contour plots.

It was observed that with a wider initial size distribution a shorter time passed before the sedimentation rate increased. And for an emulsion, with otherwise similar liquid properties, a narrow initial size distribution led to a longer period of time until the sedimentation rate increased. The non-linearity of the sedimentation was confirmed by the size profile measurements. Prior to the increased sedimentation rate an increase of the droplet size the emulsion region was observed, as illustrated in figure 5.10 b). A possible explanation for the difference in time before the sedimentation rate changed was due to the number of droplet collisions. Larger droplets will move downward with a larger velocity and with a wider droplet size distribution the emulsion will experience a higher number of collisions as the largest droplets move downwards. Since the liquid systems are the same one can assume that the coalescence time should be dependent on the droplet sizes alone. Thus, the higher number of collisions can lead to larger frequency of binary coalescence.

The second part of the article where the oil droplet stability was studied at different ion concentration and degree of dilution showed that a low ion concentration was sufficient to impact the water quality. Figure 5.11 shows the emulsion stability and zeta potential at different Ca^{2+} concentration. The presence of ions decreased the magnitude of the zeta potential which lead to a lower repulsive force between the dispersed droplets and the droplets required a lower momentum to come in physical contact and coalesce. Microscopic images also showed that the oil droplets contained water droplets. The occurrence of complex w/o/w

emulsions could have an impact on the separation on an industrial level. By performing the measurements in a larger scale the addition of salt had a less profound impact on the emulsion stability.

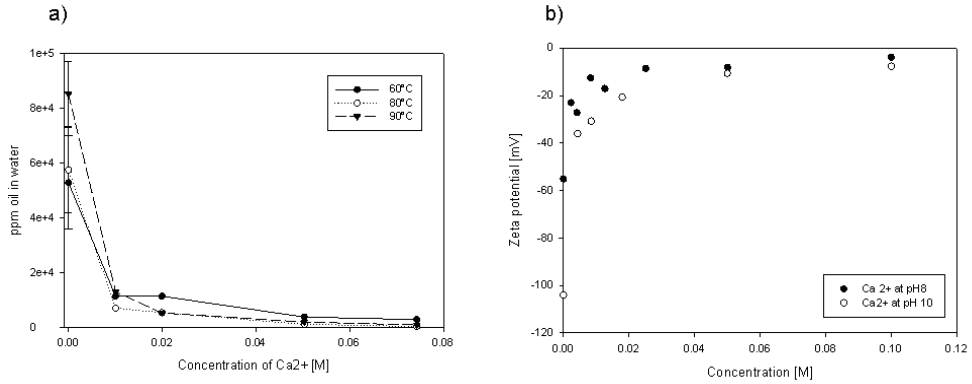

Figure 5.11 Emulsion stability, a), and zeta potential, b), for oil-in-water emulsions at different Ca^{2+} concentration.

The conclusions of the first part of paper V were that to study emulsion stability the NMR proves to be a versatile tool. The three different measurement methods used in the paper can become valuable for experimental studies alone, and such experimental results can be used in combination with modeling. It was shown that the separation of an emulsion can be greatly affected by the mixing protocol and that it is not sufficient to characterize the average size of the emulsion droplet sizes. In order to explain the separation timescale a complete droplet size distribution needs to be measured. The conclusion from the second part was that the water phase properties (ionic strength) can be a decisive parameter when considering oil droplet stability. The study also showed that care should be taken when extrapolating results from bench scale measurements.

5.6 Paper VI

"Understanding the Molecular Interactions of an Asphaltene Model Compound C5Pe in Organic Solvents Using a SFA"

In paper VI the interactions between asphaltene covered surfaces were studied. The study included both asphaltenes extracted from a crude oil and a model asphaltene compound. Asphaltene studies in general have suffered from the lack of fundamental characterization of the molecular structure. In that sense the use of a model asphaltene compound with a known structure is beneficial since the behavior of a population of molecules can be understood by the molecular structure.

Adsorption measurements were performed with a solution of toluene solubilized asphaltenes injected between two mica surfaces. By moving the surfaces together and apart the interaction forces and distances can be studied, as illustrated in figure 5.12 and 5.13. The adsorption measurements indicated that the model compounds and the extracted asphaltenes behave similar in terms of adsorption kinetics. A layer of surfactants are observed immediately and the thickness of the layer is increasing slowly. Another similarity is the evolution of the surface forces. Both setups indicated an initial adhesion force which after a time range of 20 hours. The difference between the model asphaltene and the extracted asphaltene became apparent after 2 hours, with the extracted asphaltenes exhibiting a thicker layer of surfactants.

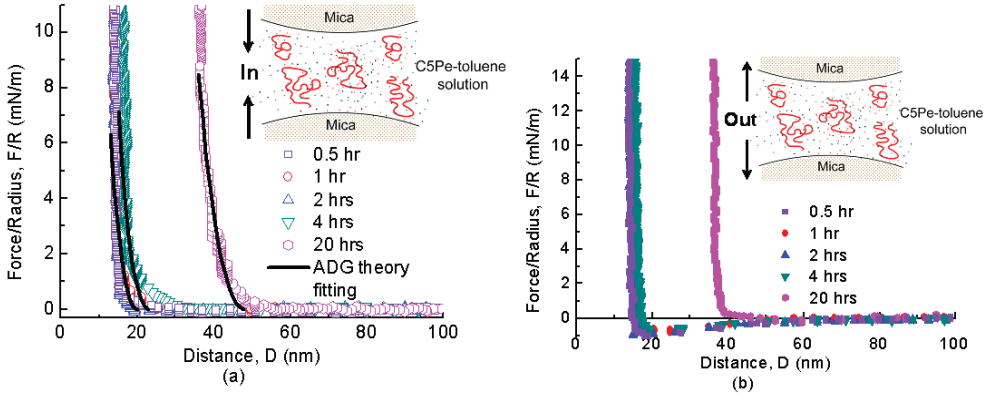

Figure 5.12 Force profiles of two mica surfaces in 0.2 mM (~ 0.02 wt%) C5Pe-toluene solution at different time intervals: (a) approaching plots and fitting curves by Alexander-de Gennes (ADG) theory; (b) retracting plots following the approaching in (a) .

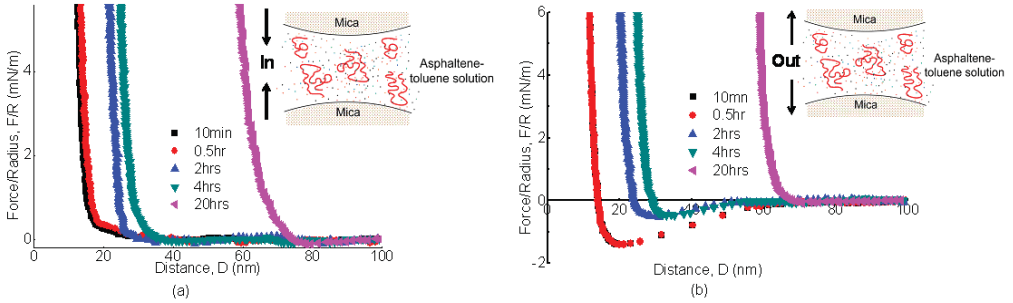

Figure 5.13 Force profiles of two mica surfaces in 0.01w% asphaltene-toluene solution at different time intervals. a) approaching plots. b) retracting plots following the approaching in a).

Mica surface with asphaltene model compounds was also prepared by dip coating. The forces between these dip coated surfaces were then examined with either toluene of heptane as a solvent between the surfaces. Figure 5.14 shows the different behavior of the surfaces depending on the solvent. As seen the interaction forces in toluene are weak, both in the symmetric and asymmetric configuration. The surfaces in heptane showed a strong adhesive force, figure 5.12 b), which is consistent with previous results on asphaltene surfaces and on the polar properties of the surfactant molecule and the apolar solvent.

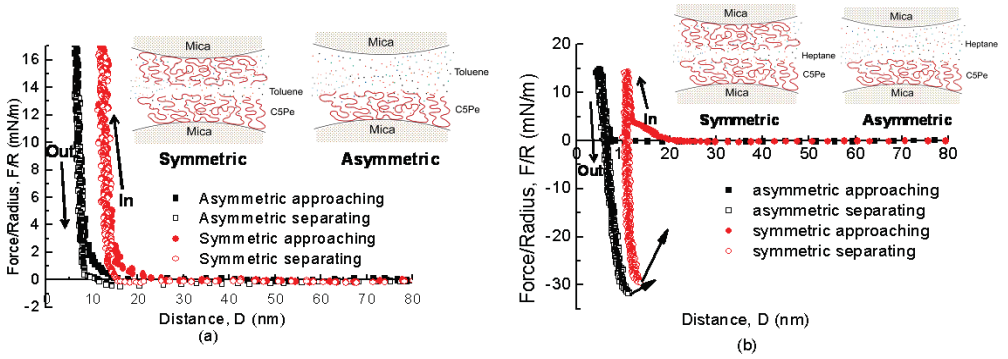

Figure 5.14 Force profiles between two C5Pe surfaces (symmetric) as well as a C5Pe surface and bare mica surface (asymmetric): a) in toluene; b) in heptane.

The study of interactions between asphaltene coated surface indicated that the solvent properties are important for attraction of asphaltene interfaces. The similarities between the model compounds and the extracted asphaltenes open up for studying mixtures of different model asphaltene molecules. Even though the single model compounds behaves similarly as extracted asphaltenes the homogeneity of using a single molecule structure might not be sufficient to understand a heterogeneous system found in the real world.

5.7 General conclusions and future work

The increasing interest in exploiting heavier crude oils necessitates the expansion of studies on crude oil emulsions behavior and characteristics. The industrial separation of heavier crude oil feedstocks can be more difficult, and to design an optimized process requires a detailed study. To be able to study emulsions in higher detail one should be able to gain more information on emulsion behavior on a macro scale. There are not many techniques available that can give information on the separation characteristics of a dark emulsion.

Low field Nuclear Magnetic Resonance (NMR) is a technique capable separating the signal from the oil and water phase, and can be used to study the droplet sizes and the vertical movement of water droplets. New NMR methods for characterizing water in oil emulsions were studied and validated against their respective reference techniques in **paper I** and **paper II**. The validation of the method to determine the droplet size distribution in **paper I** gave a good comparison with the microscope and it was also showed that the method is capable of measuring the size distribution without any assumption on the distribution shape. The validation of the method to directly study the stability in **paper II** did also give a good comparison, although there were quantitatively differences between the techniques.

After validation the NMR methods for emulsion characterization were implemented to study crude oil water emulsions. In **paper III** the demulsification of emulsions of a heavy crude oil on a macro scale and micro scale was studied. The demulsifiers were screened with the Ecrit method and further information on the separation was obtained by studying a selection of the demulsifier in the NMR. The interfacial response of the demulsifiers was also investigated with the oscillating drop method. The Ecrit method indicated that the most efficient demulsifiers required a small dosage to influence the separation. A concentration of 30 ppm was sufficient to radically reduce the emulsion stability. Closer examination on the demulsification in the NMR showed to which extent the timescale of the separation and the quality of the oil was affected. This enables a more thorough screening of the demulsifiers. The ability to directly monitor how the quality of the separation changes with the demulsifier dosage and type is important for the more hands on challenges in the industry and for a fundamental study of emulsion stability. The interfacial study showed that the most effective demulsifiers were the most interfacial active with a rapid adsorption to the interface. It was also shown that the demulsifiers reduced the interfacial elasticity and viscosity.

The experimental results on the demulsification on a heavy crude oil obtained in **paper III** were in **paper IV** compared with data from a new mathematical model. The model use the initial droplet size distribution, liquid phase properties and the interfacial properties as input and return the amount of water in a gravity settler as a function of time and position. The comparison with the results from the NMR were good; the evolution of most of the iso-volumetric curves was comparable

The emulsion stability of an extra heavy crude oil was studied in **paper V**, both w/o and o/w emulsions. The main conclusion from this paper was that in order to fully understand the behavior of an w/o emulsion, and especially its stability, the entire droplet size distribution should be determined. The paper also shows how the different NMR methods can be used to gain more information on the complete emulsion separation characteristics, including sedimentation rates, water recovery rates and the droplet growth as a function of time and axial position. The study on the o/w emulsions showed that at a low concentration of ions the

ions contributed to the decreased emulsion stability by screening the droplet charge. It was also shown that the crude oil formed complex w/o/w emulsions which could have an impact on the design of the separation process.

The study of asphaltene model compounds in **paper VI** showed that the model compounds had similar features and behavior as extracted asphaltenes. Moreover, the behavior of asphaltene interfaces was heavily dependent on the nature of the solvent. The study of model asphaltene molecules surface interactions provides insight into the behavior of asphaltenes in general.

The validation and the implementation of the various NMR methods for emulsion characterization show the potential for this technique. The methods open up for many studies on how the various relevant parameters for emulsion stability can be examined. First, a more detailed study on the emulsification and the mixing protocol could give more information on the energy input and the resulting droplet size distribution for crude oil emulsion. Accurate measurements of the droplet sizes of the stream coming into the primary separator can be difficult to perform. By knowing the fluid characteristics, volume fraction of each phases and the energy input an approximation on the droplet size distribution and their stability can be performed. **Paper III** showed how a more detailed screening of demulsifiers can be performed. Similar studies can be performed on how the various stabilizing mechanisms of crude oil emulsions affect the rates of sedimentation, binary coalescence and water recovery rates. The experimental results obtained from these studies can be used in connection with the work on modeling emulsion stability. To develop a model accounting for the complex composition and behavior of crude oils and the many different interfacial phenomenons accruing during the separation of an emulsion it is important to be able to check whether the model can predict the behavior of a real world system. Especially the phenomenon occurring in the emulsion region, for instance the thickness of any concentration droplet layers, droplet growth rates and so on.

References

1. Speight, J. G., *The Chemistry and Technology of Petroleum*. Taylor and Francis: Boca Raton, 2007.
2. Moulijn, J. A.; Makkee, M.; Diepen, A. v., *Chemichal Process Technology*. Wiley: Chichester, 2001.
3. Berkowitz, N.; Speight, J. G., *Fuel* **1975,** 54, 138-149.
4. Kharrat, A. M.; Zacharia, J.; Cherian, V. J.; Anyatonwu, A., *Energy & Fuels* **2007,** 21, 3618-3621.
5. Kilpatrick, P. K.; Spiecker, P. M., In *Encyclopedic Handbook of Emulsion Technology*, Sjöblom, J., Ed. Marcel Dekker: New York, 2001.
6. Nordgård, E. L.; Sjöblom, J., *Journal of Dispersion Science and Technology* **2008,** 29, 1114-1122.
7. Nordgård, E. L.; Landsem, E.; Sjöblom, J., *Langmuir* **2008,** 24, 8742-8751.
8. Nordgård, E. L.; Sørland, G.; Sjöblom, J., *Langmuir* **2010,** 26, 2352-2360.
9. Akmaz, S.; Iscan, O.; Gurkaynak, M. A.; Yasar, M., *Petroleum Science and Technology* **2011,** 29, 160-171.
10. Hurtevent, C.; Roussseau, G.; Bourrel, M.; Brocart, B., In *Emulsions and Emulsion Stability*, Sjöblom, J., Ed. Taylor & Francis: Boca Raton, 2006.
11. Drummond, C.; Israelachvili, J., *Journal of Petroleum Science and Engineering* **2004,** 45, 61-81.
12. Jiang, T.; Hirasaki, G.; Miller, C.; Moran, K.; Fleury, M., *Energy & Fuels* **2007,** 21, 1325-1336.
13. Jiang, T.; Hirasaki, G.; Miller, C.; Moran, K., *Energy & Fuels* **2008,** 22, 4158-4164.
14. Dang-Vu, T.; Jha, R.; Wu, S. Y.; Tannat, D. D.; Masliyah, J. M.; Xu, Z., *Energy & Fuels* **2009,** 23, 2628-2636.
15. Dang-Vu, T.; Jha, R.; Tannat, D. D.; Masliyah, J. M.; Xu, Z., *Colloids and Surfaces A: Physiochem. Eng. Aspects* **2009,** 337, 80-90.
16. Dai, Q.; Chung, K. H., *Fuel* **1996,** 75, 220-226.
17. Gu, G.; Zhang, L.; Xu, Z.; Masliyah, J. M., *Energy & Fuels* **2007,** 21, 3462-3468.
18. Saadatmand, M.; Yarranton, H. W.; Moran, K., *Industrial & Engineering Chemistry Research* **2008,** 47, 8828-8839.
19. Al-Bahlani, A.-M.; Babadagli, T., *Journal of Petroleum Science and Engineering* **2009,** 68, 135-150.
20. Arntzen, R.; Andresen, P. A. K., In *Encyclopedic Handbook of Emulsion Technology*, Sjöblom, J., Ed. Marcel Dekker: New York, 2001.
21. *Miljørapport*; The Norwegian Oil Industry Association: 2009.
22. Lundgaard, L. E.; Berg, G.; Ingebrigtsen, S.; Atten, P., In *Emulsions and Emulsion Stability*, Sjöblom, J., Ed. Taylor & Francis: Boca Raton, 2006.
23. Rubio, J.; Souza, M. L.; Smith, R. W., *Minerals Engineering* **2001,** 15, 139-155.
24. Horozov, T., *Current Opinion in Colloid & Interface Science* **2008,** 13, 134-140.
25. *Utslippsrapport 2009 for Ekofisk feltet*; ConocoPhillips: 2010.
26. EIA http://www.eia.doe.gov/aer/txt/ptb1105.html (17.02),
27. Garti, N.; Benichou, A., In *Encyclopedic Handbook of Emulsion Technology*, Sjöblom, J., Ed. Marcel Dekker: New York, 2001.
28. McClements, D. J., *Food emulsions: principles, practice, and techniques*. Taylor & Francis: Boca Raton, 2005.
29. Nielloud, F.; Marti-Meatres, G., *Pharmaceutical Emulsions and Suspensions*. Marcel Dekker: New York, 2000.

30. Washington, C., *Advanced Drug Delivery Reviews* **1996,** 20, 131-145.
31. Salager, J.; Briceño, M. I.; Bracho, C. L., In *Encyclopedic Handbook of Emulsion Technology*, Sjöblom, J., Ed. Marcel Dekker: New York, 2001.
32. Al-Roomi, Y.; George, R.; Elgibaly, A.; Elkamel, A., *Journal of Petroleum Science and Engineering* **2004,** 42, 235-243.
33. Walstra, P., *Chemical Engineering Science* **1993,** 48, 333-349.
34. Li, M.; Guo, J.; Peng, B.; Lin, M.; Dong, Z.; Wu, Z., In *Emulsions and Emulsion Stability*, Sjöblom, J., Ed. Taylor & Francis: Boca Raton, 2006.
35. Poteau, S.; Argillier, J.-F.; Langevin, D.; Pincet, F.; Perez, E., *Energy & Fuels* **2005,** 19, 1337-1341.
36. Jeribi, M.; Almir-Assad, B.; Langevin, D.; Hénaut, I.; Argillier, J.-F., *Journal of Colloid and interface Science* **2002,** 256, 268-272.
37. Arla, D.; Sinquin, A.; Palermo, T.; Hurtevent, C.; Graciaa, A.; Dicharry, C., *Energy & Fuels* **2007,** 21, 1337-1342.
38. Li, C.; Liu, Q.; Mei, Z.; Wang, J.; Xu, J.; Sun, D., *Journal of Colloid and interface Science* **2009,** 336, 314-321.
39. Hodge, S. M.; Rosseau, D., *Food Research International* **2003,** 36, 695-702.
40. Yan, Y.; Masliayh, J., *Colloids and Surfaces A: Physiochem. Eng. Aspects* **1993,** 75, 123-132.
41. Yan, N.; Masliyah, J. M., *Colloids and Surfaces A: Physiochem. Eng. Aspects* **1995,** 96, 243-252.
42. Kotlyar, L. S.; Sparks, B. D.; Woods, J. R.; Chung, K. H., *Energy & Fuels* **1999,** 13, 346-350.
43. Gu, G.; Zhou, Z.; Xu, Z.; Masliyah, J. M., *Colloids and Surfaces A: Physiochem. Eng. Aspects* **2003,** 215, 141-153.
44. Vignati, E.; Piazza, R., *Langmuir* **2003,** 19, 6650-6656.
45. Binks, B. P.; Lumsdon, S. O., *Langmuir* **2000,** 16, (8622-8631).
46. Binks, B. P.; Whitby, C. P., *Colloids and Surfaces A: Physiochem. Eng. Aspects* **2005,** 253, 105-115.
47. Zhang, L. Y.; Xu, Z.; Masliyah, J. M., *Langmuir* **2003,** 19, 9730-9741.
48. Czarnecki, J., In *Encyclopedic Handbook of Emulsion Technology*, Sjöblom, J., Ed. Marcel Dekker: New York, 2001.
49. Alvarez, G.; Poteau, S.; Argillier, F.; Langevin, D.; Salager, J., *Energy & Fuels* **2009,** 23, 294-299.
50. Yarranton, H. W.; Urrutia, P.; Sztukowski, D. M., *Journal of Colloid and interface Science* **2007,** 310, 253-259.
51. Yarranton, H. W.; Sztukowski, D. M.; Urrutia, P., *Journal of Colloid and interface Science* **2007,** 310, 246-252.
52. Acevedo, S.; Ranaudo, M. A.; Pereira, J. C.; Castillo, J.; Fernández, A.; Pérez, P.; Caetano, M., *Fuel* **1999,** 78, 977.
53. McClean, J. D.; Kilpatrick, P. K., *Journal of Colloid and interface Science* **1997,** 196, 23-34.
54. Yang, X.; Lu, W.; Ese, M.-H.; Sjöblom, J., In *Encyclopedic Handbook of Emulsion Technology*, Sjöblom, J., Ed. Marcel Dekker: new York, 2001.
55. Gafonova, O. V.; Yarranton, H. W., *Journal of Colloid and interface Science* **2001,** 241, 469-478.
56. Verruto, V. J.; Le, R. K.; Kilpatrick, P. K., *Journal of Physichal Chemistry* **2009,** 113, 13788-13799.
57. Zhang, L. Y.; Lawrence, S.; Xu, Z.; Masliyah, J. M., *Journal of Colloid and interface Science* **2003,** 264, 128-140.

58. Stokes, G. G., *Transactions of the Cambridge Philological Society* **1851,** 9:8.
59. Tcholakova, S.; Denkov, N.; Sidzhakova, D.; Ivanov, I.; Campbell, B., *Langmuir* **2005,** 21, 4842-4855.
60. Eow, J. S.; Ghadiri, M., *Chemical Engineering Journal* **2001,** 85, 357-368.
61. Kang, W.; Jing, G.; Zhang, H.; Li, M.; Wu, Z., *Colloids and Surfaces A: Physiochem. Eng. Aspects* **2006,** 272, 27-31.
62. Sjöblom, J.; Johnsen, E. E.; Westvik, A.; Ese, M.-H.; Djuve, J.; Auflem, I. H.; Kallevik, H., In *Encyclopedic Handbook of Emulsion Technology*, Sjöblom, J., Ed. Marcel Dekker: New York, 2001.
63. Krawczyk, M. A.; Wasan, D. T.; Shetty, C. S., *Industrial & Engineering Chemistry Research* **1991,** 30, 367-375.
64. Rondón, M.; Pereira, J. C.; Bouriat, P.; Graciaa, A.; Lachaise, J.; Salager, J., *Energy & Fuels* **2008,** 22, 702-707.
65. Jeelani, S. A. K.; Hartland, S., *Industrial & Engineering Chemistry Research* **1998,** 37, 547-554.
66. Nadiv, C.; Semiat, R., *Industrial & engineering chemistry research* **1995,** 34, 2427-2435.
67. Freer, E. M.; Wong, H.; Radke, C. J., *Journal of Colloid and interface Science* **2004,** 282, 128-132.
68. Hannisdal, A.; Orr, R.; Sjöblom, J., *Journal of Dispersion Science and Technology* **2007,** 28, 81-93.
69. Israelachvili, J.; Min, Y.; Akbulut, M.; Alig, A.; Carver, G.; Greene, W.; Kristiansen, K.; Meyer, M.; Pesika, N.; Rosenberg, K.; Zeng, H., *Reports on Progress in Physics* **2010,** 73, 1-16.
70. Vuillaume, K.; Giasson, S., *Journal of Physichal Chemistry C* **2009,** 113, 3660-3665.
71. Drummond, C.; Israelachvili, J., *Journal of Petroleum Science and Engineering* **2002,** 33, 123-133.
72. Christenson, H. K.; Israelachvili, J., *Journal of Colloid and interface Science* **1986,** 119, 194-202.
73. Aske, N.; Kallevik, H.; Sjöblom, J., *Journal of Petroleum Science and Engineering* **2002,** 36, 1-17.
74. Sjöblom, J.; Øye, G.; Glomm, W. R.; Hannisdal, A.; Knag, M.; Brandal, Ø.; Ese, M.-H.; Hemmingsen, P. V.; Havre, T. E.; Oschmann, H.-J.; Kallevik, H., In *Emulsions and Emulsion Stability*, Sjöblom, J., Ed. Taylor & Francis: Boca Raton, 2006.
75. Vankova, N.; Tcholakova, S.; Denkov, N.; Ivanov, I.; Vulchev, V.; Danner, T., *Journal of Colloid and interface Science* **2007,** 312, 363-380.
76. Dalen, G. v., *Journal of Microscopy* **2002,** 208, 116-133.
77. Paso, K.; Kallevik, H.; Sjöblom, J., *Energy & Fuels* **2009,** 23, 4988-4994.
78. Miller, D. J., *Colloid & Polymer Science* **1987,** 265, 342-346.
79. Darbeau, R. W., *Applied Spectroscopy Reviews* **2006,** 41, 401-425.
80. Packer, K. J.; Rees, C., *Journal of Colloid and interface Science* **1972,** 40, (2), 206-218.
81. Durand, E.; Clemancey, M.; Quoineaud, A.; Verstraete, J.; Espinat, D.; Lancelin, J., *Energy & Fuels* **2008,** 22, 2604-2610.
82. Denkova, P. S.; Tcholakova, S.; Denkov, N. D.; Danov, K. D.; Campbell, B.; Shawl, C.; Kim, D., *Langmuir* **2004,** 20, 11402-11413.
83. Aichele, C. P.; Flaum, M.; Jiang, T.; Hirasaki, G. J.; Chapman, W. G., *Journal of Colloid and interface Science* **2007,** 315, 607-619.
84. Carr, H. Y.; Purcell, E. M., *Physical Review A* **1954,** 94, (3), 630-638.
85. Meiboom, S.; Gill, D., *The Review of Scientific Instruments* **1958,** 29, (8), 688-691.

86. Hollingsworth, K. G.; Sederman, A. J.; Buckley, C.; Gladden, L. F.; Johns, M. L., *Journal of Colloid and interface Science* **2004,** 274, 244-250.

Paper I

diffusion-fundamentals.org

The Open-Access Journal for the Basic Principles of Diffusion Theory, Experiment and Application

Methods for Droplet Size Distribution Determination of Water-in-oil Emulsions using Low-Field NMR

Nils van der Tuuk OPEDAL[1], Geir SØRLAND[2], Johan SJÖBLOM[1]

[1]Ugelstad Laboratory, Department of Chemical Engineering, the Norwegian University of Science and Technology (NTNU), N-7491 Trondheim, Norway.
[2] Anvendt Teknologi AS

Corresponding author: Nils van der Tuuk Opedal, Dept of Chemical Engineering, the Norwegian University of Science and Technology (NTNU), E-Mail: nils.opedal@chemeng.ntnu.no

Abstract

A method using Pulsed Field Gradient Nuclear Magnetic Resonance PFG-NMR for water-in-crude oil emulsion droplet size determination has been optimized and compared with optical microscope for validation. The method applies a combination of Pulsed-Field Gradient (PFG) NMR, Stimulated Echo (STE), and Carr-Purcell-Meimboom-Gill (CPMG) sequences for measuring diffusion, resolving oil and water signal and for measuring the attenuation due to a distribution in T_2 values. This returns the droplet size distributions of water-in-oil emulsions within a minute. No prior assumption is made on the shape of the droplet size distribution, which enables the method to resolve for instance bimodal distributions. To validate this method, three different crude oils were used in the experiment. The emulsions prepared had water cuts from 10 to 40 %. The correlation between PFG-NMR and optical microscopy was good for the emulsions. Any potential discrepancies between the two techniques are discussed, so are the limitations and advantages of the methods.

Keywords:
Water-in-oil Emulsions, Droplet Size Distribution, PFG, NMR, Diffusion.

1 Introduction

The behavior of emulsions is of great importance for a variety of industries and sciences. Independent of the origin of the emulsion, whether it be the mostly unwanted emulsions relevant for the petroleum industry, or emulsions within daily life products such as food and pharmaceuticals. Either way, the mechanisms of emulsion formation and stability are more or less similar for all industries. So, in order to fully appreciate the behavior of an emulsion, a complete characterization is purposeful. One of the important features of an emulsion is its Droplet Size Distribution (DSD). The droplet size influences many characteristics, for instance the rheology[1] [2], and the stability of an emulsion [3] and emulsion liquid membrane performance [4]. There are presently several different techniques available to obtain the DSD. The suitability of the techniques, the quality and reliability of the measurements, and the ease at which to use them depends on the system to be studied. Some of the techniques require some kind of preparation which may alter the state of the sample. Other techniques consider only a small portion of the sample, making the results less representative. For instance, the use of light scattering to obtain the DSD for a petroleum emulsions is not ideal due to the impermeability of light through the sample. Thus, if any droplets are measured at all, only the droplets in vicinity of the container wall are included in the measurement. This technique is also not ideal for concentrated emulsions. In addition, light scattering does not discriminate between single droplets and clusters. [5] The microscope is another popular technique. This technique often requires dilution, and in addition to being potentially tedious and labour intensive, there are wall effects to consider when the emulsion drop is flattened between two glass slides, and only a small part of the sample is analyzed. [6] The advantages by using NMR to obtain the DSD are several. The entire sample is considered, no sample preparation or dilution is required and the measurements can be relatively fast. The non-perturbing handling of the sample means that the same sample can be analyzed several times. For characterization of water-in-crude oil emulsions, the technique is especially useful due to the opacity of petroleum crude oils.

Stejskal and Tanner [7, 8] pioneered the work on restricted diffusion by studying the diffusion using the pulsed field gradients (PFG-NMR) experiment, where they utilized the difference in the relaxation times for oil and water to separate the signals. Since this initial work on restricted diffusion, the method has been further developed to its current status where it

amongst a broad range of applications may be used to characterize various food emulsions [9, 10] [11] [12] and crude oil emulsions [13]. As the NMR experiment can be performed in numerous ways, a large variety of approaches have been developed for this purpose. Even though the size determination using different NMR approaches has been compared with other techniques with promising results, many of the methods are based on the work by Packer and Rees [14] with the assumption that the shape of the distribution follows a log-normal distribution [15] [12] [16] [17] [9] [18]. Most droplet size distributions do follow a log-normal distribution. However, it might not be the case for all systems. The loss of accuracy in the determined distribution shape can be of importance in order to fully understand the behavior of an emulsion.

Peña and Hirasaki [19] included a CPMG sequence to avoid the a priori assumption of a well defined shape of the distribution. But they still applied the same diffusion model as used by Packer and Rees to find the droplet sizes. One should also bear in mind that these methods assumes a mono exponential decay of the oil signal due to longitudinal relaxation. This is not the case in for example crude oil emulsion, where the relaxation components from the crude oil may vary several orders of order of magnitude.

Aichele et al [13] presented a technique using PFG-NMR with diffusion editing (DE) to quantify brine/crude oil emulsions. This technique made no assumptions on the distribution shape. However, each measurement was relatively long, 5 -7 hours, and proved sensitive to coalescence.

This work presents a new method which uses a combination of Pulsed Field Gradient (PFG), Stimulated Echo (STE) and CPMG sequences to obtain the DSD for crude oil emulsions within a minute. The method combines either the short diffusion time model developed by Mitra et al [20] or a slight modification of the method presented by Packer and Rees [14] with a method for determination of pore size distributions in brine saturated rock core plugs developed by Sørland et.al [21]. The major difference from brine saturated rock core plugs is that the continuous phase, being either oil or water, returns an NMR signal that may overlap in the T_2 distributions. Thus we have included a so called z-storage interval for resolving oil and water due to non overlap in the T_1 distributions instead. As will be shown in the theoretical section this combined sequence can be used to find the short time diffusion coefficient, the average surface to volume ratio (yielding the average droplet size), the surface relaxivity and the droplet size distribution. The methods make no assumptions on the shape of the distributions, enabling it to resolve less trivial distributions. In order to test the performance of the methods, emulsions of three different crude oils at different water cuts

(volume % of water) were investigated. As a comparison, the droplet sizes of the same emulsions were studied with optical microscope.

2 Theory

2.1 Extracting droplet size distribution from water in oil or oil in water emulsions

Here we recapture the theory leading the functionality between the diffusion coefficient at short observation times and the surface to volume ratio. It is also shown how this can be related to a droplet size distribution. A simple way to combine the asymptotical approach [14] at long observation times with the T_2 distribution from the CPMG experiment to result in droplet size distribution is given in section 2.1.3.

The equation of motion for the diffusing molecules within the cavities may be described by the standard diffusion equation:

$$\frac{\partial G}{\partial t} = D_0 \nabla^2 G \tag{2.1}$$

where the diffusion propagator $G = G(\mathbf{r}_0, \mathbf{r}, t)$, is the conditional probability [22] , defined as

$$G = p(\mathbf{r}_0, 0) \times P(\mathbf{r}_0, \mathbf{r}, t) \tag{2.2}$$

where $p(\mathbf{r}_0, 0)$ is the probability of finding the molecule at position $\mathbf{r}_0$ at time t = 0, and $P(\mathbf{r}_0, \mathbf{r}, t)$ is the probability of finding this molecule at position $\mathbf{r}$ at a later time t.

When including the effect from relaxation at the pore walls, the boundary condition can be stated as

$$D_0 \, \mathbf{n} \cdot \nabla G_{r \in S} + \rho \, G_{r \in S} = 0 \tag{2.3}$$

Here **n** is the outward normal vector on the pore surface S and ρ is the surface relaxivity. The boundary condition merely states that the surface may act as a sink for the coherence of the NMR signal of the molecules, while in the physical picture the molecules collide with the surface and bounce back into the cavity. As seen by the NMR experiment, the molecule, if it relaxes at the surface, vanishes from the heterogeneous system. This is why it is difficult to relate the NMR diffusion experiments to physical properties as described by the diffusion

equation (eq. 2.1) without the surface relaxation term in the boundary condition (eq. 2.3). The existence of a surface relaxation term makes the true physical picture of particles different from the picture of the nuclear magnetic moments of the molecules. Compared to brine saturated rock core plugs, we have found the surface relaxivity, as experienced by the brine, to be approximately two orders of magnitude smaller in emulsion systems ($\rho_{emulsion} \leq 10^{-6}$ m/s while $\rho_{rock} \geq 10^{-4}$ m/s). In the following we will focus on two regimes of the ratio between the mean squared displacement and the typical droplet sizes; the asymptotic level of the diffusion coefficient where $(6\ D_0\ t)^{1/2} >> R_{cavity}$ and the short observation time expansion of the diffusion coefficient where $(6\ D_0\ t)^{1/2} << R_{cavity}$. What is important for these two regimes is the absence of dependency on the surface relaxivity within the equation governing the PFG-NMR experiments. As will be shown in the next sections it is then possible to solve out the surface relaxivity, and thus transform the T_2 relaxation time distributions to droplet size distributions.

2.1.1 The short observation time expansion of the diffusion coefficient

As shown by Mitra et al [20], there is a situation where the surface relaxation term is absent in the solution of the diffusion propagator, i.e. the short time expansion. By assuming piecewise smooth and flat surfaces and that only a small fraction of the particles are sensing the restricting geometries, the restricted diffusion coefficient can be written as

$$\frac{D(t)}{D_0} \approx 1 - \frac{4}{9\sqrt{\pi}} \sqrt{D_0 t}\, \frac{S}{V} + \varphi(\rho, R, t) \tag{2.4}$$

where $D(t)$ is the time dependent diffusion coefficient, D_0 is the unrestricted diffusion coefficient, in bulk fluid, and t is the observation time. The higher order terms in t, $\varphi(\rho, R, t)$ holds the deviation due to finite surface relaxivity and curvature (R) of the surfaces. At the shortest observation times these terms may be neglected such that the deviation from bulk diffusion depends on the surface to volume ratio alone.

In a porous system a large span in pore sizes must be assumed. eq. (2.4) must be expected to be valid also for a heterogeneous system. If ξ_i is the volume fraction of the pores with surface to volume ratio $(S/V)_i$, eq. (2.4) can be expressed as

$$\sum_i \xi_i \frac{D_i}{D_0} \approx \sum_i \xi_i \left[1 - \frac{4}{9\sqrt{\pi}} \sqrt{D_0 t} \left(\frac{S}{V} \right)_i \right] = \left(1 - \frac{4}{9\sqrt{\pi}} \sqrt{D_0 t} \overline{\left(\frac{S}{V} \right)} \right) \tag{2.5}$$

Measurements of the early departure from bulk diffusion combined with a linear fit of the experimental data to the square root of time will thus result in a value for the average surface to volume ratio $\overline{(S/V)}$.

2.1.2 Transforming a T_2 distribution to a droplet size distribution

Assuming that the water molecules are probing the droplets within the sample, there is a simple relation [23] between T_2 values and the droplet sizes

$$T_2 \approx \frac{V}{S\rho} \tag{2.6}$$

This couples the surface to volume ratio to the surface relaxivity, ρ, and makes it difficult to assign the T_2 distribution to a (V/S) distribution. However, if we make the assumption that eq. (2.6) holds for any droplet size, with ξ_i being the volume fraction of pores with surface to volume ratio $(S/V)_i$ and corresponding relaxation time T_{2i}, we may follow Uh and Watson [24] and write

$$\sum_{i=1}^{n} \xi_i \frac{1}{T_{2i}} = \sum_{i=1}^{n} \xi_i \rho_i \left(\frac{S}{V} \right)_i \approx \rho \sum_{i=1}^{n} \xi_i \left(\frac{S}{V} \right)_i = \rho \overline{\left(\frac{S}{V} \right)} \tag{2.7}$$

Here we have made the basic assumption that the surface relaxivity ρ is independent of droplet size. The left hand side of eq. (2.7) is the harmonic mean $\overline{1/T_2}$ of the T_2-distribution weighted by the fraction ξ_i of nuclei with relaxation time T_{2i} and n is the number of subdivisions of droplet sizes. This average can be calculated from the T_2-distribution obtained in a CPMG measurement where the magnetization attenuation $M^{obs}(t)$ is converted to a T_2 distribution by solving an inverse problem using e.g. an Inverse Laplace Transform (ILT) routine [25]. Then the surface relaxivity ρ can be calculated from eq. (2.7) if the average surface to volume ratio $\overline{(S/V)}$ is already found from the diffusion experiment. Finally, the measured T_2-distribution can be transformed into an absolute droplet size distribution (V/S) by means of the relationship inherent in eq. (2.7).

To sum up, the procedure for deriving absolute droplet size distributions is as follows:

1) The average surface to volume ratio $\overline{(S/V)}$ is found from fitting eq. (2.5) to a set of diffusion measurements at short observation times.

2) The average (S/V) can be correlated to the average ($1/T_2$) found from a CPMG experiment. From eq. (2.7) eq. (2.6) can then be written as

$$\overline{\left(\frac{1}{T_2}\right)} \approx \rho \overline{\left(\frac{S}{V}\right)} \qquad \Rightarrow \qquad \rho = \overline{\left(\frac{1}{T_2}\right)} \times \overline{\left(\frac{S}{V}\right)}^{-1} \tag{2.8}$$

hence we find the relaxivity, ρ, which then is assumed to be droplet size independent.

3) Under the assumption of droplet size independency of the relaxivity the value of ρ can then be used in eq (2.6) thus resulting in a linear relation between T_2 and the volume to surface ratio which is a measure of the droplet size. By multiplying the T_2 distribution by the calculated surface relaxivity the distribution is normalized to a droplet size distribution in absolute length units.

2.1.3 The asymptotic level of the measured diffusivity

As shown by Packer et.al [14], there is a situation where the surface relaxation term is absent in the solution of the diffusion propagator, i.e. for diffusion within closed cavities and when the diffusing molecules have covered mean free path lengths >> cavity dimension [$(6\ D_0\ t)^{1/2}$ >> R_{cavity}]. In such a situation the attenuation of the NMR signal from diffusion within the closed droplet can be simplified to [14] [26]

$$\left(\frac{I}{I_0}\right) \approx \exp^{-\frac{1}{5}\gamma^2\delta^2G^2R^2} \tag{2.9}$$

where δ is the gradient pulse length, G is the applied gradient strength and R is the droplet radius. In a heterogeneous system a large span in droplet sizes must be assumed. Thus eq. (2.9) must be expected to be valid also for a heterogeneous system. If ξ_i is the volume fraction of the droplets with surface to volume ratio $(S/V)_i$, eq. (2.9) can be expressed as

$$\left(\frac{I}{I_0}\right) \approx \sum_i \xi_i \exp^{-\frac{1}{5}\gamma^2\delta^2 G^2 R_i^2} \tag{2.10}$$

When the exponent in Equation 2.10 is small for all *i*, we may expand the exponential functions using its two first terms:

$$\left(\frac{I}{I_0}\right) \approx \left(\sum_i \xi_i - \sum_i \xi_i \frac{1}{5}\gamma^2\delta^2 G^2 R_i^2\right) = 1 - \frac{1}{5}\gamma^2\delta^2 G^2 \overline{R}^2 \tag{2.11}$$

Where $\overline{R}^2$ yields the average value of the square of the droplet radius. Measurements of the early departure from I_0 as a function of applied gradient strength may then result in a value for the average surface to volume ratio. This can be used in combination with a T_2 distribution to result in a droplet size distribution as shown in section 2.1.2. The only difference is that the value of the surface relaxivity now must be given as

$$\rho = \sqrt{\left(\frac{1}{\overline{T_2^2}}\right) \times \left(\frac{\overline{R^2}}{9}\right)} \tag{2.12}$$

2.2 Separation of crude oil and brine signal

There are several ways to separate the NMR contribution of the crude oil and brine components. One method is to suppress the brine using the oneshot method [27] . This applies when the molecular mobility of the oil is more than a decade slower than the mobility of the brine. Another method applies when the T_1 distributions of brine is longer than the T_1 distribution of the crude oil. Then one may store the NMR signal for full recovery of the crude oil signal back to thermal equilibrium while the brine signal still can be measured on. If one of the two methods can be used, the theory above can be applied in achieving a droplet size distribution for the brine droplets. In the following we will focus on the method using z-

storage delay for suppression of the crude oil signal using the sequence shown in figure 3.1. Then we find the following T_2 distributions for short and long z-storage (Δ) intervals, as shown in figure 2.1. By increasing the duration of the z-storage one can thus omit the oil signal. The two peaks at short Δ corresponds to the oil signal (left peak) and water signal(right peak).

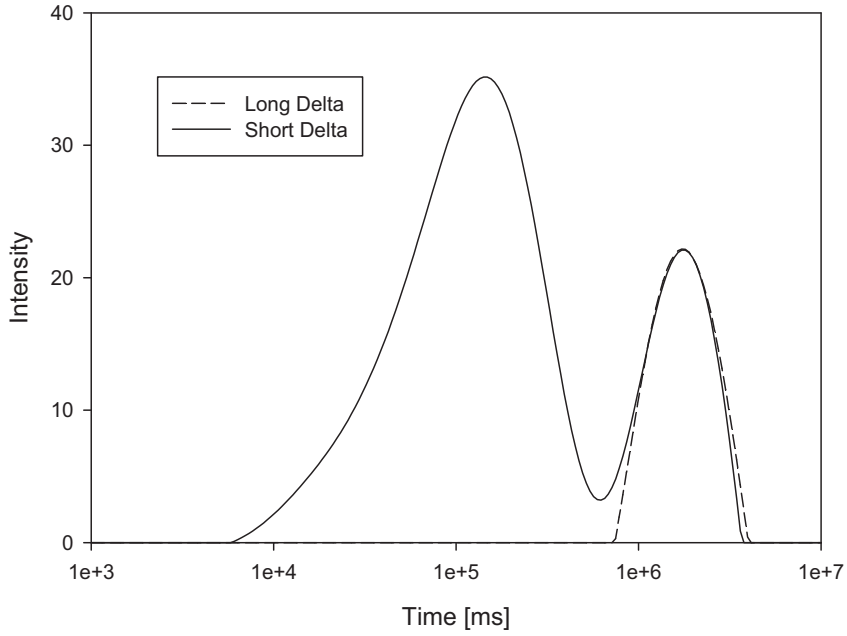

Figure 2.1 The effect of using z-storage to obtain the T_2 distribution of water alone.

3 Experimental

3.1 Materials

Three different petroleum crude oils were used; some of the key properties of the crude oils are given in table 3.1. The crude oils will henceforth be denoted as A, B and C. The water was Milli-Q grade (18,2 mΩ).

Table 3.1 Summary of key crude oil properties at 25 °C.

Crude oil	Density [g/cm^3]	Viscosity [mPas]
A	0.905	53
B	0.932	220
C	0.970	2500

3.2 Methods

3.2.1 Emulsion preparation

The emulsions were prepared by mixing the crude oils with water at room temperature (25°C). The total sample volume of all the emulsions was 15 mL. Water cuts higher than 40% were not investigated as these emulsions were not stable for crude A and B, and since it proved difficult to properly mix the viscous crude C and water at higher water cuts at room temperature. The mixing was performed by an IKA Ultra Turrax homogenizer (10 mm head) with a stirring speed of 24 000 rpm for 2 minutes. The emulsions were analyzed immediately after mixing. Parallel to the NMR measurements, the same emulsions were analyzed with the microscope.

3.2.2 Droplet Size Distribution from Microscope

The microscope consist of a Nikon Eclipse ME 600L Microscope and a CoolSNAP-Pro cf camera with Image-Pro PLUS 5.0 software of Media Cybernetics. By utilizing a costum-made macro that identifies and measures the size and shape of dark objects in a picture, the distribution of the droplets was obtained. The shape measurement was useful to exclude droplets with a non-spherical shape and clusters of droplets. In order to obtain a droplet size distribution by using the microscope technique, the emulsions had to be diluted. The original emulsions were too concentrated for the macro to properly separate and distinguish the

droplets. The dilution was performed by adding ~0,2 g emulsion drop wise to ~2 g of the crude oil, and thereby gently mixing. The droplet size distribution was obtained by placing a small drop of the diluted emulsion on a glass slide. The drop was then flattened by placing a smaller glass slide on top of the droplet. Thereafter, several pictures of the emulsion drop were taken. In order to get a credible impression of the droplet sizes for each emulsion, more than 800 droplets were counted in the distribution population. However, this method proved insufficient for crude C emulsions. Visual observation of the droplets from emulsions prepared with this particular oil was difficult due to its dark appearance and high viscosity. In order to observe the droplets formed from crude oil C, a technique that has been performed previously on heavy viscosity crude oils was used [28]. By placing a small drop of the emulsion on the glass slide, and then placing a small drop of toluene in contact with the emulsion drop, the water droplets diffuse into the toluene phase/drop. The droplets diffused into the toluene zone were then registered and measured in the same manner as the other two crude oils.

3.2.3 Droplet Size Distribution from NMR

The NMR sequences that were used for measuring the droplet size distributions of the oil/water systems are explained in the following section. The NMR measurements were performed on a low field Oxford Instruments MARAN Ultra spectrometer, 23 MHz tempered at 40°C, with the ability of producing shaped gradients up to 400 G/cm. The NMR sample tubes of 18 mm diameter were filled with ~3 mL of the emulsion.

The PFG-NMR as shown in figure 3.1 makes use a combination of three different sequences to obtain the DSD. The first part is the 11-interval PFG sequence used to weight the NMR signal with a diffusion dependent term. Originally this sequence was developed for diffusion studies in the presence of internal magnetic field gradients. In an emulsion system we find the internal gradient strengths to be negligible, but still we are using the 11-interval PFG sequence in order to minimize the effect from eddy current transients. Thus we may use eddy current dead times of just 500 μs without any sophisticated preemphasis adjustment. In the second part the signal is stored along the z-direction for a period of Δ, which is used for letting the oil signal relax towards thermal equilibrium. Then we are left with water signal only that is subjected to a CPMG sequence [29] in the last part of the sequence. This part may then return a T_2 distribution from water/brine only. This distribution is diffusion weighted depending on the strength on the applied magnetic field gradient *g* used in the first part of the sequence. When setting the applied gradient strength to zero and Δ long enough to suppress

the crude oil signal, the T_2 distribution obtained can be used to calculate the droplet size distribution. This will then obtain the volume weighted droplet size distribution of the dispersed droplets. An important feature about the CPMG sequence is that it does not make any assumptions on the distribution shape.

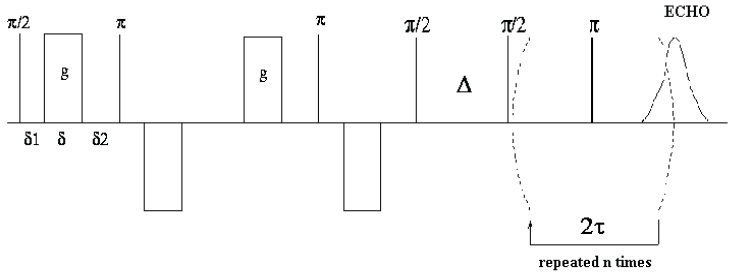

Figure 3.1 Combined Pulsed Field Gradient - Stimulated Echo – CPMG sequence.

3.2.4 The Diffusion-T_1-weighted profile experiment

In the PFG-NMR sequence shown in figure 3.2 we have replaced the CPMG part with spin echo acquisition during a read gradient. This yields a position dependent NMR signal once it has been Fourier transformed, i.e. a distribution of signal intensities that depends on position within the sample. The gradients in the first part of the sequence may be used to suppress signal from the water, leaving us with the profile of the crude oil component. This may act as a probe of emulsion stability, as a variation of the crude oil profile indicates instability of the emulsion.

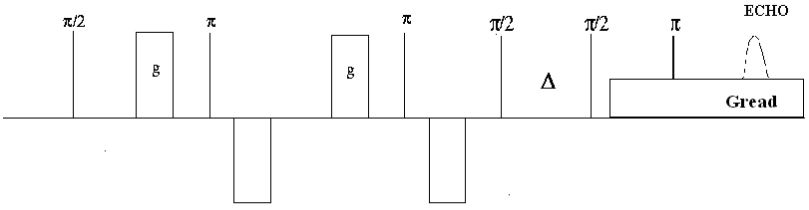

Figure 3.2 The Diffusion-T_1-weighted profile sequence.

One may also use set the gradients in the first part to zero, and instead make use of the z-storage delay Δ either to measure the profile of the entire sample (short Δ), or the water profile of the sample (long Δ). This is shown in figure 3.3, where the dashed line (long Δ)

indicates that water is moving to the bottom of the sample. The solid lines (short Δ) giving the signal of all components present in the sample tubes indicates a flat intensity profile.

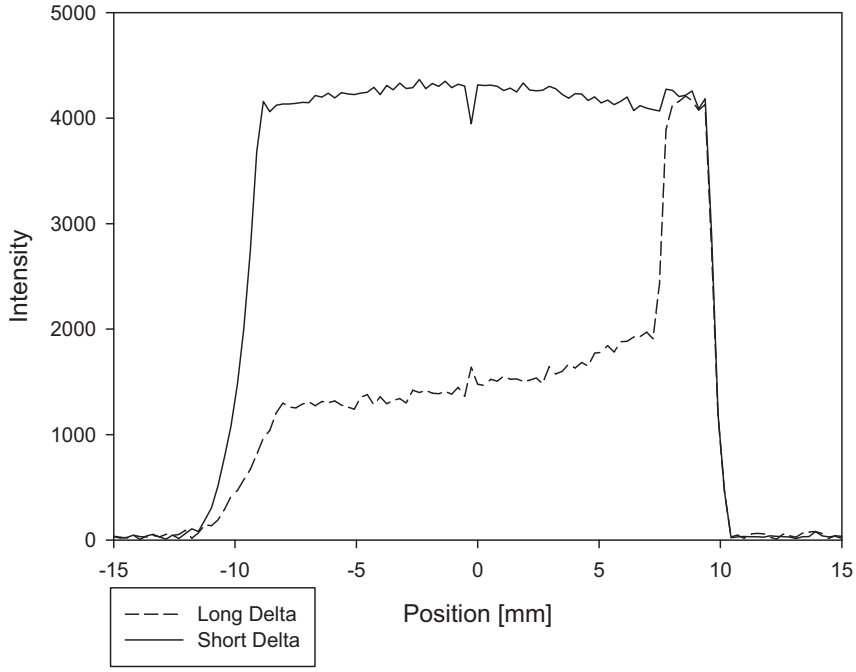

Figure 3.3 The effect of using z-storage to obtain the water profile of the sample. The bottom of the sample is at ~10 mm, and the top of the sample is at ~ - 10 mm.

As the NMR magnet is tempered to 40°C, and the emulsions were prepared at room temperature, the NMR tubes containing sample had to be tempered for about 15 minutes to reach the magnet temperature. The emulsions were then subjected to the NMR measurements. Depending on the T_2 values of the crude oil, the water signal was separated from the crude oil signal by setting the Δ to 1.5 seconds +- 0.5 seconds, depending on the T_2 distribution of the crude oil being investigated. In order to study any instability of the emulsions, the NMR experiments were repeated after certain time intervals. The diffusion measurements were calibrated with Milli-Q grade water, and the value of the unrestricted diffusion coefficient, D_0, was measured to be 3.2 x 10^{-9} m^2/s.

4 Results & Discussion

The outline of the experimental data obtained will here be presented. However, the manner in which the results from the two techniques will be presented requires a short comment. A distribution obtained from image analysis of droplets in a microscope will give a size distribution based on number intensity. The NMR method yields a volume-based size distribution; the droplet dimensions are calculated from the surface to volume ratio. This means that a direct comparison of the results from the two techniques might not give the best correlation. A number based size distribution will yield a smaller mode and be differently shaped compared to a volume based size distribution. Figure 4.1 illustrates the difference of weighting by a number- and volume-based distribution obtained by the NMR. In a volume-based distribution, the smallest droplets will be discriminated by the larger ones, and vice versa. In the section where the two techniques are compared, the volume based distribution obtained from the NMR has been changed/transformed to a number based distribution by dividing the volume intensity of each diameter interval by its volume. The opposite could have been done; transforming the number-based distribution of the microscope to a volume-based one. However, due to the low amount of data points compared to the NMR data, such a transformation could easily become flawy. If a certain data set would contain one or two droplet relatively larger than the other ones, the transformed distribution would be skewed by these particular droplets. The distributions presented from both techniques are also normalized.

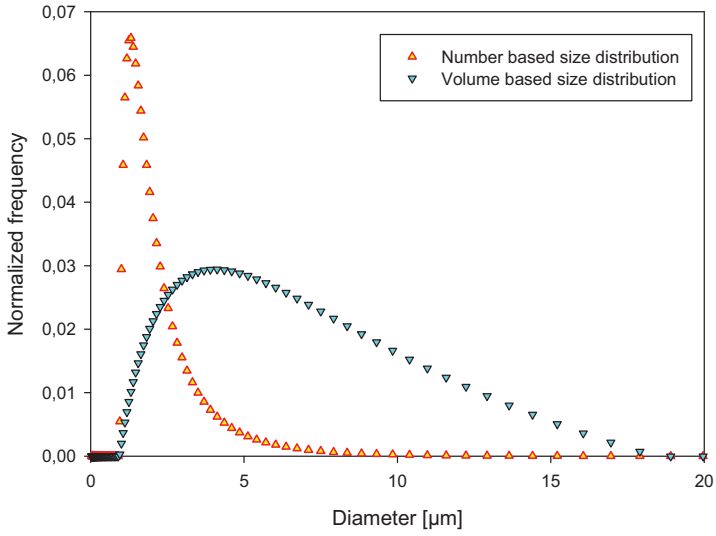

Figure 4.1 Volume-based and number-based size distribution of crude A emulsion with 10 % water cut obtained by NMR.

4.1 Separation of oil and water signal in the NMR

The NMR technique herein presented utilizes the fact that the relaxation times of the ^{1}H spin are dependent on the molecular structure. And so, separating the signal from oil and water phases is dependent on the nature of the particular phases. The structure of a water molecule is not changeable, but the average molecule size and structure of hydrocarbons found in crude oils may vary. As seen in figure 4.2, the ease at which to distinguish the water and oil signal increases with the viscosity. The signal from the droplets of the emulsion from crude A partially overlaps with the oil signal, making it less trivial to separate the two contributions. Thus, depending on the delay time at which the signal recording starts (Δ, see figure 2.1), either signal from the smallest water droplets might be excluded or signal from the oil might be included. However, there is a clear cut-off between the contribution of water and oil signal in the T_2 distribution for crude B and C.

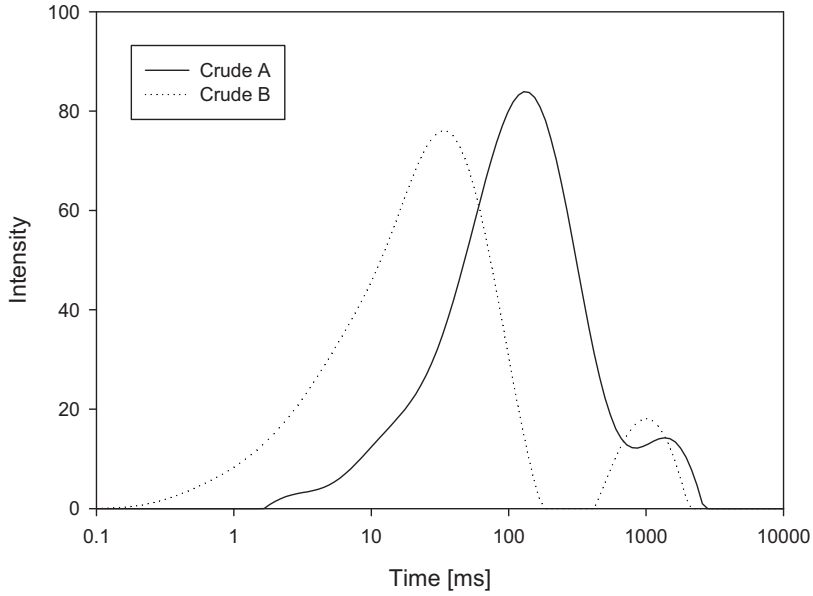

Figure 4.2 T_2 distributions of emulsions with 10 % water cut formed from Crude A and B.

4.2 Accuracy of the Microscope

The microscope technique has its advantage that it gives a direct view of the droplets. A study regarding the accuracy of the microscope technique for obtaining size distributions was performed by Denkova et al [30]. The experimental error of the technique itself proved to be minor. The largest contribution to the error was attributed to the resolution limit of the microscope used. As can be seen from figure 4.3, analyzing an emulsion with different magnification might yield different results. The inclusion of the smallest droplets is dependent on the microscope resolution. Another issue regarding the microscope technique is the dilution of the emulsion. Diluting the continuous phase can be a major intrusion for some systems. For instance, the dilution of margarine can induce coalescence due to the breakdown of crystal networks within these emulsions [16], other emulsions might exhibit increased stability due to addition of more surfactant. Crude oils are known to contain several surfactants. [31] The effect of the dilution on the systems studied herein has not been further explored. Though, diluting could stop droplet collision and coalescence. Another factor is the possible change in solubility properties of interfacial active compounds. This means that even though the same emulsions were studied parallel in the NMR and the microscope, the dilution might result in a different behavior.

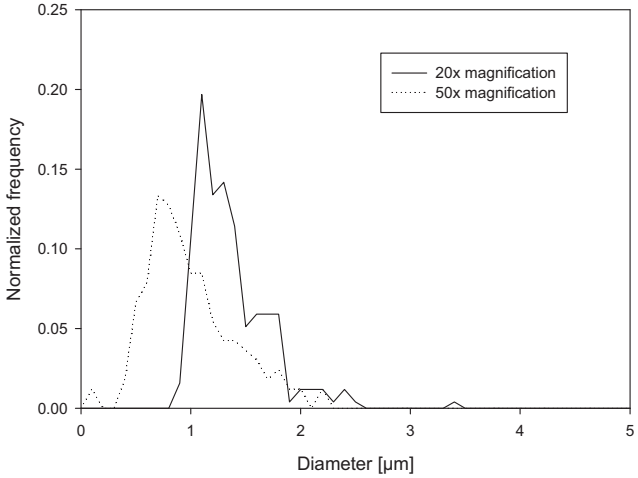

Figure 4.3 Droplet size distribution of an emulsion studied with microscope with different magnification.

4.3 Comparison of the two techniques

Even though the NMR model presented in this paper makes no assumptions of the shape of the distributions, the results indicate that the log-normal fitting is suitable for the number based distributions. Most unimodal emulsion droplet size distributions follow the log-normal distribution [32] [33] [9] The distribution obtained from the microscope were also fitted with the log-normal distribution. The result of the fitting is given in table 4.1. The log-normal equation is given below:

$$f(a) = \frac{1}{\sqrt{2\pi}\sigma 2a} e^{-\left[\frac{(\ln(2a)-\mu)^2}{2\sigma^2}\right]} \quad (4.1)$$

where a is the droplet radius and σ is the width of the log-normal distribution.

The comparison of the DSD from an emulsion with 10 % water cut for crude A is given in figure 4.4 below. The two distributions correlate well, the distribution peak and the distribution shape are similar for both techniques. As seen from table 4.1 below, the difference of both the mean diameter and standard deviation is minimal. There is a difference between the two graphs for the smallest droplets. The NMR method indicates a distribution with droplets ranging from about 1 µm, whereas the microscope indicates that the smallest droplets are about 0.5 µm in diameter. The difference can be explained due to the T_2

distribution and the selected delay time at which the NMR recording starts; figure 4.2. As mentioned above, an overlapping T_2 distribution means that the signals from the two phases coincide. With that, there is a risk that the contribution from the smallest droplets will not be properly registered with the selected Δ.

Table 4.1 Summary of the log-normal fitting for emulsions of crude A and B.

Crude Oil	Water cut	Parallel	Method	d_0 [μm]	σ
A	10 %	1	Microscope	1,34	0,26
			NMR	1,67	0,30
		2	Microscope	1,42	0,30
			NMR	1,49	0,32
	20 %	1	Microscope	1,43	0,27
			NMR	2,31	0,28
		2	Microscope	1,40	0,34
			NMR	2,83	0,30
B	10 %	1	Microscope	1,34	0,25
			NMR	1,20	0,31
		2	Microscope	1,31	0,29
			NMR	1,01	0,37
	20 %	1	Microscope	1,46	0,20
			NMR	1,84	0,34
		2	Microscope	1,47	0,24
			NMR	1,70	0,36

Figure 4.5 displays the size distribution for an emulsion from crude B. The correlation between the NMR and the microscope is good. The shapes of the two distributions are comparable, and the registered dimensions of the smallest and largest droplets present in the emulsion are similar for both techniques. The fact that the quantification of the smallest droplets tallies for both techniques for crude B, and not for crude A, can be understood by figure 4.2. There is a distinct gap between the T_2 time for the oil and water phases for emulsions of crude B, making it is easier to set Δ for the recording of the water signal without excluding any of the water signal. Hence, there is a higher probability that the contribution

from the smallest droplets will be included. The peak of the distribution between the two techniques does not correlate equally well as to what was the case for crude A. The NMR indicates a distribution peak around 1 µm. However, the accuracy of droplet detection for the microscope decreases with droplet diameters smaller than 1 µm. It is possible to visually detect the smallest droplets, but it is increasingly difficult to properly detect the droplets by the automatic counting macro due to low contrast. This can be a plausible explanation as to why the peak of the distribution from the microscope is slightly larger than the one of the NMR.

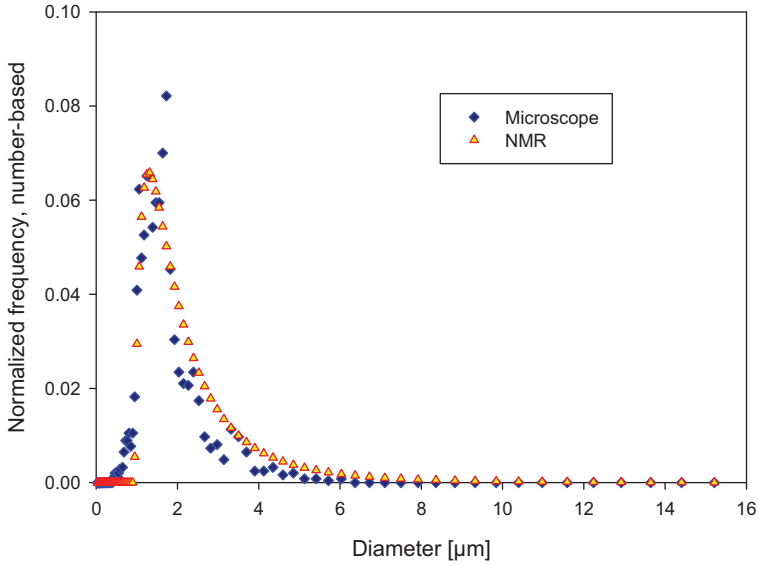

Figure 4.4 Comparison of the DSD of crude A from NMR and microscope; 10% water cut.

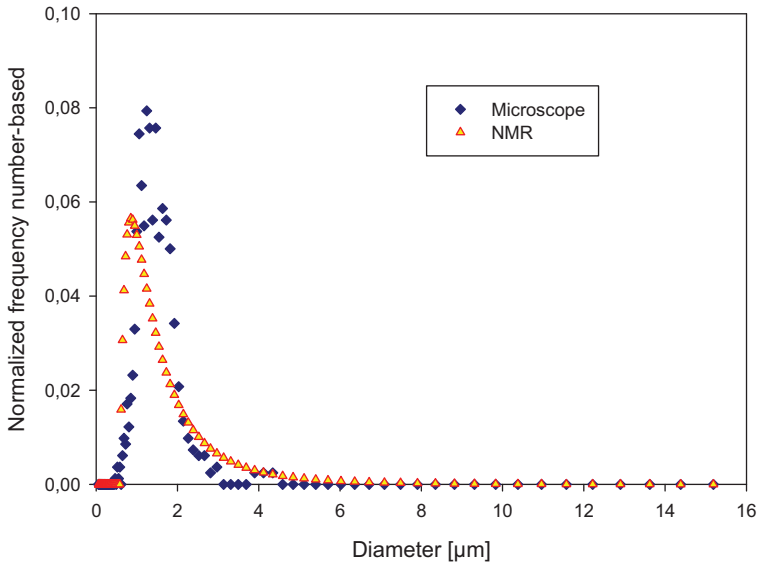

Figure 4.5 Comparison of the DSD of crude B from NMR and microscope; 10% water cut.

4.4 Reasons for discrepancies between the two techniques

As can be seen in table 4.1, the comparison of the two techniques are indeed promising. The correlation between the NMR and microscope was good the emulsions at water cuts 10 – 20 %. Both techniques used in this work have their limitations, and these limitations and how they can affect the data will be further discussed.

Considering the NMR, there are three potential effects that can influence the results. As indicated by table 4.1, the mean diameter from the NMR method increases more with the water cut than what is the case of the mean diameter from the microscope. The first explanation for the increased mean diameter from the NMR method is that of convection of the water droplets. If the droplets are moving during the diffusion measurements, the movement may affect the accuracy and influence the final droplet size distribution. Convection of water droplets will ultimately result in a distribution indicating larger droplets [34]. With increased water cut the overall viscosity of the emulsion changes, leading to a possible onset of convection of brine to the bottom of the sample tube. This movement largely exceeds the self diffusion which is used for probing the droplets size distribution. This may be wrongly interpreted as larger droplets as the apparent measured diffusion is biased towards

larger values due to convection. Another factor influencing the correlation between the two techniques is the stability of the emulsions formed. The stability of the emulsion is an important factor for the NMR measurements. Formation of a free water phase at the bottom of the NMR tube will perturb the final distribution since a free water phase will be perceived by the diffusion probing as large droplets. With a free water phase in the sample, the separate T_2 distribution of the water will not be representative of only the droplets in the emulsion phase, but will also include the bulk water. Figure 4.6 exhibits the NMR signal intensity as a function of the sample height of emulsions from crude B at different water cuts. The emulsions with water cuts from 10 to 30 % were all stable, as seen by the flat signal intensity, and a signal that increases with the water cut. Whereas for the emulsion of 40 % water cut sedimentation and coalescence of the droplets clearly occurs. The increase in signal intensity in the middle and lower part of the tube for the 40 % emulsion can be interpreted as an accumulation of droplets, and the large peak at the bottom of the NMR tube is indicative of the formation of a free water phase. The intensity profiles of figure 4.6 where also confirmed by visually examining the sample tube containing the emulsion after the measurements were completed. The emulsion of water cut 40% for crude B had formed a separate water phase.

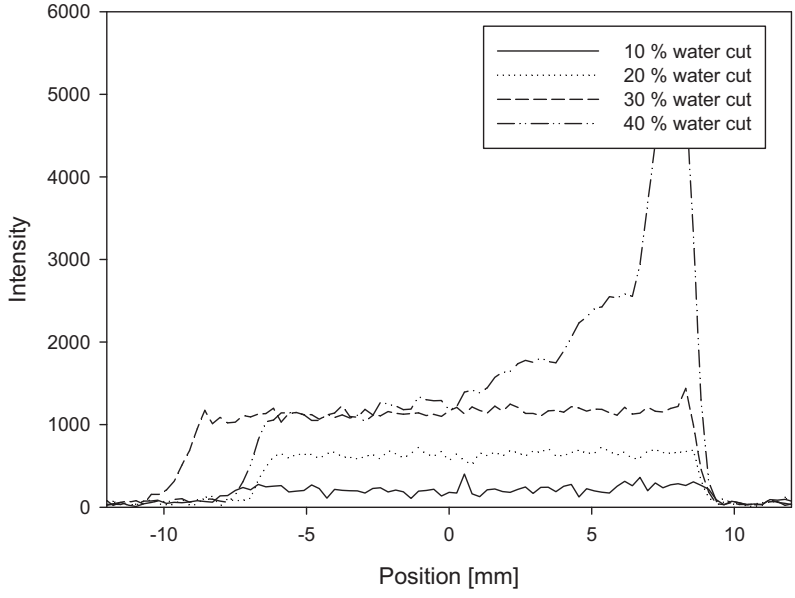

Figure 4.6 NMR signal intensity profile of crude B emulsions as a function of position. Bottom of sample is at ~10 mm, and top of sample is at ~ -10 mm.

There is ongoing work to develop a NMR-method capable of monitoring and measuring the size distribution of unstable emulsions. The position dependent signal intensity illustrated in figure 4.6 is a promising feature to study emulsion stability.

The third possible effect for decreasing correlation is due to the model used for NMR data interpretation. Depending on droplet size, the echo attenuation of the diffusion measurements can be modeled differently. The model used herein is based on diffusing molecules for which the mean squared displacement for unrestricted movement is much larger than the actual droplet sizes (section 2.1.3). With an observation time of a few milliseconds this model applies for droplets with diameter around ~1 μm. This is not the case for all the droplets within the emulsions with a higher water cut, as demonstrated by table 4.1. The validity of the simplification leading to equation 2.11 may not be valid for the larger droplets. However, as will be shown below, the correlation of the distributions from the microscope and the NMR is good for emulsions from crude C at various water cuts. Hence, the importance of this effect seems to be of minor importance compared to the other two effects as mentioned above.

4.5 Bimodal droplet size distribution

The emulsions prepared from crude C exhibited a bimodal distribution from the NMR data, as seen in figure 4.8. The bimodal shape of the distribution exemplifies the usefulness of the NMR method. In figure 4.8, the volume-based normalized frequency of the droplet sizes for 10 and 40 % water cut emulsions have been plotted. And the figure indicates a bimodal distribution, with modes around 1,8 μm and 4,5 μm in diameter for the emulsion of 10 % water cut. As the water cut increases, an increase in the modes and a shift of the share of the respective modes can be observed.

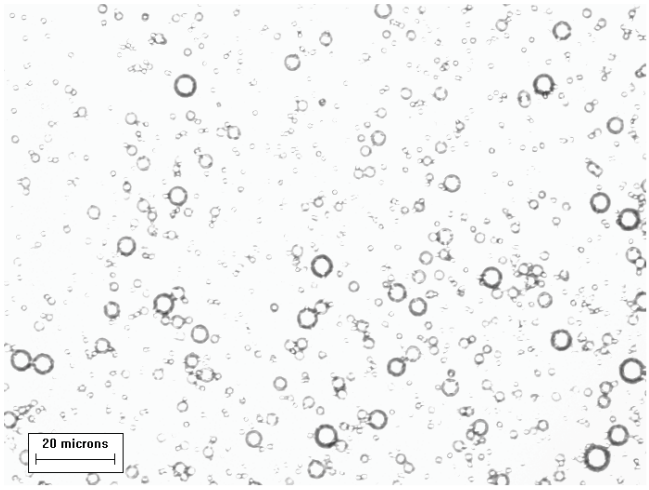

Figure 4.7 Microscope image of an emulsion of crude C, 40% water cut.

The increase in the share of larger droplet with increasing water cut is expected; increased water cut increases the probability of formation of larger droplets. The bimodal nature of the distributions of these emulsions was confirmed by the distribution obtained from the image analysis plotted in figure 4.9. The modes of the distributions from the image analysis are reasonably similar to the NMR results; around 1.3 μm and 4 μm in diameter, depending on the water cut. The bimodality is not that distinct for the emulsion with water cut 10 % in the microscope. However, at 40 % two peaks are clearly visible. The difference in modes and the amount of the different droplet sizes for the NMR and microscope data can be explained by the different weighting of the plots. The data plotted from the NMR is volume-based, whereas the data from the microscope is number-based. And as previously mentioned these two bases are not directly comparable. A volume-based distribution will underestimate the amount of the smallest droplets and vice-versa.

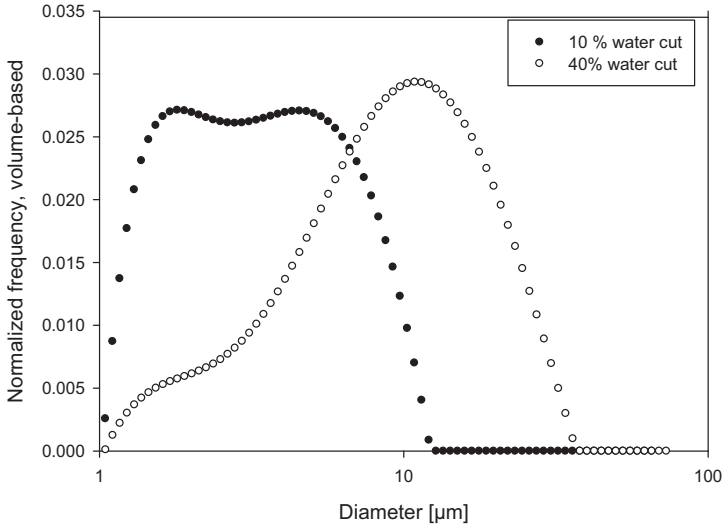

Figure 4.8 Emulsion droplet size distributions of crude C at different water cuts obtained by the NMR.

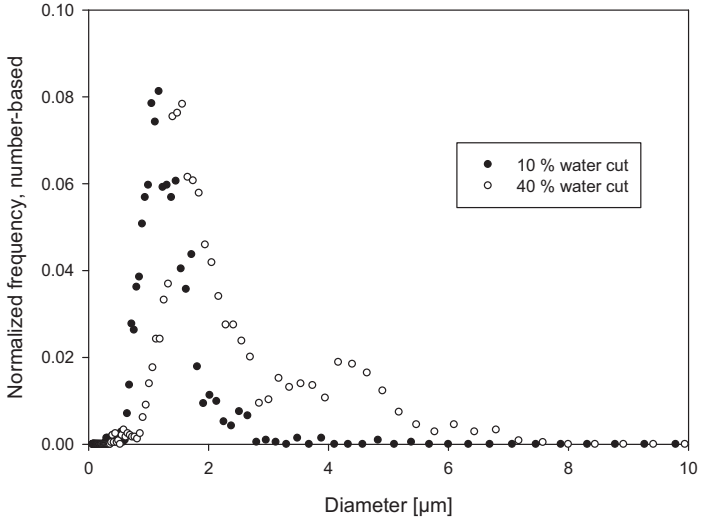

Figure 4.9 Emulsion droplet size distributions of crude C at different water cuts obtained by the microscope.

4.6 On the approximations in the pore size (S/V) distribution model

To be able to transfer the NMR measurements one must make an important approximation that relates to the duration of the gradient pulses. The literature makes use of three length scales, the diffusion length, the dephasing length and the pore length [37]. In the short time expansion developed by Mitra et al. [20] it was assumed piecewise smooth surfaces that only a small fraction of the probing molecules experienced, i.e. the diffusion length is much less than the pore length. Thus one could apply the square root of time attenuation of the diffusion coefficient to get the surface to volume ratio. As the droplets are getting smaller, the dephasing length may become comparable to the pore/droplet length. As long as there is a small deviation one should apply the corrected effective diffusion times as developed by Fordham et al. [38]. This correction will lead to larger average droplet sizes as the restricted diffusion during the gradient pulses is corrected for. However, in systems mainly consisting of small droplets, where the diffusion length becomes much larger than the droplet size, the Mitra model fails anyway due to a deviation from the square root of time dependency on the measured diffusivity. If it is apparent that the measured diffusion coefficient is attenuated significantly at the shortest observation time possible (~1 ms), the S/V ratio then cannot be found accurately. To measure the S/V for such a system by NMR the asymptotic level of the diffusion coefficient must be used. Then one may choose the experimental parameters such that $(6\ D_0\ t)^{1/2} >> R_{cavity.}$ Still there is a lower limit to what droplet sizes one may measure using this method. As the droplet sizes gets smaller the validity of the Gaussian approximation of the phases of the nuclear spins fails due to restricted diffusion during the gradient pulses, i.e the dephasing length becomes comparable and even larger than the typical droplet size. One may compensate for this effect by measuring the attenuation at different gradient pulse lengths and get a measure for the droplet size as a function of gradient pulse length. Then a fit of this functionality including an extrapolation back to zero gradient pulse length yields a gradient pulse length independent average droplet size.

Conclusion

This work has evaluated a LF-NMR method for the applications of obtaining droplet size distributions of petroleum crude oil emulsions with different water cut. An optical microscope was used as a reference technique. The correlation between the two techniques was overall good.

Compared to many other techniques, the NMR can analyze concentrated and opaque samples, such as petroleum emulsions. Measurements are performed within one minute, and no sample preparation is needed. One of the major advantages with the presented technique is its ability to obtain the droplet size distribution without making any assumptions on the shape of the distribution. This means that the method is capable of obtaining bimodal size distributions. Another potentially promising feature is the NMR signal profile which can be used to study emulsion stability.

Acknowledgments

The authors thank Sèbastien Simon for proof-reading the paper. Nils van der Tuuk Opedal thanks StatoilHydro for a PhD grant.

References

1. Asano, Y. and K. Sotoyama, Food Chemistry, 1999. **66**: p. 327-331.
2. Otsubo, Y. and R.K. Prud'homme, Rheologica Acta, 1994. **33**: p. 303-306.
3. Basheva, E.S., et al., Langmuir, 1999. **15**: p. 6764-6769.
4. Chakraborty, M., C. Bhattacharya, and S. Datta, Colloids and Surfaces A: Physiochem. Eng. Aspects, 2003. **224**: p. 65-74.
5. Coupland, J.N. and D.J. McClements, Journal of Food Engineering, 2001. **50**: p. 117-120.
6. Hemmingsen, P.V., et al., *Droplet Size Distributions of Oil-in-Water Emulsions under High Pressures by Video Microscopy*. 2nd Edition ed. Emulsion and Emulsion Stability, ed. J. Sjöblom. Vol. 132. 2006, Boca Raton: Taylor & Francis.
7. Tanner, J.E. and E.O. Stejskal, The Journal of Chemical Physics, 1965: p. 288-292.
8. Tanner, J.E. and E.O. Stejskal, The Journal of Chemical Physics, 1968. **49**: p. 1768-1777.
9. Goudappel, G.-J.W., J.P.M.v. Duynhoven, and M.M.W. Mooren, Journal of Colloid and interface Science, 2001. **239**: p. 535-542.
10. Fourel, I., J.P. Guillement, and D.L. Botlan, Journal of Colloid and interface Science, 1995. **169**: p. 119-124.
11. Duynhoven, J.P.M.v., et al., European Journal of Lipid Science and Technology 2007. **109**: p. 1095-1103.
12. Kiokias, S., A.A. Reszka, and A. Bot, International Dairy Journal, 2004. **14**: p. 287-295.
13. Aichele, C.P., et al., Journal of Colloid and interface Science, 2007. **315**: p. 607-619.
14. Packer, K.J. and C. Rees, Journal of Colloid and interface Science, 1972. **40**(2): p. 206-218.
15. Li, X., J.C. Cox, and R.W. Flumerfelt, The American Institute of Chemical Engineers Journal, 1992. **38**(10): p. 1671-1674.
16. Balinov, B., O. Söderman, and T. Wärnheim, Journal of the American oil Chemists' Society, 1994. **71**(5): p. 513-518.
17. Enden, J.C.v.d., et al., Journal of Colloid and interface Science, 1990. **140**(1): p. 105-113.
18. Callaghan, P.T., K.W. Jolley, and R.S. Humphrey, Journal of Colloid and interface Science, 1983. **93**(2): p. 521-529.
19. Peña, A.A. and G.J. Hirasaki, Advances in Colloid and Interface Science, 2003. **105**: p. 103-150.
20. Mitra, P.P., P.N. Sen, and L.M. Schwatrz, Physical Review B, 1993. **47**(14): p. 8565-8574.
21. Sørland, G.H., et al., Diffusion Fundamentals, 2007. **5**: p. 4.1-4.15.
22. Kärger, J. and D.M. Ruthven, *Diffusion in Zeolites and other Microporous Solids*. 1992, New York: Wiley.
23. Hurlimann, M.D., et al., Journal of Magnetic Resonance, Series A, 1994. **111**(2): p. 169-178.
24. Uh, J. and A.T. Watson, Industrial & engineering chemistry research, 2004. **43**: p. 3026-3032.
25. Cohen, M.H. and K.S. Mendelson, Journal of Applied Physics, 1982. **53**: p. 1127.
26. Balinov, B. and O. Söderman, *Emulsion - the NMR Perspective*. Encyclopedic handbook of Emulsion Technology, ed. J. Sjöblom. 2001, New York: Marcel Dekker.

27. Sørland, G.H., *Method for measuring the content of fat/oil in multi component system. Patent number 6946837*. 2005: United States.
28. Gu, G., et al., Colloids and Surfaces A: Physiochem. Eng. Aspects, 2003. **215**: p. 141-153.
29. Meiboom, S. and D. Gill, The Review of Scinetific Instruments, 1958. **29**(8): p. 688-691.
30. Denkova, P.S., et al., Langmuir, 2004. **20**: p. 11402-11413.
31. McClean, J.D. and P.K. Kilpatrick, Journal of Colloid and interface Science, 1997. **196**: p. 23-34.
32. Peña, A.A. and G.J. Hirasaki, *NMR Characterization of Emulsions*. Emulsion and Emulsion Stability, ed. J. Sjöblom. Vol. 132. 2006, Boca Raton: Taylor & Francis.
33. Dalen, G.v., Journal of Microscopy, 2002. **208**: p. 116-133.
34. Zhang, X., C.-G. Li, and M.-L. Liu, Analytical Chemistry, 2001. **73**: p. 3528-3534.

Paper II

Energy Fuels **2010,** *24,* 3628–3633 · DOI:10.1021/ef100268x
Published on Web 06/02/2010

energy&fuels
article

Emulsion Stability Studied by Nuclear Magnetic Resonance (NMR)

Nils van der Tuuk Opedal,*,† Geir Sørland,‡ and Johan Sjöblom†

†*Ugelstad Laboratory, Department of Chemical Engineering, Norwegian University of Science and Technology (NTNU), N-7491 Trondheim, Norway, and* ‡*Anvendt Teknologi AS Munkvollveien 56, N-7022 Trondheim, Norway*

Received March 8, 2010. Revised Manuscript Received May 10, 2010

A method using low-field nuclear magnetic resonance (NMR) for measurement of water-in-crude oil emulsion stability has been optimized and compared to light transmission measurements. Two NMR sequences have been used; one of them applies a diffusion T_2-weighted profile measurement sequence, which can return a water profile of an emulsion within 30 s. The stability of the emulsions was compared by studying emulsions in parallel in Turbiscan and NMR. Three different crude oils were used in the experiment. The emulsions prepared had water cut at 50%. The correlation between NMR and Turbiscan regarding the free water formation was good for the emulsions. The potential limitations and advantages of the technique are discussed.

1. Introduction

The extraction of petroleum is often performed offshore with the inevitable presence of water or with water used to aid the exploitation. Crude oils are known to contain several emulsion-stabilizing compounds, making the process to remove water potentially difficult. Asphaltenes and resins are two solubility classes of crude oils proven to form barriers at the interface between water and oil, retarding water droplet coalescence.[1−4] In addition, solid particles originating from the reservoir adsorbed to the water−oil interface may also contribute to the stability of the water droplets.[5,6] With that said, a lot of resources are spent to study the mechanisms of crude oil emulsion stability. In addition, the reasons for that are plentiful. Pipeline and process equipment are prone to corrosion with water present in the fluid stream. Another important factor is that the viscosity of an emulsion increases with an increasing amount of dispersed liquid, making the transportation potentially more energy-consuming than necessary. Finally, the oil refinery has a limit on the accepted amount of water in its incoming oil stream. All of these factors highlight the importance of emulsion stability.

One of the most used methods to study the emulsion stability of crude oil is the bottle test.[1,3,7,8] With this method, oil and water is mixed and allowed to stand for a defined time in a graduated cylinder. Thereafter, the height of the water phase is recorded, and the quality of the water phase is determined by visual observation. This method is often performed together with addition of certain chemicals, centrifugation, and/or heating of the mixture depending upon the goals of the study. The advantage of this method is its easy concept and implementation. A possible disadvantage is the error because of the difference in the perception of the height of the water−oil interface of the sample by different researchers. In addition, studying the kinetics of free water formation can be very time-consuming with this method.

Using electric field and conductivity measurements is another method to characterize water-in-oil emulsion stability. With no field applied, the water droplets move randomly according to Brownian motion and Stoke's law. However, with increasing field strength, the droplets tend to align between the electrodes because of polarization. After a critical value of the electric field (E_{crit}), the water droplets have coalesced and formed a bridge of water between the two electrodes. The electrolytes in the water cause an increase in the measured conductivity. The study of emulsion stability at electric fields is purposeful, but no information regarding sedimentation and coalescence rates can be obtained. In addition, there is no quantification as to how much water has coalesced. The conductivity measurement is only sensitive to the formation of a bridge of free water. That means that, even though coalescence is indicated, a substantial amount of water can still be in the form of droplets.[9,10]

Light transmission measurements on unstable emulsions have been performed in previous studies.[11,12] When the transmission of a light source applied to an emulsion is recorded, the stability can be studied. The automated acquisition of transmission profiles is useful to study the kinetics in the formation of the free water phase. In addition, clearification of the water phase can be quantified without the possible difference in results because of different research. With that,

*To whom correspondence should be addressed. Telephone: +47-735-50924. Fax: +47-735-94080. E-mail: nils.opedal@chemeng.ntnu.no.

(1) McClean, J. D.; Kilpatrick, P. K. *J. Colloid Interface Sci.* **1997**, *196*, 23–34.
(2) Graham, B. F.; May, E. F.; Trengove, R. D. *Energy Fuels* **2008**, *22*, 1093–1099.
(3) Gafonova, O. V.; Yarranton, H. W. *J. Colloid Interface Sci.* **2001**, *241*, 469–478.
(4) Sjöblom, J.; Aske, N.; Auflem, I. H.; Brandal, Ø.; Havre, T. E.; Sæther, Ø.; Westvik, A.; EJohnsen, E.; Kallevik, H. *Adv. Colloid Interface Sci.* **2003**, *100−102*, 399–473.
(5) Angle, C. W. *Can. J. Chem. Eng.* **2004**, *82*, 722–734.
(6) Binks, B. P.; Lumsdon, S. O. *Langmuir* **2000**, *16*, 8622–8631.
(7) Payet, L.; Terentjev, E. M. *Langmuir* **2008**, *24*, 12247–12252.
(8) Arla, D.; Sinquin, A.; Palermo, T.; Hurtevent, C.; Graciaa, A.; Dicharry, C. *Energy Fuels* **2007**, *21*, 1337–1342.
(9) Aske, N.; Kallevik, H.; Sjöblom, J. *J. Pet. Sci. Eng.* **2002**, *36*, 1–17.
(10) Kallevik, H.; Kvalheim, O. M.; Sjöblom, J. *J. Colloid Interface Sci.* **2000**, *225*, 496–504.
(11) Dalmazzone, C.; Noïk, C. SPE, Oilfield Chemistry. International Symposium of the Society of Petroleum Engineers, Houston, TX, Feb 13−16, 2001.
(12) Miller, D. J. *Colloid Polym. Sci.* **1987**, *265*, 342–346.

light transmission measurements are a significant improvement of the bottle test. However, for samples with little or no transmission, such as crude oil emulsions, this technique is not ideal to use because of difficulties with interpreting transmission profiles of crude oil emulsions. Still, keeping the improvement compared to the bottle test in mind, the use of light transmission does not give reliable information on the vertical movement of the droplets. Only the formation of free water can be studied. Another automated and nonperturbing method used to study emulsion stability is the use of ultrasound. Ultrasonic characterization can give information on both the sedimentation and the coalescence of an emulsion.[13] However, polydisperse samples can lead to anomalous results because the velocity of ultrasound is dependent upon the droplet size.

Using low-field nuclear magnetic resonance (NMR) to study water-in-oil emulsion, emulsion studies have reached a higher level. The main advantage of the technique is that the entire sample is considered. Not only can the NMR give information of the time of formation of free water, but it can also yield information on the sedimentation of the droplets in the continuous phase. NMR is routinely used to measure the water content of crude oil samples.[14,15] However, such methods consider the sample as a whole; position-dependent differences are not taken into account. However, NMR can also give more detailed information about a sample. For instance, McDonald et al. used NMR to study position-dependent droplet size distributions of oil-in-water emulsions.[16] Another way of using NMR is to study the brine profiles of settling emulsions. Jiang et al.[17,18] studied the stability of diluted bitumen water-in-oil emulsions using a NMR sequence, which returned brine profiles, enabling us to calculate the sedimentation rate.

This paper has compared the formation of the free water rate obtained from the profile measurement of the NMR with the acquisition of transmission profiles of Turbiscan. The aim of the comparison between the two techniques is to examine the performance of the NMR sequences for emulsion stability measurements. Some of the older NMR sequences reported in the literature have a long resolution time. One of the sequences in this paper can return a profile after 30 s, increasing its range of application. Emulsions have been prepared from different crude oil samples, all with a water cut of 50%.

2. Experimental Section

2.1. Materials. Three different crude oils were used in this study, key properties of which are found in Table 1. The water cut for all emulsions was 50%. The brine (3.5 wt % NaCl) had an initial pH of ~6.5.

2.2. Emulsion Preparation. The emulsions were prepared by mixing the crude oils with brine at 33 °C in a water bath. The total sample volume of all emulsions was 30 mL. The mixing was performed with a four-bladed propeller at a stirring speed of 1500 rpm for 5 min. The emulsions were immediately distributed after mixing to the NMR and Turbiscan sample tubes for simultaneous analysis.

Table 1. Summary of the Key Crude Oil Properties at 40 °C

crude oil	density (g/cm^3)	viscosity (mPa s)	T_2 relaxation peak (ms) (33 °C)
A	0.895	25.6	173
B	0.922	85.6	63.3
C	0.996	21100	7.60
C diluted with 30% toluene	0.952	35.8	63.6
C diluted with 50% toluene	0.925	5.6	241

2.3. Turbiscan. Turbiscan is a commercial tool for dispersion analysis. It consists of a light source of near-infrared light with a wavelength at 850 nm moving vertically and two detectors moving simultaneously for recording of backscattered and transmitted light. One measurement takes approximately 20 s.

Because the NMR magnet is tempered at 33 °C to maintain the homogeneity of the magnetic field, the measurements performed in Turbiscan were also performed at 33 °C to avoid any potential differences because of the temperature. The free water formation rate was obtained by calculating the thickness/height of the area with transmission.

2.4. Low-Field NMR. The NMR measurements were performed on an Oxford Instruments MARAN Ultra spectometer. The magnetic field is 23 MHz and 0.5 T, with a gradient strength of 4 T/m. The duration of the sinusoidal gradient pulse is 0.4 ms, and the direction of the gradient is along the length of the tube. Two NMR sequences where used in this study. The first NMR sequence used for obtaining brine profiles in this paper is given in a previous work. This sequence returns a brine profile every 2 min.[19] The same work explains the method and sequence for measuring the initial droplet size distribution.

In Figure 1, we have shown the second NMR sequence used for measuring the brine profile. Initially, the NMR signal contains a crude oil and brine contribution. Because of a significantly lower transverse relaxation time for the crude oil, one may use the C1 loop to suppress the contribution from the crude oil. The first gradient echo is then from brine only, and a Fourier transform of this echo yields a brine profile. The second loop is used to measure a gradient echo at an even longer observation time, which gives another brine profile. These two profiles may then be used to correct for transverse relaxation of the brine signal, ending with a third brine profile, which is unaffected by transverse relaxation processes. This profile is proportional to the brine content along the sample, and by calibrating with a sample that contains 100% brine, one can measure the brine content along the length of the emulsion (see Figure 2).

The first NMR sequence is time-consuming because it only records one profile per scan. Thus, two scans at different Δ are required to account for relaxation of the brine signal and acquire relaxation-weighted brine content. In addition, four scans are required to run through a proper phase cycle.[20] The second method records two profiles at different observation times per scan and may account for relaxation effects in one scan. The second sequence consists of two loops of spin echoes, where convection terms (as found in unstable emulsions) are compensated. Thus, one may measure true convection-compensated profiles for every second echo in the sequence.

To be able to set the optimum acquisition parameters for the NMR droplet size distribution measurement and the brine profile measurement, a CPMG measurement was performed

(13) McClements, D. J. *Adv. Colloid Interface Sci.* **1991**, *37*, 33–72.
(14) Peña, A. A.; Hirasaki, G. J. In *NMR Characterization of Emulsions*; Sjöblom, J., Ed.; Taylor and Francis: London, U.K., 2006; Vol. 132.
(15) Peña, A. A.; Hirasaki, G. J. *Adv. Colloid Interface Sci.* **2003**, *105*, 103–150.
(16) McDonald, P. J.; Ciampi, E.; Keddie, J. L.; Heidenreich, M.; Kimmich, R. *Phys. Rev. E: Stat., Nonlinear, Soft Matter Phys.* **1999**, *59*, 874–884.
(17) Jiang, T.; Hirasaki, G.; Miller, C.; Moran, K.; Fleury, M. *Energy Fuels* **2007**, *21*, 1325–1336.
(18) Jiang, T.; Hirasaki, G.; Miller, C.; Moran, K. *Energy Fuels* **2008**, *22*, 4158–4164.
(19) Opedal, N.; Sørland, G.; Sjöblom, J. *Diffus. Fundam.* **2009**, *9* (7), 1–29.
(20) Fauth, J.; Schweiger, A.; Braunschweiler, L.; Forrer, J.; Ernst, R. *J. Magn. Reson.* **1986**, *66*, 74.

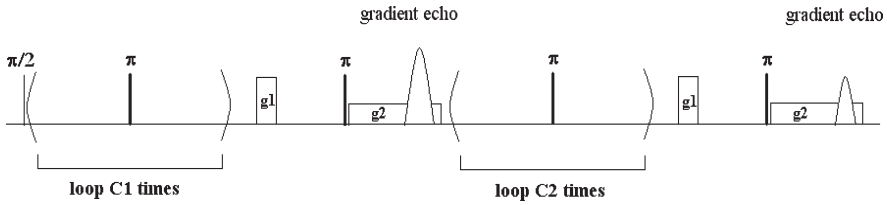

Figure 1. NMR sequence used for acquiring the brine profile.

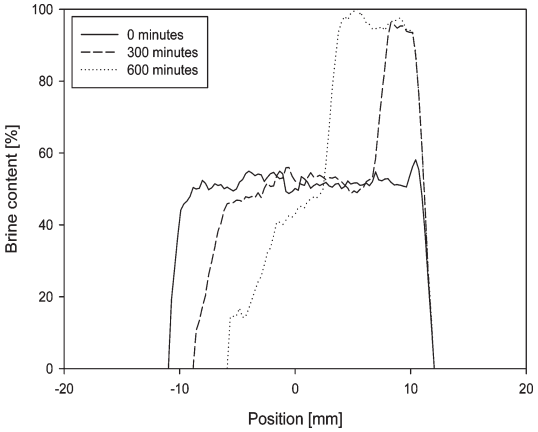

Figure 2. Different brine profiles that give the brine content along the sample. The bottom of the sample is situated around position ~12 mm, and the top of the sample is situated around position ~−11 mm.

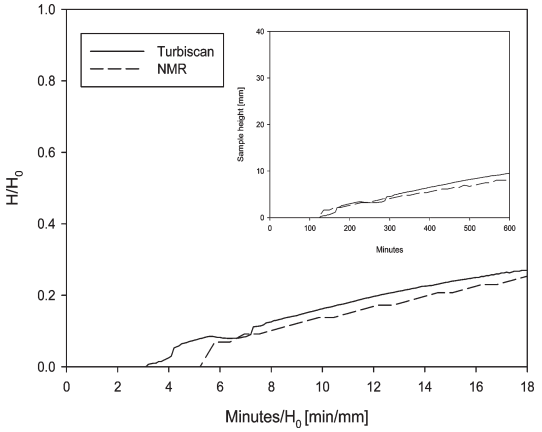

Figure 3. Development of free water of a crude A emulsion. The y axis is normalized sample height (H/H_0), and the x axis is normalized time (minutes/H_0). The inset shows the raw data.

on the different crude oils and the pure brine phase, yielding a T_2 distribution.[21,22] Dependent upon the T_2 values of the crude oil, the water signal was separated from the crude oil signal by letting the water signal be recorded after the oil signal had relaxed. The same procedure applies for the NMR sequence given in Figure 1 that measures the brine profile. However, then, one must set the C1 value correct, such that the crude oil signal has relaxed to an insignificant value at the time of the first gradient echo that gives the first brine profile.

3. Results and Discussion

3.1. Differences between the Two Techniques. When the performance of two different methods is compared, it is important to keep in mind any differences in the technique of the methods used. Light transmission measurements can be highly sensitive to wall effects. If, for instance, a thin film or a droplet of dark crude oil is sticking to the wall of the sample tube, this can affect the measurement of phase separation. Another feature of gravity batch separation is the sample tube dimensions. The NMR requires a sample volume of about 3 mL. This corresponds to a height of roughly 20 mm in the sample tubes used in this experiment. On the other hand, the sample tubes used in Turbiscan require a sample height of 40 mm. That means that droplets prepared from the same batch will not sediment the same distance when their instability is studied in different sample tubes. The sample tube diameter is also different, which can influence the effect of retarded droplet movement along the wall. Thus, the difference in sample tube diameter can have an influence on the coalescence time. Another possible source of error is the techniques themselves. A water−oil interface can be curved. The position of a curved interface can be interpreted differently depending upon the technique used. For instance, a layer of densely packed water droplets at the oil−water interface can be interpreted as oil by the light transmission technique, whereas the NMR can interpret the same region as mostly water. With the mentioned differences in mind, it is not necessarily expected to see a perfect agreement between the two methods. Because of the difference in height of the sample tubes, the comparison of the results has been illustrated with normalized sample heights (H/H_0) on the y axis and normalized time (minutes/H_0) on the x axis.

3.2. Formation of Free Water: Comparison between NMR and Turbiscan. In the figures giving the comparison between Turbiscan and NMR, the rate of free water formation has been obtained by plotting the width of the area with 90% water. As seen in Figure 2, even though a region of free water has formed, the brine profile does not indicate accurately 100% of water in that region. An example of the comparison between the two techniques can be seen in Figure 3. The two curves indicate the boundary between free water and the emulsion phase. Both techniques indicate an appearance of free water after approximately 120 min for the given sample. Three runs with similar experimental conditions were studied with this particular oil−water system. The NMR indicated that the first appearance of free water came after 144 ± 18 min, whereas Turbiscan indicated a time of 134 ± 50 min. The further increase in the height of the water phase seems to be almost linear and reasonably similar for

(21) Carr, H. Y.; Purcell, E. M. *Phys. Rev. A: At., Mol., Opt. Phys.* **1954**, *94* (3), 630–638.
(22) Meiboom, S.; Gill, D. *Rev. Sci. Instrum.* **1958**, *29* (8), 688–691.

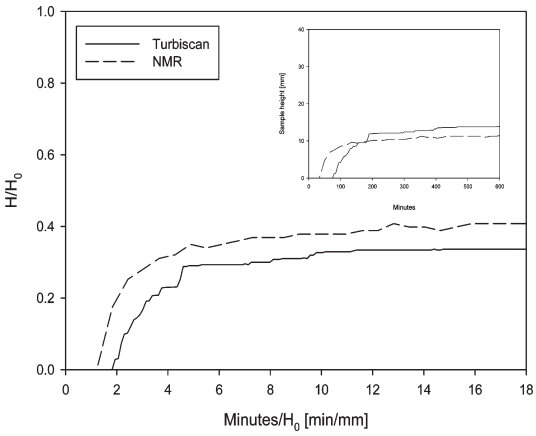

Figure 4. Development of free water of a crude C emulsion diluted with 30% toluene with 50% water cut. The *y* axis is normalized sample height (H/H_0), and the *x* axis is normalized time (minutes/H_0). The inset shows the raw data.

both techniques. A feature evident for all samples was that the height of free water in the NMR parallels was higher than that from the Turbiscan measurements.

The three mentioned runs from the NMR indicated that on average ~55% of the initial water had coalesced after 600 min, whereas Turbiscan indicated an average of ~36% free water. The reason for this difference can be attributed to the parameters mentioned in section 3.1. Even for systems that were separated before 600 min had passed exhibited a difference in the total amount of free water. Figure 4 illustrates the difference of the amount of free water for an emulsion of crude C diluted with 30 wt % toluene. The separation is complete after approximately 200 min. Still, the NMR indicates a ~20% difference in terms of the amount of free water.

When the data from NMR are analyzed, it is important to check whether the water profiles return the same amount of water as was added in the emulsions. This can be performed by integrating each position with regard to the amount of water over the total sample height. Figure 5 shows the results of this integration. As can be seen, there is a good recovery of the water for all of the profiles, making the profiles credible for further analysis. The emulsions studied in this paper contained 50% water. Had the integration showed in Figure 5 given an amount of water higher than 50%, it would indicate inclusion of the oil signal. All samples exhibited a small decrease in the amount of water as a function of time. The reason for the small decrease is not yet determined.

The second NMR sequence, illustrated in Figure 1, was able to obtain the water profiles of unstable emulsions within 30 s. The rate of free water formation was compared to similar measurements in Turbiscan. Figure 6 illustrates the development of free water formation over time. It should be noted that these emulsions were not studied in parallel because of the high degree of instability. This could contribute to any miscorrelations. The oil-phase viscosity was 5.6 mPa s, and as the figure indicates, the emulsion is not very stable. The rate of free water formation from the NMR indicates the appearance of free water even after the first scan is complete. After approximately 5 min, most of the water droplets have coalesced.

3.3. Sedimentation from NMR. Unlike Turbiscan, the NMR can give information on the water content in the entire sample.

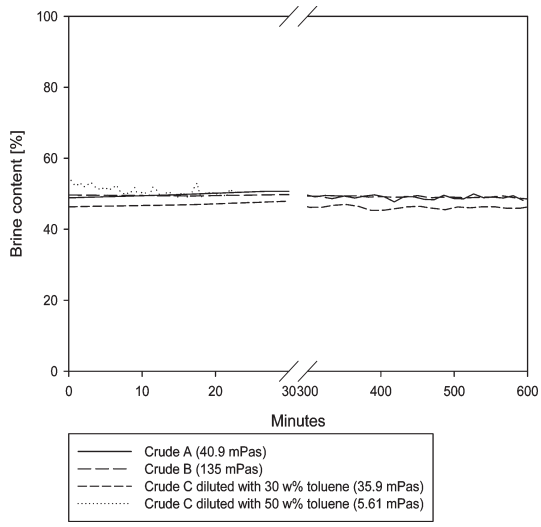

Figure 5. Brine balance for the emulsions studied. The oil-phase viscosity is given in parentheses in the legend.

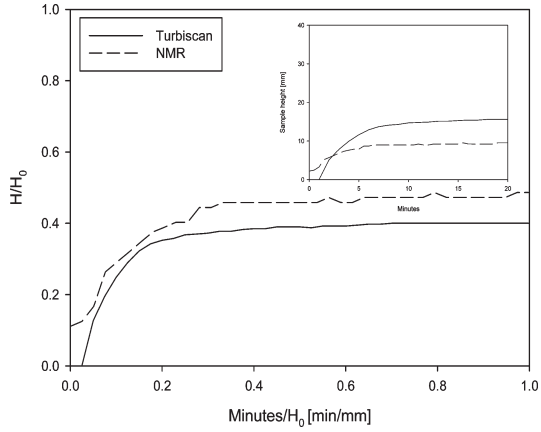

Figure 6. Development of free water of a crude C emulsion diluted with 50% toluene with 50% water cut. The *y* axis is normalized sample height (H/H_0), and the *x* axis is normalized time (minutes/H_0). The inset shows the raw data.

This can give information on the vertical movement of the water in the oil phase, in addition to the formation of pure water. Figure 7 shows an example of the information one can collect from this method. The figure displays the development of an emulsion from crude A. The figure has been obtained by plotting the movement of five different fronts from the water profile scans (Figure 2). Three of the lines are representative of sedimentation of the droplets. An emulsion will in most cases have a distribution of droplet sizes, and the sedimentation velocity of droplets of different sizes will be different. The first line, the 0% water line, indicates the end point at which the NMR detects water. The movement of this line can be considered as the sedimentation of the smallest and most stable droplets, and the area above this line can be considered as a pure oil phase. In the literature, this have been previously been called the sedimenting interface.[23] The next line is the 25% line.

(23) Jeelani, S. A. K.; Hartland, S. *Ind. Eng. Chem. Res.* **1998**, *37*, 547–554.

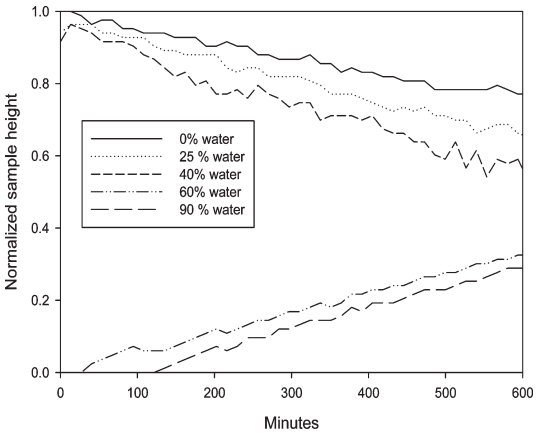

Figure 7. Vertical movement of water in a crude A emulsion studied in the NMR.

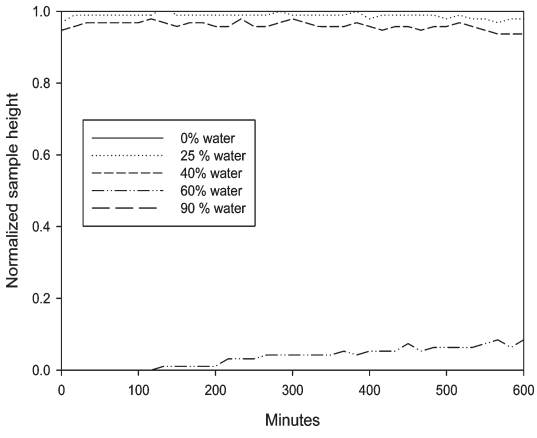

Figure 8. Vertical movement of water in a crude B emulsion studied in the NMR.

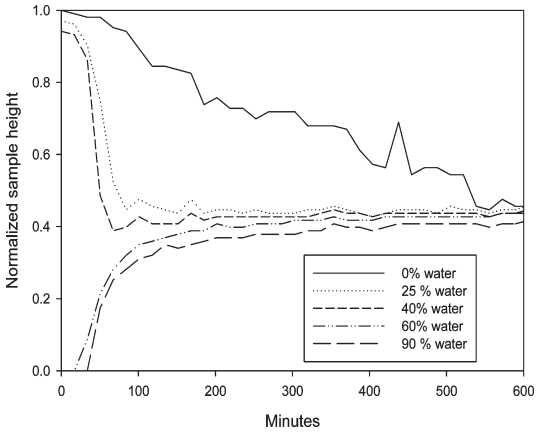

Figure 9. Vertical movement of water in a crude C emulsion diluted with 30 wt % toluene studied in the NMR.

This represents half of the amount of water compared to the initial emulsion concentration and can loosely be thought of as the sedimentation of the average/mean-sized droplets. The next line is the 40% line. This can be considered to represent the sedimentation of the fraction of the largest droplets in the emulsion.

The two last lines can be considered as the accumulation of water at the bottom of the tube. The 60% water line represents a region of increased water concentration compared to the original emulsion concentration. That means that the area between the 40% water line and the 60% water line can be considered as the area of the sample with the water content more or less similar to the initial state of the emulsion. The last line, the 90% water line, has already been discussed in the section above. This can be considered to be representative of a free water phase.

When a simple linear regression is performed on the 25% water line in Figure 7, a crude estimation on the sedimentation velocity can be calculated. The fit gave a R^2 of 0.98 and a sedimentation velocity of 0.011 mm/min. When the initial droplet size distribution of the emulsion is analyzed, Stokes' sedimentation velocity can be calculated. The mean droplet size was measured to be 9.4 μm, giving a velocity of 0.014 mm/min. Although Stokes' sedimentation velocity has been derived with the assumption of no droplet−droplet interactions, the two velocities are within the same order of magnitude. This indicates that the droplets sediment largely without any increased sedimentation because of binary coalescence or clustering/flocculation or hindered sedimentation because of the high water cut. The development of the 60 and 90% water lines indicates that free water only after a certain amount of droplets accumulates at the bottom of the tube.

Figure 8 illustrates the development of a crude B emulsion. In comparison to Figure 7 and the crude A emulsion, this emulsion exhibits little vertical movement of droplets. The initial droplet radius was measured to be 3.0 μm. That gives Stokes' sedimentation velocity of 0.000 27 mm/min, which correlates well with the stability of the emulsion. However, the same trend as seen in Figure 7 regarding the accumulation of droplets at the bottom can be observed for this emulsion with the 60% water line.

The sedimentation and coalescence of an emulsion of crude C diluted with 30 wt % toluene is displayed in Figure 9.

The 0% water line in Figure 9 is a bit undulating/oscillating but appears linear overall. However, the 25 and 40% water lines both abruptly increase the sedimentation velocity. This can be explained by enhanced sedimentation because of droplet−droplet interactions. The initial droplet size was measured to be 9.1 μm, giving a calculated sedimentation velocity of 0.007 mm/min for this system, a value much lower than what is observed in the figure. The reason for the undulating behavior of the 0% line in Figure 9 can be that the amount of water is low in that area. The local low concentration of the water can increase the uncertainties of the measurements.

The oil-phase viscosity of crude C diluted with 30 wt % toluene is quite similar to the viscosity of crude A. The viscosity of both oils is given in the legend in Figure 5. The initial droplet size was also similar for both systems, but still, the emulsion of diluted crude C exhibited a lower stability than the emulsion of crude A. The reason for this has not been further investigated, but an explanation could be due to the dilution with toluene. The dilution with toluene could change the solubility properties enough to change the stabilizing properties of the surfactants present in the oil. Thus, unperturbed oil, with similar viscosity, could exhibit a higher degree of stability. The importance of the solubility properties

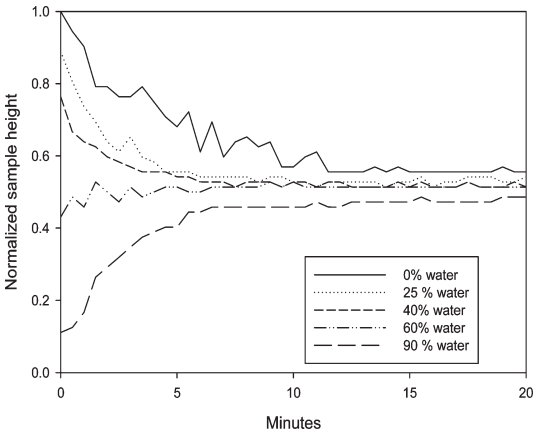

Figure 10. Vertical movement of water in a crude C emulsion diluted with 50 wt % toluene studied in the NMR.

in context with crude oil emulsion stability has been studied before.[1]

An emulsion of crude C diluted with 50 wt % toluene is displayed in Figure 10. The oil phase had a viscosity of 5.6 mPa s. The separation for this emulsion is operating at a completely different time scale than the one shown in Figure 9. As can be seen, the separation is more or less complete after about 10 min. Because of the low viscosity of the oil phase and the high degree of instability of the emulsion, it was not possible to measure the initial droplet size distribution. The same trend as seen in Figure 9 with regard to the undulating behavior of the 0% water line is observed in Figure 10. It should also be noted that the emulsion has already formed free water before the first brine profile was obtained; free water formed approximately 2 min after the mixing was turned off.

A feature observed for the last two emulsions, Figures 9 and 10, in this study indicated that a small fraction of the droplets exhibited a very high stability. For instance, the emulsion displayed in Figure 10 does not achieve complete phase separation. The figure includes scanning until 20 min, but analyzing the same sample after several hours showed little or no difference in the amount of free water formed. This could mean that a small fraction of the droplets is highly resistible to coalescence or that the water−emulsion interface is curved.

4. Conclusions

Coalescing water-in-oil emulsions have been studied with light transmission measurements and NMR. The comparison of the two techniques indicated a good correlation regarding the rate of formation for free water. The NMR method can, in addition to the coalescence rate, give information on the sedimentation of the droplets. The acquisition time for the second NMR sequence is 30 s, which can be useful to study emulsions with high sedimentation and coalescence rates. Oils with viscosity down to 5 mPa s can be studied.

Acknowledgment. Nils van der Tuuk Opedal thanks Statoil for a Ph.D. grant.

Paper III

Enhanced Sedimentation and Coalescence by Chemicals on Real Crude Oil Systems

Nils van der Tuuk OPEDAL, Iva KRALOVA, Caterina LESAINT, Johan SJÖBLOM

Ugelstad Laboratory, Department of Chemical Engineering, the Norwegian University of Science and Technology (NTNU), N-7491 Trondheim, Norway.

Corresponding author: Nils van der Tuuk Opedal, Dept of Chemical Engineering, the Norwegian University of Science and Technology (NTNU), E-Mail: nils.opedal@chemeng.ntnu.no

Abstract

Water-in-oil emulsions of a crude oil were prepared and destabilized by addition of demulsifiers. The goal of the study was to compare two different techniques used to evaluate demulsification effectiveness and to study the interfacial response of the demulsifiers. The stability of these emulsions was determined in the E_{Crit} cell and low field NMR and the interfacial response of the demulsifiers was measured in with the oscillating drop method. The E_{Crit} cell measures the electric field required to induce the formation of free water and the NMR monitors the vertical movement of dispersed water droplets. The stability measurements and the interfacial response gave different indications on the demulsifier effectiveness at different demulsifier concentrations. The difference could be attributed to the difference between how the stability is measured or by the effect of the electric field on the demulsifiers. The separation profiles obtained in the NMR illustrated that the demulsifiers increase the sedimentation velocity at increasing demulsifier concentration. The water recovery rates indicated that the demulsifiers had different properties. The interfacial study showed that low concentrations of demulsifiers decrease both the elastic and viscous modulus of water-crude oil interface. At higher dosages both moduli increase. The different trends can be explained by considering the ratio between the total interfacial area and the demulsifier doseage. The demulsifier dosage was kept similar, but the amount of available area varied from the emulsion stability measurements and the interfacial study.

Keywords:

Emulsions stability, Sedimentation rate, Coalescence rate, Interfacial rheology, Demulsifiers, NMR.

1 Introduction

Stable w-o emulsions are a common industrial challenge within the crude oil industry. During the transportation of a multi phase mixture from the reservoir enough energy can be provided to break up and emulsify water droplets. A crude oil is a mixture of both molecules and particles with a wide range of sizes and functionalities and several of these contribute to the formation and the stability of emulsions. Solid particles of waxes [1 2], clays [1 3] or minerals [4 5] have been studied in connection with emulsion stability. Asphaltenes and resins are two solubility classes of crude oil identified as other important factors for the enhanced stability of water-in-crude oil emulsions. The interplay between the asphaltenes and resins form strong and elastic films at the oil-water interface. [6 7 8 9] The basic understanding of emulsion stability can be understood by two parameters: drop-drop collision frequency and collision success rate. There are various industrial applications used to manipulate these two parameters and destabilize emulsions. Most separation processes utilize a combination of mechanical [10], electrical [11], thermal [12] and/or chemical methods [13] to improve the separation.

When discussing the chemical aspect of emulsion treatment, one should differentiate between emulsion inhibitors and demulsifiers. Inhibitors are added before the liquids have been subjected to mixing, whereas demulsifiers are added after the emulsion has been formed. For emulsion inhibitors, one can predict a stability minimum using different parameters. The Hydrophilic-Lipophilic-Balance (HLB) is one such parameter, the Hydrophilic-Lipophilic-Deviation (HLD) is another more accurate parameter. The HLB balance indicates whether a surfactant, or a mixture of surfactants, will form an o/w or w/o emulsion. Low values typically form the latter, whereas higher values will favor the former. There are some limitations to this approach; the HLB-value does not take into account all relevant physicochemical parameters. The HLD takes into account the chain length, type of oil, temperature etc. However, due to the complexity of crude oil composition it is difficult to extrapolate the HLD concept as a universal rule of thumb. [14 15 16 17]

Although how interesting the use of the HLD and HLB concept to understand the process of adding an inhibitor is, one should keep in mind that in practice emulsion inhibition and demulsification are two entirely different processes; a surfactant successfully inhibiting the formation of a stable film might not be equally successful in destroying an already existing film. [18] Previous work has indicated that a successful demulsifiers should be able to influence several parameters. Firstly, the demulsifiers should be interfacial active and be able to change the film properties, such as reduce the interfacial viscosity, interfacial elasticity [19 20 21]. Another property of importance can be the changing of the wettability of solid particles at the

oil-water interface. [13] A third phenomenon is the ability to flocculate droplets. [22] There are many different patented demulsifiers, and most of the on-field industrial dosages consist of a mixture of different chemicals which all have different roles in the demulsification process. In terms of treating already formed droplets, the aging effect of the film is important to keep in mind. At similar dosages of a demulsifiers, an aged film might be less inclined to be destabilized. [23] Other important parameters are the resin to asphaltene ratio and the solvent quality of the crude oil. Given the complexity of a crude oil, and large differences between different reservoirs, to determine the correct dosage and chemical for a given oil-field does requires testing on a macroscopically level.

On a macroscopically level, the by far most used method to compare the effectiveness of demulsifiers has been the bottle test. The methodology of the bottle test is easy to understand, and on a practical level it is easy to perform the measurements. The major drawback is the lack of data one can obtain from this method. The only data possible to extract is the amount of water resolved. In some cases it is possible to monitor the sedimentation, but that requires a sample permitting enough transparency in the oil phase. In addition, the method only allows the determination of a sedimentation front. An emulsion with a distribution of droplet sizes will exhibit a distribution of sedimentation rates. Thus, measuring a sedimentation front will give limited information on the actual behavior of the system; position dependent differences are not elucidated. [24 25] Another drawback with the bottle test is the unknown state of the oil phase; little is known of the amount of water in the oil phase. It is possible to expand the information by using Karl Fischer to gain insight into the question. But the Karl Fischer method is again rather time consuming, and it can be troublesome to collect a sample from exactly the same location. Another technique used to compare optimum demulsifier and dosage is the E-critical measuring cell. With this technique, the emulsion is placed in an electrical field, and the magnitude of the applied field is increased. The current passing through the cell is continuously monitored, and when the droplets have coalesced and formed a bridge between the two electrodes the measured current is rapidly increasing. The field strength necessary to promote the increased current is label as E_{crit}. The technique is helpful for industrial plants which will use chemicals and electro-coalescence in combination. However, a demulsifier might behave different in an electrical field, so this method might not the perfect tool for determining the optimum dosage and the correct demulsifier for an industrial process without electro-coalescence. In addition, with the E_{crit} method there is no quantification on the water recovery. [26]

This study has used low-field NMR to study demulsifier efficiency for crude oil emulsions. The main advantage with the NMR is that it can be used to monitor the changes of water concentration of the entire sample in a non-intrusive way. [27] That means that both the rate of free water formation (interfacial coalescence rate) and the sedimentation rates of dark samples can be monitored. The method has showed to be very helpful for the comparison of different demulsifiers in terms of sedimentation rates, final oil quality and the thickness of layers of extra stable emulsion. The film properties of some of the demulsifiers were studied with the oscillating drop technique. Another goal of the work is the study the link between emulsion behavior on macro scale (sedimentation and coalescence rates) and micro scale (film properties) with the effect of different demulsifiers.

2 Experimental

2.1 Materials

The water phase was 3.5 w% NaCl with an initial pH of 6.5. The water cut was 40 % for all samples. Table 1 gives some key crude oil parameters.

Table 1 Key crude oil parameters.

Saturates (%)	37
Aromatics (%)	44
Resins (%)	16
Asphaltenes (%)	2.5[a]
Particle content (w%)	0.04
TAN (mg/g)	2.15
TBN (mg/g)	2.81
Density (kg/m^3, 33°C)	927
Viscosity (mPas, 33 °C)	156

[a] Using hexane.

Nine different demulsifiers were used in this study. They were described as polymerized polyols derived from substituted glycols. Since no other characterization was given by the suppliers, they are henceforth denoted as chemical 1, 2, 3, etc. The demulsifiers were dissolved in a xylene/methanol mixture (75:25 wt %) according to the procedure from the suppliers and selected amounts of the demulsifiers were added after the emulsification was complete.

2.2 Methods

2.2.1 Emulsion preparation

Emulsions were prepared by mixing water and oil with a four-bladed turbine for 5 minutes at a mixing speed of 2000 rpm at a temperature of 33°C. The total sample volume during mixing was 30 mL. Immediately after mixing, the demulsifiers were added and the solution was gently mixed for a few seconds. After addition of demulsifier, the samples were transferred to NMR tubes or the E-critical cell and analyzed.

2.2.2 Analysis by E-critical cell

The critical electric field was determined using the same apparatus and procedure developed by Aske et al. [28] The technique monitors the droplet coalescence by measuring the conductivity through an emulsion. The apparatus can in principle be used in two ways. One way is to gradually increase the electrical field. When there is free water in a continuous bridge between the two electrodes, the measured conductivity is increasing rapidly. The applied electric field which induces this jump in the measured current is called E_{crit} value, where a higher value of the E_{crit} indicates more stable emulsions. Another method is to keep the field strength constant and register the time necessary to induce droplet coalescence and increase in conductivity. In this study the emulsions were injected into the cell and power supply was started at 0 V and increased by steps of 0.2 V/s. Five parallel measurements were performed on each emulsion and the average value and standard deviation were calculated. The experiments were performed at 33 °C with a 0.25 mm thick Teflon plate between the electrodes.

2.2.3 Analysis by NMR

A low field Oxford Instruments Maran Ultra 23 MHz NMR was used to obtain both the droplet size distribution and the separation profiles of the emulsions. The Droplet Size Distribution is obtained by measuring the diffusion of water confined as droplets in combination with measurement of the T_2 distribution of the water. [29] The separation profiles were obtained by measuring the position dependent signal of the sample at short and long observation times. [27 30] A more elaborate description of the sequences and the NMR technique can be found in the references. The NMR magnet was tempered to 33 °C.

2.2.5 Oscillating drop

The interfacial tension and rheology of the oil-water films was studied with a Sinterface PAT-1. The apparatus consist of a camera that monitors the shape of a droplet attached to a syringe needle. Measurements of the droplet shape make it possible to calculate the interfacial tension of the oil-water interface. The syringe is connected to a computer controlled piston and is capable of changing the droplet volume. By changing the droplet volume periodically in a sinusoidal manner the interfacial response can be studied. The Gibbs interfacial dilational modulus E can be described by the change in interfacial area and tension.

$$E = \frac{d\gamma}{d\ln A}$$

The interfacial dilational modulus is a complex function of the angular frequency ω, where the real part, E_d, is attributed to the interfacial elasticity and the imaginary part, $i\omega\eta_d$, is attributed to the interfacial viscosity.

$$E = E_d + i\omega\eta = E' + iE''$$

Where E' is the storage modulus and E'' is the loss modulus of the interface. In this study a freshly formed oil droplet was immersed in the saline water in a small cuvette via a u-bent needle of diameter 0.7 mm. The volume was varied in a sinusoidal manner with a period of 100 seconds and the interfacial tension was recorded. The drop volume oscillated around 25 mm^3 with amplitude of 1 mm^3.

2.2.6 Multivariate Analysis (MVA)

Multivariate data analysis is a useful tool for visualizing and extracting information from large data sets where more than one variable is analyzed simultaneously. [31] For the data analyzed in this study, the 9 demulsifiers were used as category variables and as normal variables the initial droplet size, interfacial tension, water recovery (80% recovery), sedimentation rate, high of water layer and thickness of emulsion layer all after 30 minutes of testing were used. Principal component analysis (PCA) was used to visualize and extract the major trends in the data sets by constructing (extracting) a new set of variables called principal components (PCs). Mathematically, PCA is an eigenvector type decomposition of the covariance matrix where successively orthogonal scores and loadings vectors are extracted

according to the principle of maximal explained variance. Given a data matrix **X** with *m* rows of samples and *n* columns of variables, the covariance matrix is defined as

$$\mathrm{cov}(X) = \frac{X^T X}{m-1} \tag{2}$$

The result of the PCA procedure is a decomposition of the data matrix **X** into principal components (*k*) called score and loading vectors

$$X_{n\times m} = t_1 p_1^T + t_2 p_2^T + t_i p_i^T + \ldots + t_k p_k^T + E_{n\times m} \tag{3}$$

where t_i is the score vector, p_i is the loading vector and E is the residual matrix. The score and loading vectors contain information on how the samples and variables relate to each other. A PCA transforms the data into a new orthogonal coordinate system of dimension k, where the first coordinate is called the first principal component (PC1); the second coordinate second principal component (PC2) and so on. The plot of score vectors against each other is called the score plot. The most common score plot is the score vector for PC1 versus the score vector for PC2, since these two often contain the major variance in the data.

PLS regression is used to fit a model to observed data in order to quantify the relationship between two groups of variables. This regression gives the size of the effects and interactions, the direction of the effects on the response and a model describing the relationship between the data blocks. The regression coefficients can be used to identify the most important variables in the model which will correspond to the effects found to be most significant by PCA. To avoid over fitting of the regression model, cross validation is used to determine the number of latent variables. The cross validation checks a model by repeatedly taking out different subsets of calibration samples from the model estimation and then the model is built using the remaining data and the eliminated part is predicted by this model. [32]

3 Results & Discussion

Emulsion stability in electric field

The demulsifier effectiveness and the optimum demulsifier dosage in terms of breaking emulsions were screened in the E-critical cell. Higher values of the E_{crit} mean that the emulsions are more stable. The ability to destabilize emulsions in an electrical field was varied for the demulsifiers, as seen in figure 1. Chemicals 7, 8 and 9 required a small dosage to decrease the E_{Crit} value. At a concentration of 30 ppm, the necessary field to induce destabilization is reduced from 0.55 kV to around 0.1 kV. At higher dosages the instability decreased somewhat, but not significantly. Chemicals 5 and 6 were also active, but had a less

pronounced effect on the stability. At a dosage of 90 ppm the E_{Crit} value was reduced to approximately the same value as chemicals 7,8 and 9. Chemicals 1, 2 and 3 exhibited an intermediate effect on the stability of the emulsions. Concentrations in the range of 30 – 50 ppm did not affect the stability much, however, at dosages higher than 90 ppm the E_{Crit} was reduced to half its initial value. Chemical 4 exhibited limited effect on the emulsion stability, even at a demulsifier concentration of 200 ppm. Dosages higher than 200 ppm did not affect the emulsion stability considerably for any of the chemicals. The low concentration necessary to reduce the stability for the most effective demulsifiers is common for many of the demulsifier system reported in the literature. A concentration optimum in the range of 20-100 ppm is reported. [33 34 19]

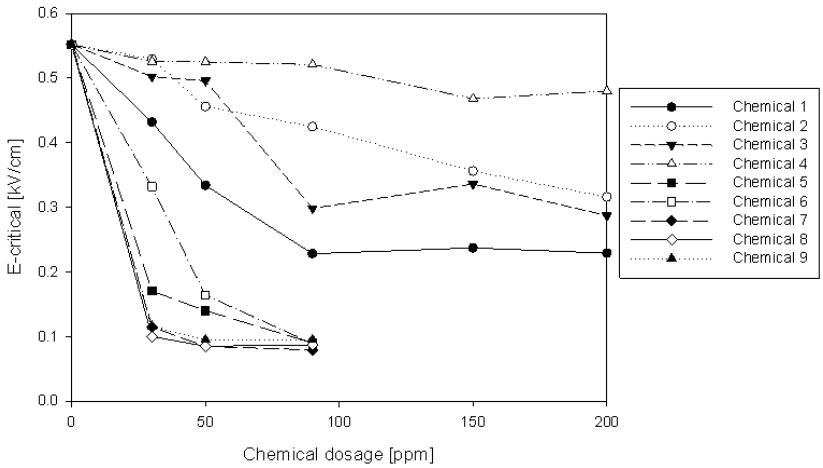

Figure 1 Effect of chemical dosage on the emulsion stability in an electrical field. Water cut 40%.

Separation data from NMR

Screening the demulsifiers with the E_{Crit} stability test shows the effectiveness with regard to the emulsion stability, and is a simple way for categorizing the demulsifiers in terms of coalescence. But the method does not quantify the amounts of water that has separated. To study the separation in detail, three of the demulsifiers were selected to be studied in the NMR. Two of the most effective demulsifiers, chemical 5 and 7, and a less effective demulsifier, chemical 4, were selected for further examination in the NMR. The separation data for the emulsions are given in figure 2. The contour plot shows the amount of water as a function of position and timescale for the emulsions. The solid lines highlight the iso-

volumetric curves of 0 %, 20 %, 40 %, 60 %, 80 % and 100 % of water. Red areas contain between 0 and 20 % water, yellow areas contain between 20 and 40 % water, green areas contain between 40 and 60 % water, the light blue areas contain between 60 and 80 % of water and the dark blue area contain between 80 and 100 % water. The crude oil used in this study is characterized as a heavy crude oil. A low density difference between water and oil and a high viscosity suggest that separating water droplets from such a crude oil can be difficult. Figure 2 a) illustrates this. The plot of the iso-volumetric curves in this figure indicates very slow vertical movement of the droplets for the timescales used in this study. All the iso-volumetric curves moves horizontally and there are no signs of accumulation of water at the bottom of the sample tube. However, by adding a small amount of demulsifier, it is possible to alter the separation time of the crude oil emulsions. As seen in figure 2 b), chemical 4 was added with a final concentration of 90 ppm and a larger sedimentation rate is observed. By following the iso-volumetric curve of 40 %, the sedimentation of a fraction of the water droplets is faster. After approximately 100 minutes there is breakthrough of free water. The distinction between the emulsion phase and free water is very sharp. There is no sign of accumulation of droplets for this emulsion. From the separation profile it seems as if the droplets are moving downwards and coalesce into free water rapidly after they have reached the bulk interface. Though the chemical is enhancing the sedimentation of some of the droplets, the iso-volumetric curves of 0 and 20 % appear to be moving as slowly as the one seen for the untreated emulsion in figure 2 a). That means that the oil phase still contains a considerable amount of dispersed water. After 300 minutes 85 % of the water is still present as dispersed droplets, and in the top quarter section of the vessel the amount of water has decreased from 40 % down to 16 %.

Chemicals 5 and 7 proved to be more efficient in breaking the emulsions, figure 2 c) and d) respectively. The sedimentation rates are much faster with the presence of these demulsifiers. The rate of free water formation indicates that both demulsifiers have similar effect on water recovery. However, the oil phase quality shows that chemical 5 is performing better than chemical 7. Within a similar time scale a larger fraction of the water droplets in the oil phase have been removed. After 180 minutes the amount of dispersed water in the sedimentation region is lower for the emulsion treated with chemical 5. Approximately 10 % of the water has not reached the oil-water bulk interface, where the amount of water in the top quarter position has gone down to 2 % from the original emulsion water cut of 40 %. For the droplets in the emulsion treated with chemical 7, around 21 % of the water has not reached the oil-water bulk interface and the amount of water in the top quarter region of the separation vessel

is 5 %. By judging the iso-volumetric curves in figure 2 d), the sedimentation velocity of the droplets in the sedimentation region is very slow, suggesting that these droplets have not been sufficiently affected by the chemicals.

Another difference between chemical 5 and 7 is the rate of interfacial coalescence and formation of droplet layers between the oil and water phase. The emulsion treated with chemical 5 can be seen forming a dense packed layer of droplets in the time interval between 7 and 20 minutes, after which the layer is collapsing. There is no sign of a dense packed layer of droplets resisting coalescence after 40 minutes. Even after 180 minutes of separation, when most of the droplets have reached the bulk water interface, there was no sign of significant accumulation of droplets. The distinction between the emulsion layer and the free water appears sharp. The emulsion treated with chemical 7 on the other hand has a less pronounced distinction between the free water and the emulsion region. The build up of a layer of droplets with a high resistance towards coalescence is seen in the time interval between 40 and 180 minutes with little changes in the extent of the layer.

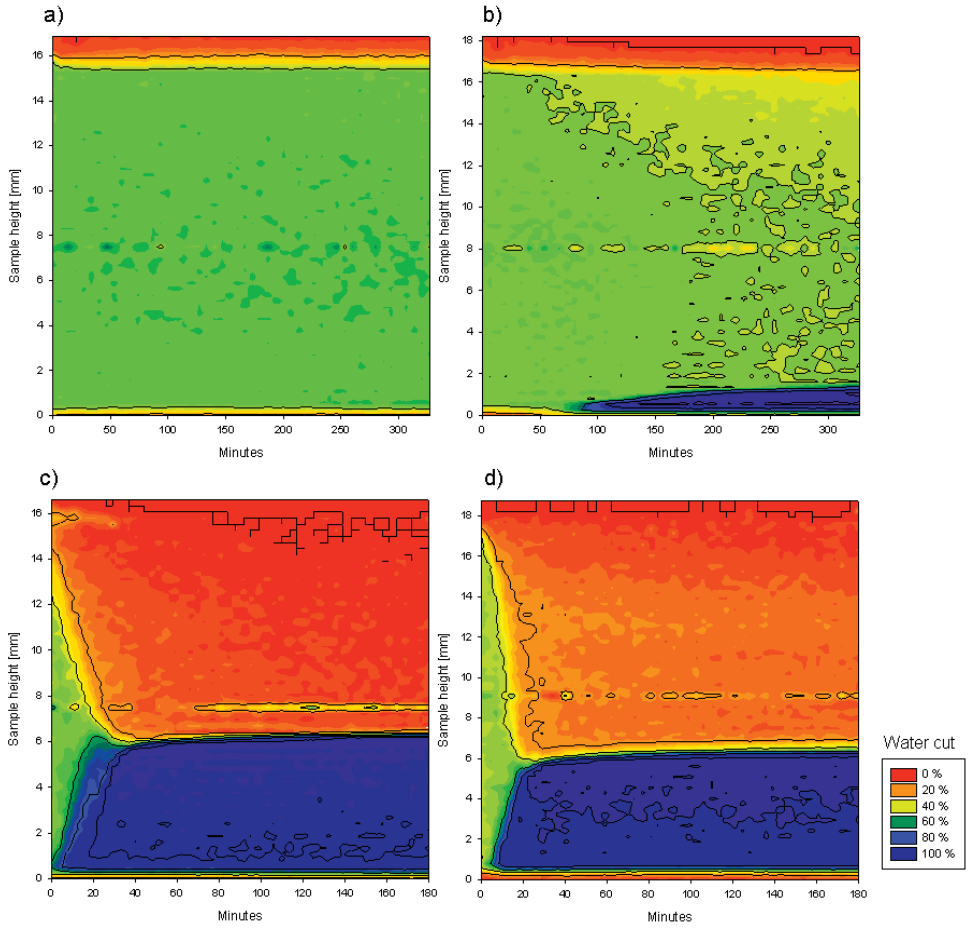

Figure 2 Collection of iso-volumetric contour plots for the crude oil emulsions. Water cut 40 %. a) No chemicals added. b) 90 ppm of chemical 4 c) 90 ppm of chemical 5 d) 90 ppm of chemical 7.

In figure 3 the iso-volumetric curves of 20 % and 90 % water for the four emulsions are plotted together. The 20 % water line can be considered to represent half of the original emulsified water and as an example of a single sedimentation rate. The 90 % line has been chosen to represent the threshold of free water presence. The sedimentation fronts moves downwards and the free water formation curves moves upwards, and when the separation is complete the two curves meet. As seen in the figure, the sedimentation of the emulsions treated with chemical 5 and 7 exhibit rather similar sedimentation velocities. By assuming an initial linear slope, the sedimentation velocity can be approximated. The emulsion treated with chemical 5 has a sedimentation velocity of approximately 0.34 mm/min, whereas the

emulsion treated with chemical 7 has a velocity of approx 0.18 mm/min. Both these values indicate an unstable emulsion by considering the length of the emulsion sample in the NMR measurements. Comparing the separation of the non-treated emulsion and the emulsion treated with chemical 4, one can conclude that they have approximately the same slow sedimentation velocity. But the plot including all the iso-volumetric curves shows that there is more vertical movement in the emulsion treated with chemical 4. By comparing the separation illustrated in figure 2 and 3, one can see how presenting one sedimentation rate alone for an unstable emulsion can be insufficient.

The same approach can be used on the rate of free water formation. By assuming a linear initial slope, one can approximate the rate of water recovery. The emulsion treated with chemical 5 has a water recovery rate of about 0.059 mL/min, whereas chemical 7 gives a recovery rate of 0.072 mL/min. The performance by chemical 5 and 7 differs somewhat, with chemical 5 giving a higher sedimentation velocity, and chemical 7 has a higher interfacial coalescence rate. This suggests two different properties for the two demulsifiers. The higher sedimentation rate of the emulsion treated with chemical 5 compared to chemical 7 suggests that the former have a slightly higher propensity for binary coalescence, or that this demulsifier is slightly better to flocculate the droplets. The emulsion with chemical 7 seems to have a higher rate of interfacial coalescence than the emulsion with chemical 5. But the higher interfacial coalescence rate from chemical 7 seems only to be valid in the firs stages of the separation. As seen in figure 2, the emulsion treated with chemical 7 forms a thin layer of non coalescing droplets, something that chemical 5 does not exhibit.

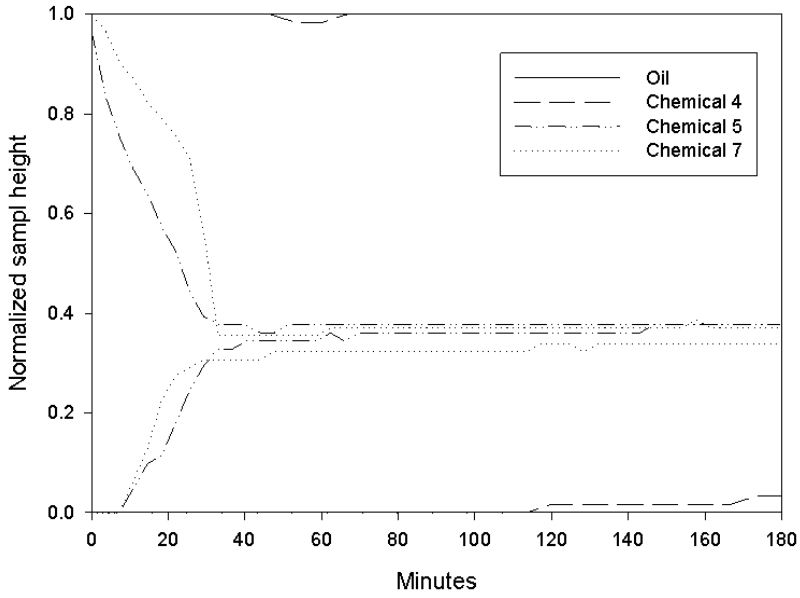

Figure 3 Comparison of sedimentation and free water formation of the different chemicals at demulsifier concentration of 90 ppm. The sedimentation fronts are the 20% iso-volumetric curves and the free water formation rates are the 90 % iso-volumetric curves from figure 2.

Figure 4 shows the droplet size distributions of the emulsions. The measurement was performed immediately after the mixing was complete, and can thus be considered as the initial droplet size distribution. The rapid effect the demulsifier has on the emulsion explains why the four distributions give a different shape and average size, even though the emulsification was performed similarly. As seen in figure 2 and 3, the emulsions treated with chemicals 5 and 7 are unstable and the droplet size measurements takes approximately three minutes. Within three minutes the droplets have moved been considerably, and it is fair to assume that a large fraction of the droplets have already coalesced into larger ones. That means that the only size distribution in figure 4 that can accurately be called an initial size distribution is the non-treated emulsion. The separation plots indicate a high stability and it seems reasonable to assume no binary coalescence within three minutes for this sample. The trend regarding which demulsifiers is the most efficient in inducing binary coalescence follows the trend from the separation profiles. Chemical 4 is increasing the binary coalescence to a certain level, but chemical 5 and 7 are much more efficient in increasing the droplet size distribution.

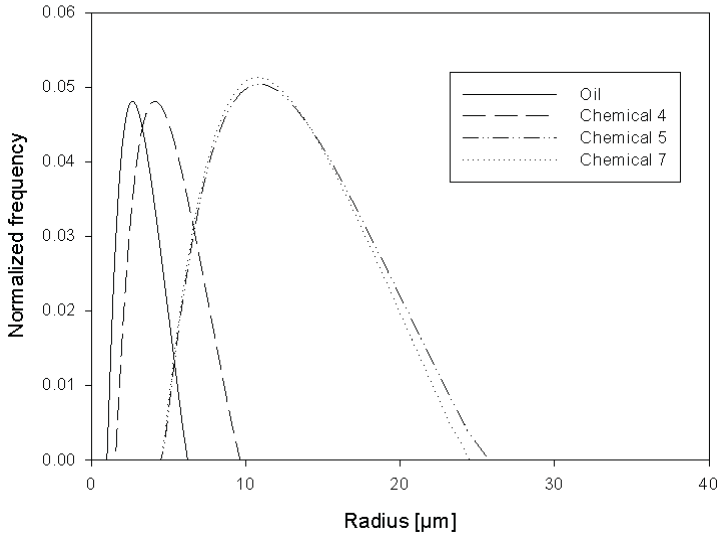

Figure 4 Droplet size distributions of the emulsions.

Table 2 shows the Stokes' [35] sedimentation rate calculated from the initial droplet sizes for the 4 emulsions. The velocity was calculated from equation 4:

$$v = \frac{2a^2 g \Delta\rho}{9\mu} \qquad \text{(I)}$$

Where a is the droplet radius, g is the gravity constant, Δρ is the density difference between the dispersed and continuous phase and μ is the continuous phase viscosity. The values of the theoretical initial sedimentation velocity do not match the observed velocities seen in figure 3. By assuming that the emulsion with no chemicals added reflects the true initial droplet size distribution, one can approximate a droplet growth rate for the emulsion treated with demulsifiers. The growth rate was calculated by considering the emulsion without any demulsifiers added as a base line. The difference between the average droplet radius of the emulsion treated by chemicals and the base line emulsion without chemicals was then divided by the measurement time (i.e three minutes). The difference between the observed sedimentation velocity and the Stokes' coincides with the trend of the droplet growth rate. The chemical which induces the largest droplet growth has the largest deviation between Stokes' and observed sedimentation velocity.

Table 2 Average droplets sizes, sedimentation velocities and average droplet growth rate of the emulsions.

Chemical	Average initial droplet radius [μm]	Stokes' sedimentation velocity [mm/min]	Observed sedimentation velocity [mm/min] [a]	Average droplet growth rate [μm/s]
No	3.0	0.00054	0	0
4	4.0	0.00095	1.6 E(-4)	0.0052
5	10.9	0.0071	0.34	0.041
7	10.7	0.0068	0.18	0.040

[a] Initial sedimentation velocity of the iso-volumetric curve of 20 % (figure 3).

Two of the demulsifiers were evaluated by their efficiency in the NMR at different concentrations with the results shown in figure 5. The figure shows the 20 % and 90 % iso-volumetric curves as representatives for the sedimentation and water recovery rate, respectively. As explained in the legend in figure 5 a), four different dosages of chemical 5 have been added to the emulsions. The higher dosage gives a faster sedimentation velocity for both demulsifiers. The concentration dependence on the water recovery rate appears different. The dosages of 90, 50 and 30 ppm does not give a big difference in the initial slope of the water recovery, but the time of appearance of free water is different. For the emulsions in figure 5 a) the dosage of 30 ppm gives the fastest appearance of free water. At this dosage free water appears after 6 minutes, whereas the dosage of 50 and 90 ppm gives free water after 9 and 11 minutes respectively. A possible explanation for this is that at a concentration of 30 ppm the demulsifier activity is optimized in terms of facilitating interfacial coalescence, at least in the initial timescale of the separation. Though, after the initial linear slope another difference between the dosages can be seen. After ~50 minutes the amount of recovered water has stagnated for the dosages of 90, 50 and 30 ppm, with lower chemical dosage giving less free water and a thicker layer of non coalescing droplets at the water-emulsion interface. The emulsions have formed a densely packed layer of droplets.

The sedimentation rates of the emulsions treated with chemical 7 (figure 5 b)) appear to give a similar trend as what is seen in figure 5 a); higher concentration of demulsifiers gives higher sedimentation velocities. But the water recovery rates for the different dosages of chemical 7 show a different trend. An increased demulsifier concentration gives an earlier breakthrough of free water and a faster recovery rate. This indicates that the separation process for emulsions where chemical 7 is added is driven by the binary coalescence; the binary coalescence will give a higher sedimentation rate which consequently gives a higher water

recovery rate. For emulsions with chemical 5 added, the separation process seems to be driven by the interfacial coalescence rate. The binary coalescence gives a higher sedimentation rate, but the water recovery rate is not affected in the same manner as the sedimentation rate. However, without being able to directly measure the binary coalescence for the samples the underlying mechanisms are still not completely elucidated.

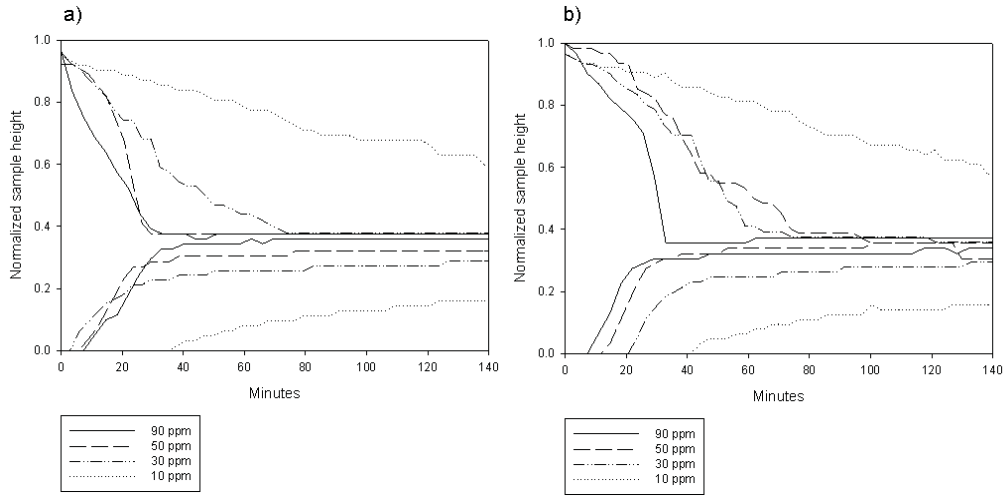

Figure 5 Sedimentation and free water formation at different concentrations for two demulsifiers: a) chemical 5, b) chemical 7. The sedimentation fronts are the 20% iso-volumetric curves and the free water formation rates are the 90 % iso-volumetric curves.

To further study the time of appearance of free water and the kinetics of water recovery for chemicals 5 and 7 the emulsion stability was also examined with bottle test. The main motivation was to observe whether the trend of the stability studied in the NMR could be found in a slightly larger scale. The sample tubes used in the NMR study were cylindrical and had an inner diameter of 18 mm and a sample height of approximately 18 mm. The bottle tests were performed in cylindrical tubes with inner diameter of 31 mm and a sample height of 45 mm. All other conditions, such as mixing protocol, demulsification dosage etc, were kept equal. Figure 6 shows the time of appearance for the different tube dimensions with chemical 5 and 7 added at dosage ranging from 10-90 ppm, and as seen the difference between the two conditions becomes more profound when the emulsions are more stable. At 90 ppm of demulsifier concentration the difference is low, whereas at 10 ppm the difference between the two sample tube dimensions becomes substantial. At 90 ppm the demulsifiers act

so effectively that the sedimentation and subsequent coalescence into free water occurs almost instant. At a lower dosage and lower activity of the demulsifiers the sedimentation distance becomes important. The difference in the stability kinetics is important with regard to scaling of the separation to industrial dimensions. Comparing the data from figure 5 and 6 shows that by increasing the separation vessel dimension slightly the timescale of the separation can change substantially if the dosage is not optimized. It should be noted that the registration of the time of free water appearance is somewhat arbitrary. The first "free" water in the bottle test is observed as a large droplet in the bottom of the settler. A question related to the NMR data is how the point of free water breakthrough is interpreted. In the NMR data the threshold of free water was set to follow the 90 % curve. However, given the small sample size it can be difficult to relate to the visual appearance of the free water and this study has not visually observed what the sample inside the NMR tube looks like when the 90 % curve emerge.

Table 3 Initial water recovery rates for emulsions treated measured with the NMR and the bottle test with various concentrations of chemicals 5 and 7. Data calculated from figure 5 (NMR) and figure 6 (bottle test).

	Chemical 5		Chemical 7	
Concentration (ppm)	Bottle test (mm/min)	NMR (mm/min)	Bottle test (mm/min)	NMR (mm/min)
10	n/a	0.025	n/a	0.14
30	0.0083	0.17	0.076	0.26
50	0.082	0.19	0.097	0.35
90	0.049	0.18	0.077	0.35

The kinetics of free water formation studied with the bottle test at different concentrations of chemical 5 and 7 also showed that the initial water recovery rate had an almost to linear behavior. Thus, by assuming a linear relationship in the early stages of the separation one can make a comparison on the velocity in the same manner as was done with the emulsions studied in the NMR. The result of the linear regression is shown in table 3. Compared to the kinetic behavior shown in figure 5, a similar trend is observed albeit with different absolute values. A trend observed for both techniques is that an increased demulsifier concentration gives a faster free water recovery rate, except for the dosages of 50 and 90 ppm. At this level the velocity is approximately equal; with the difference between the concentrations is the time of appearance of free water. The differences between the acquired data from the two techniques become visible on the absolute value of the velocity. The bottle test gives an

overall lower recovery rate than the NMR does. The initial recovery velocity for both chemicals measured with the NMR is approximately 4 times larger than the one obtained from the bottle test. Nadiv and Semiat [25] studied the separation time at different dispersion heights of an o/w emulsion system and found that the difference in height of the sample could increase the timescale by a factor of ~2.4. Given the differences in the cylinder diameter between the studies the small difference in the factor is expected. They operated with settler diameters of 2.3 and 6.3 cm, whereas this study has slightly smaller sample tube diameters. Another difference between the two studies is that Nadiv and Semiat studied the time of complete separation whereas table 3 contains the initial water recovery rate. These two parameters are not exactly comparable.

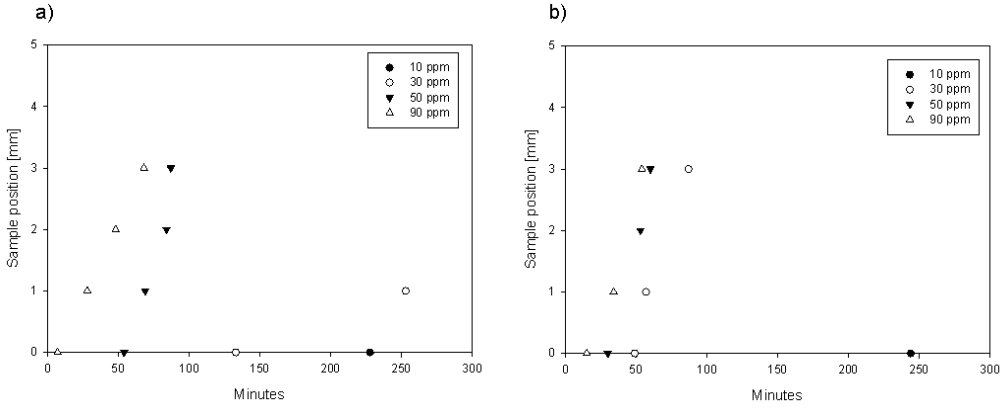

Figure 6 The time of free water appearance and development of water recovery studied with the bottle test with chemicals at different concentration. a) chemical 5. b) chemical 7.

By comparing the results from the demulsifier effect in the electric field (figure 1) with the result in figures 2, 5 and 6 some differences in the behavior are observed. Figure 1 indicates that at dosages 30 and 50 ppm, chemical 7 is slightly more effective than chemical 5. At 90 ppm they seem to be similarly effective in breaking the emulsion. The separation in the NMR indicates that chemical 5 is slightly more efficient with less dispersed water in the oil phase. Another difference between the two techniques in terms of determining emulsion stability is the effect of dosage. The E_{Crit} method suggests that the difference between 30, 50 and 90 ppm is not very large, but analyzing the sedimentation data from the NMR a more accurate observation of the differences between the dosages can be done. The E_{Crit} method only gives an indication of appearance of free water, not any quantification on the amount or any kinetic data. Another explanation for the difference is that demulsifiers act differently when confined

in an electrical field. The same point can be made with the bottle test results. These data indicated that chemical 7 was slightly more efficient than chemical 5 at similar dosages. This shows the importance of being able to monitor the entire emulsion sample, and gives an illustration on the flexibility of the NMR technique. If the main goal of adding the chemical is to increase the dewatering of the oil phase than the demulsifier should be chosen based on the oil phase quality, not on indirect measurements of the emulsion stability.

Interfacial rheology

Oscillating drop measurements were performed to study how chemicals 4, 5 and 7 affect the film properties of the droplets. However, by studying the interfacial rheology with the oscillating drop technique one should keep in mind that the method assumes that the only forces acting on the droplet shape are gravity and the interfacial tension. At certain experimental conditions, viscous and inertial forces can perturb the measured response. Freer et al [36] showed that the measured interfacial response of samples can be influenced by the viscosity of the droplet. Hannisdal et al [37] also showed that the contribution of viscous forces could be the explanation of an apparent viscoelastic behavior for non-surfactant systems. The limit at which the measurements are affected is governed by the Capillary number.

$$Ca = \frac{\Delta\mu\omega\Delta V}{\gamma_0 a^2} \qquad (5)$$

Where $\Delta\mu$ is the difference in viscosity for the two phases, ω is the frequency of drop volume oscillation, ΔV is the volume oscillation amplitude, γ_0 is the equilibrium interfacial tension and a is the radius of the capillary tube. With no influence of viscous forces, a plot of the relative interfacial amplitude, $\Delta\gamma_a/\gamma_0$, versus the capillary number should yield a flat relationship. If the measurements of interfacial tension are distorted by viscous forces the amplitude will increase linearly with the capillary number. Given the heavy character of the crude oil used in this study, a compromise has to be made with regard to the study of the interfacial rheology. By studying the undiluted crude oil with the oscillating drop method, there is a risk of measuring an apparent interfacial tension influenced by the high oil phase viscosity.

One way avoiding this problem is to extract the interfacial active compounds in the crude oil, namely resins and asphaltenes and re-dissolve them in a model oil of lower viscosity. Another method is to dilute the crude oil with heptane, toluene or other diluents. Both methods have

their shortcomings and the accuracy and how representative such perturbations are to the properties of a real system is always under scrutiny. By using extracted resins and asphaltenes in model oil solutions the diffusion and intermolecular properties of the surfactants can be different than in the original crude oil solution. By diluting the crude oil the concentration of the resins and asphaltenes are changing and their activity can be changes depending on the nature of the diluents. In this study we have chosen to dilute the crude oil in a mixture of 1:1 weight ratio of toluene and heptane, henceforth named heptol. Both Freer et al and Hannisdal et al showed that the measurements were distorted at Capillary number higher than approximately 0.002. The viscosity of the diluted oil phase was reduced and in combination with the frequency and volume amplitude the capillary numbers used in this study was well below 0.002.

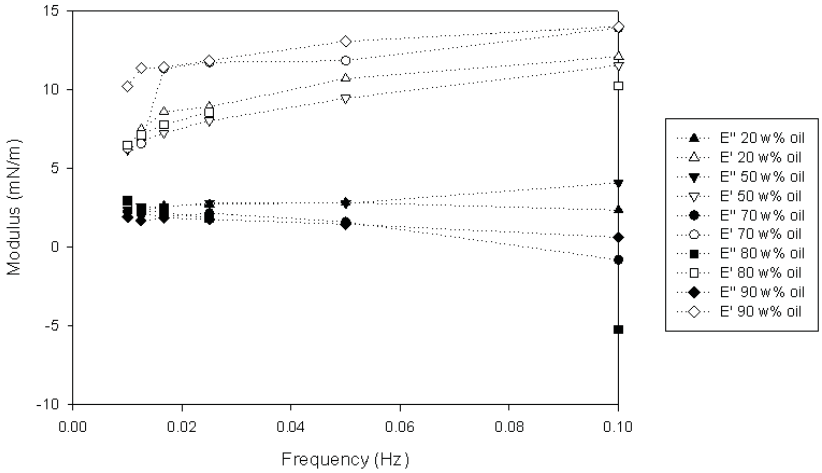

Figure 7 The elastic and viscous modulus of the diluted crude oil as a function of frequency. The crude oil was diluted with different amount of 1:1 weight ratio of heptol. The percentage shown in the legend gives the weight percentage of heptol of the sample, i.e. 80 % corresponds to 80% crude oil and 20 % 1:1 heptol.

Figure 7 shows the elastic (E') and viscous (E'') modulus of the crude oil diluted with different amounts of 1:1 weight ratio heptol at different frequencies. The response of all the different dilutions was mainly elastic. As seen in the figure, negative values of E'' at the highest frequencies for some of the dilutions with the highest oil content. The negative values of the loss modulus at the highest frequency indicate that the measurements are perturbed by the viscosity of the droplet, since negative values are unrealistic for the interfacial viscosity.

This indicates that the combination of high frequency and high bulk viscosity can affect the accuracy of the interfacial tension measurements. At lower frequency, the difference between the various dilutions is not profound. Figure 8 shows the dynamic Interfacial Tension (IFT) for the water-crude oil interface where the crude oil has been diluted with 20 w% of 1:1 weight ratio of heptol and with various dosages of chemicals 5 and 7. As seen in both figures 8 a) and b) the tension decreases in a monotone manner at increasing chemical dosage. The only deviation is at a concentration of 10 ppm, a feature observed for both chemicals. There are no good explanations for this anomaly. However, in the rheology measurements the dosage of 10 ppm also gave the highest variance in the measurements. At a dosage of 90 ppm the tension is decreasing rapidly for both chemicals and at a concentration of 90 ppm of chemical 5 the droplet let go of the capillary tube after ~4800 seconds due to the low interfacial tension.

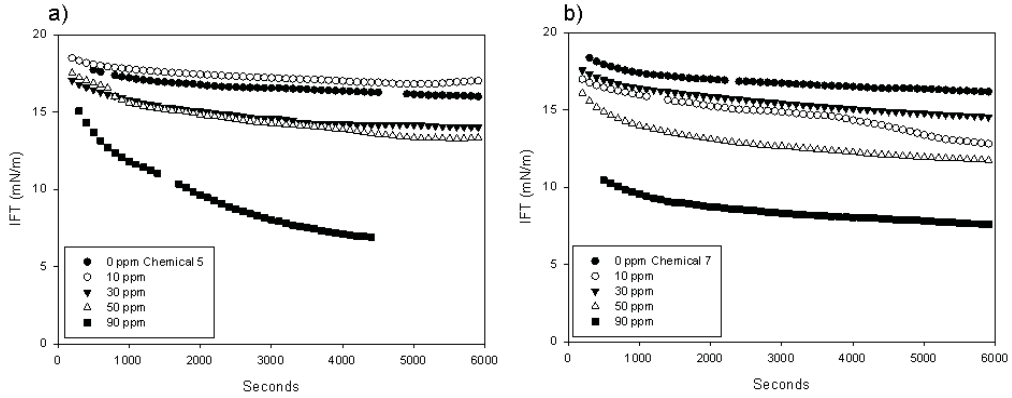

Figure 8 Dynamic Interfacial Tension with the crude oil diluted with 20 w% of 1:1 heptol with different concentration of: a) chemical 5 b) chemical 7.

The kinetics of film formation at different chemical dosage was studied and the general response was similar to the response of crude oil interfaces at different dilutions in figure 6, with mainly an elastic response. An example of the time dependency on film formation is seen in figure 9. The figure shows the elastic (E') and the viscous (E'') response of interface with no demulsifier added and with chemical 5 added at a concentration of 90 ppm. The interface with no demulsifier present shows very slow development of the film formation. The addition of 90 ppm of chemical 5 increases both the elastic and viscous modulus substantially, and as seen after approximately 4000 seconds the droplet let go of the capillary tube.

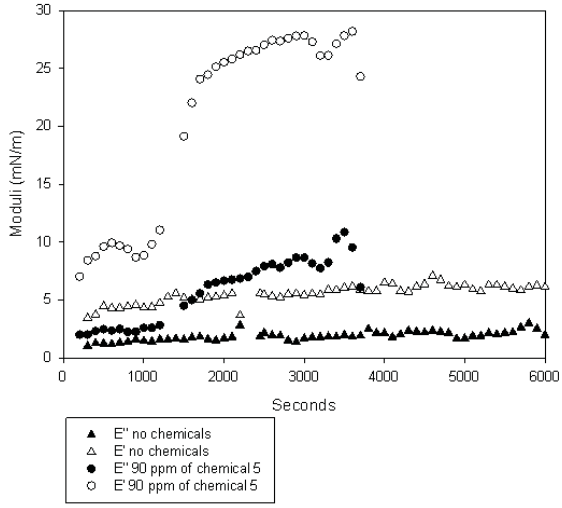

Figure 9 Kinetic development of the elastic and viscous modulus of crude oil water interfaces.

Apart from the behavior with an addition of 90 ppm of chemical 5, as seen in figure 8, the kinetic behavior of the interface at other dosages was rather similar. The curves appear to have the same shape, similar to the curve for the interface with no chemicals added shown in figure 8. Table 3 shows the values of E' and E'' after 6000 seconds of measurements for the interfaces in the presence of different concentrations of chemical 5 and 7. The reproducibility was good except for the dosage at 10 ppm; a feature observed for both chemicals. The values of 90 ppm of chemical 5 after 3000 seconds are given in table 3 due to the broken droplet; the development of E' and E'' can be seen in figure 9. The values in table 3 indicates that both the elastic and viscous modulus pass through a minimum with increasing demulsifier concentration. That observation is in contrast to the separation plots shown in figure 5. The separation seems to be improving with increasing demulsifier concentration. An explanation for the difference in the trend between the separation results and interfacial rheology could be that in the stability studies the demulsifiers were added after the formation the interface, i.e. after emulsification was complete. In the interfacial studies the demulsifiers were added to the oil phase prior to film formation, and thus the demulsifiers will compete with the indigenous crude oil surfactants on the composition on the film. Another factor that can affect the comparison is the dilution of the crude oil. The dilution with heptol can change the diffusion properties of the demulsifiers, and more importantly there is a possibility of formation of organic particles through aggregation of asphaltenes. A third explanation is the concentration of demulsifiers and the available interfacial area. In the separation measurement the total

interfacial area is much larger than in the oscillating measurements were a large but single droplet gives the interface. This could mean that the dosages per unit area used in the oscillating measurements are higher than the ones used in the separation measurements. In that sense it seems reasonable that both the elastic and viscous modulus decreases at the small concentrations, and the reason for the increased value of the modulus at higher concentration is an overdose of demulsifiers. The volume of the droplet in the oscillating measurements was around 25 mm^3 which corresponds to approximately an interfacial area of 4.1 x 10^{-5} m^2. An approximation of the total interfacial area for the freshly formed emulsions can be obtained by assuming a uniform droplet size of 4 μm and considering the total volume available from an emulsion with 40 v% water cut and total liquid volume of 30 mL. This approximation gives a total interfacial area of ~9 m^2. By considering the ratio between demulsifier concentration and available interfacial area the data from table 3 are more reasonable. It shows that considering the dosage alone is not sufficient to compare the data sets and a likely reason for the increase of both the loss and storage modulus at higher demulsifier concentration is because the interface is overpopulated with surfactants. The comparison between the separation data and the interfacial behavior then shows that the active demulsifiers decrease both the viscous and elastic modulus of the oil-water interface.

Table 4 Elastic and viscous modulus after 6000 seconds.

	Chemical 5		Chemical 7	
	E' (mN/m)	E'' (mN/m)	E'(mN/m)	E''(mN/m)
0 ppm	6.8 ± 0.7	2.0 ± 0.1	6.8 ± 0.7	2.0 ± 0.1
10 ppm	3.8 ± 1.1	1.2 ± 0.2	5.7 ± 2.0	1.2 ± 0.4
30 ppm	7.8 ± 0.2	1.5 ± 0.1	6.0 ± 0.1	1.1 ± 0.1
50 ppm	8.4 ± 0.4	1.9 ± 0.2	5.1 ± 0.1	1.0 ± 0.1
90 ppm	27.4 ± 0.5[a]	8.1 ± 0.5[a]	7.3 ± 0.5	1.7 ± 0.1

[a] after 3000 seconds the droplet broke

Multivariate Analysis (MVA)

Since our tested matrix is quite complex the multivariate analysis was used as a tool for comparison of the effect of chemicals on separation of w/o emulsions in terms of enhancing free water evolution. For the data analyzed in this study, the 3 crude oils and 9 demulsifiers are used as category variables and as normal variables are used initial droplet size, equilibrium interfacial tension, water recovery (80% recovery), sedimentation rate, height of

water layer and thickness of emulsion layer all after 30 minutes of testing. Principal component analysis (PCA) was effectively used for reducing the number of original variables and understanding which parameters contribute the most with demulsifier efficiency. Figure 7 shows the result from PCA where the variation in the data set is well explained by 2 PCs, because PC1 explained 62% of variance in the data and PC2 explained 16%. The score plot reveals similarities between individual chemicals which are grouped regarding their efficiency to break up w/o emulsions and how they enhance the evolution of free water. The loading plot represents the correlations between original variables where difference in interfacial tension between pure crude oil and crude oil with demulsifier after 30 minutes (IFT_30min) correlates to PC2, free water evolution represented by height of emulsion layer (water_Layer_30mi), initial droplet radius (MDR_init) and sedimentation rate (sedim_velocity) significantly correlates with PC1. The thickness of emulsion layer (Emul_Layer_30mi) and 80% water recovery (80% recovery) correlates together and anti-correlates with previous parameters.

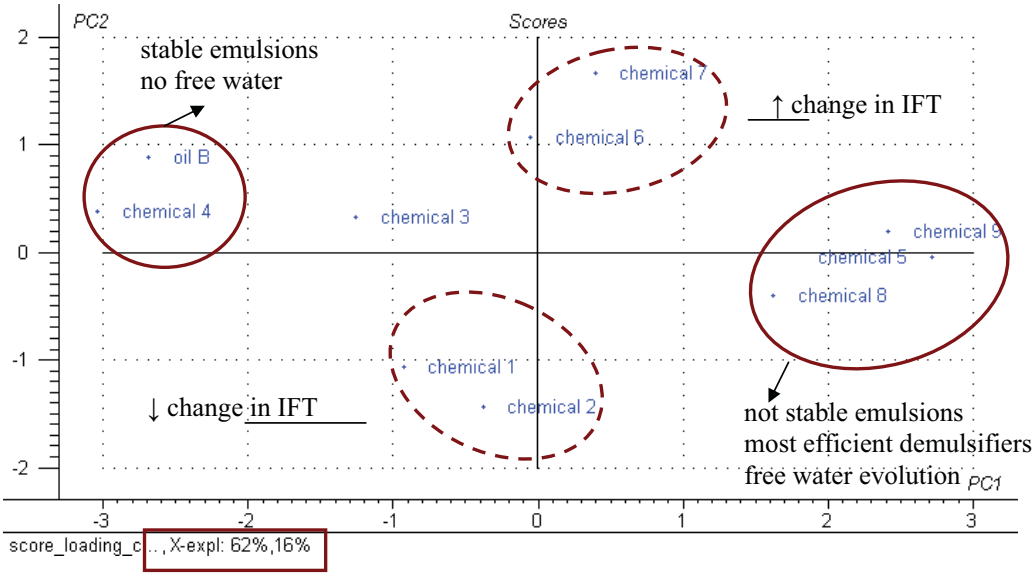

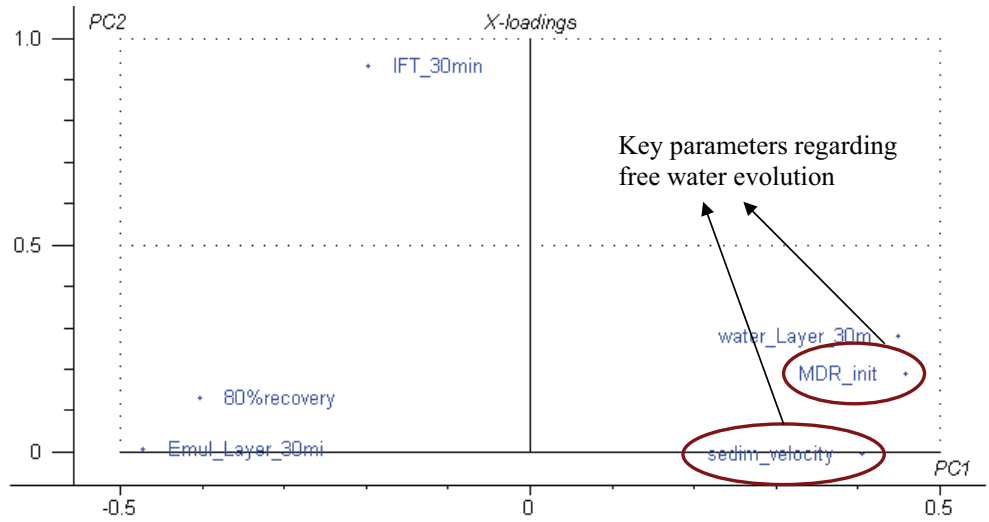

Figure 10 Score (top) and loading (bottom) plots of PC1 versus PC2. The groupings seen in score plot correspond to free water evolution induced by chemicals and consequently with demulsifier efficiency. Loading plot represents the relationship between variables where IFT_30min corresponds to difference between interfacial tension of pure acrude oil and crude oil contains demulsifier after 30 minutes, 80% recovery to water recovery 80%, Emul_Layer_30mi to thickness of emulsion layer after 30 minutes, water_Layer_30mi to hight of emulsion layer after 30 minutes, MDR_init to initial droplet radius and sedim_velocity to sedimentation rate.

This means that the most efficient demulsifiers are on the right side of score plot. These demulsifiers enhance the separation of free water, reach faster 80% water recovery and have higher value of initial droplet radius. In contrary demulsifiers on the left side of score plot create stable emulsions and their initial droplet radius is similar as initial droplet radius for pure crude oil. Loading plot shows strong correlation between free water evolution, initial droplet radius and sedimentation rate which is in accordance with correlation coefficients (regression coefficients) obtained from PLS analysis of same test matrix. Figure 8 confirms previous findings and indentifies initial droplet radius and sedimentation rate as essential parameters regarding to free water evolution and explains efficiency of demulsifiers.

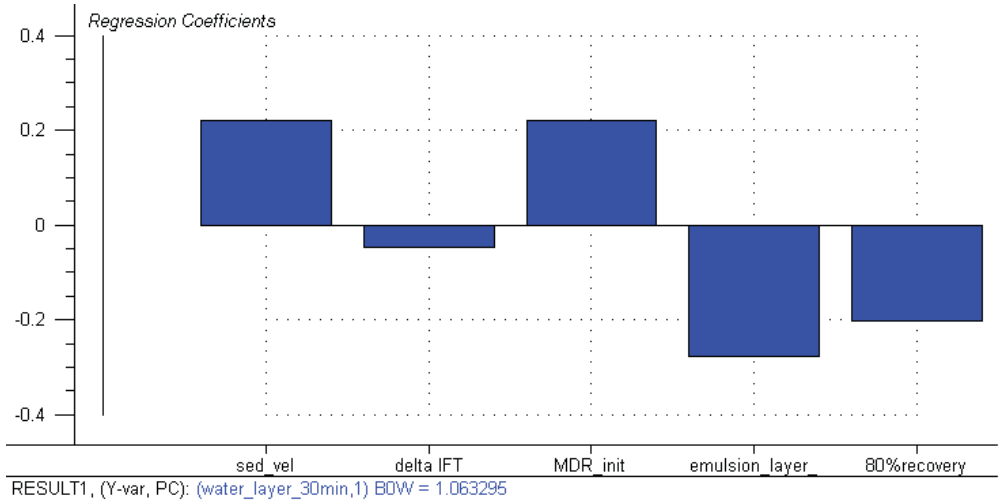

Figure 11 Regression coefficients for the model explaining the main effects on the efficiency of demulsifiers in terms of w/o emulsion stability. The positive coefficients represent variables that break up w/o emulsions and enhance free water evolution.

4 Conclusions

Measurements of chemical destabilization of water-in-oil emulsion were performed in the critical electric field, bottle tests and in low field NMR. The destabilization in the electrical field showed that the most efficient demulsifiers require a small dosage to induce droplet coalescence. A concentration of 30 ppm was sufficient for the most efficient chemicals; higher concentrations did not improve the stability substantially. For the medium effective demulsifier the concentration limit was at ~100 ppm. The study shows that the NMR technique is an important tool for screening demulsifiers. Multiple parameters are possible to monitor with the NMR technique, such as the sedimentation of the entire water fraction dispersed in the oil phase, the rate of water recovery and the droplet size distribution. The monitoring of the entire water fraction can give an indication whether the separation meets the criteria of oil quality or not. With the possibility of obtaining these parameters, a preliminary screening can be performed with regard to determination of optimum dosage and chemical. The results from the bottle tests and the NMR show a slightly different demulsifier concentration dependence than from the E_{Crit} method, though only three demulsifiers were studied in the NMR. In the NMR one can observe that the sedimentation velocity for both of the effective demulsifier increased at increasing demulsifier concentration, the same trend was

observed with the bottle tests. Regarding the rate of free water formation the behavior was more dependent on each demulsifier. One of the demulsifier gave faster water recovery at increasing concentration, whereas another demulsifier shows stagnation on the water recovery rate.

The interfacial experiments showed that at low demulsifier concentrations the elastic and viscous moduli of the interface was reduced and at higher demulsifier concentration both moduli increased. Even though there was a mismatch between the behavior at similar concentration ranges in the separation experiments and the interfacial experiments, the relation between the available interface area and demulsifier concentration indicated that the chemicals decrease the interfacial elasticity and the interfacial viscosity. However, only the two most effective demulsifiers were studied at different concentrations, and additional studies should be performed to make further conclusions on the interfacial response of the demulsifiers.

The study shows that in order to choose the appropriate demulsifier type and dosage one should consider not only the demulsifier dosage but also the amount of dispersed interfacial area. In addition, in order use the information obtained from laboratory measurements it is important to consider how the separation vessel dimensions affect the emulsion stability and the optimum demulsifier dosage.

Acknowledgements

The authors are thankful for the proof reading and the discussion with Dr Sebastien Simon and for the financial contribution from the participants in the Joint Industrial Project, JIP-1 hosted by the Ugelstad Laboratory at the Norwegian University of Science and Technology. Nils van der Tuuk Opedal acknowledges Statoil for a PhD grant.

References

1. Li, C.; Liu, Q.; Mei, Z.; Wang, J.; Xu, J.; Sun, D., *Journal of Colloid and interface Science* **2009,** 336, 314-321.
2. Hodge, S. M.; Rosseau, D., *Food Research International* **2003,** 36, 695-702.
3. Jiang, T.; Hirasaki, G.; Miller, C.; Moran, K., *Energy & Fuels* **2008,** 22, 4158-4164.
4. Wu, X. A., *Energy & Fuels* **2008,** 22, 2346-2352.
5. Hannisdal, A.; Ese, M.-H.; Hemmingsen, P. V.; Sjöblom, J., *Colloids and Surfaces A: Physiochem. Eng. Aspects* **2005,** 276, 45-58.
6. Zhang, L. Y.; Xu, Z.; Masliyah, J. M., *Langmuir* **2003,** 19, 9730-9741.
7. Nordgård, E. L.; Landsem, E.; Sjöblom, J., *Langmuir* **2008,** 24, 8742-8751.
8. Kilpatrick, P. K.; Spiecker, P. M., In *Encyclopedic Handbook of Emulsion Technology*, Sjöblom, J., Ed. Marcel Dekker: New York, 2001.

9. Gafonova, O. V.; Yarranton, H. W., *Journal of Colloid and interface Science* **2001,** 241, 469-478.
10. Ekott, E. J.; Akpabio, E. J., *Journal of Engineering and Applied Sciences* **2010,** 5, 447-452.
11. Lundgaard, L. E.; Berg, G.; Ingebrigtsen, S.; Atten, P., In *Emulsions and Emulsion Stability*, Sjöblom, J., Ed. Taylor & Francis: Boca Raton, 2006.
12. Nikiforidis, C.; Kiosseoglou, V., *Food Hydrocolloids* **2006,** 21, 1310-1318.
13. Angle, C. W.; Dabros, T.; Hamza, H. A., *Energy & Fuels* **2007,** 21, 912-919.
14. Fan, Y.; Simon, S.; Sjöblom, J., *Energy & Fuels* **2009,** 23, 4575-4583.
15. Rondón, M.; Bouriat, P.; Lachaise, J.; Salager, J., *Energy & Fuels* **2006,** 20, 1600-1604.
16. Rondón, M.; Pereira, J. C.; Bouriat, P.; Graciaa, A.; Lachaise, J.; Salager, J., *Energy & Fuels* **2008,** 22, 702-707.
17. Borges, B.; Rondón, M.; Sereno, O.; Asuaje, J., *Energy & Fuels* **2009,** 23, 1568-1574.
18. Sjöblom, J.; Aske, N.; Auflem, I. H.; Brandal, Ø.; Havre, T. E.; Sæther, Ø.; Westvik, A.; EJohnsen, E.; Kallevik, H., *Advances in Colloid and Interface Science* **2003,** 100-102, 399-473.
19. Krawczyk, M. A.; Wasan, D. T.; Shetty, C. S., *Industrial & Engineering Chemistry Research* **1991,** 30, 367-375.
20. Tambe, D.; Paulis, J.; Sharma, M. S., *Journal of Colloid and interface Science* **1995,** 171, 463-469.
21. Kang, W.; Jing, G.; Zhang, H.; Li, M.; Wu, Z., *Colloids and Surfaces A: Physiochem. Eng. Aspects* **2006,** 272, 27-31.
22. Angle, C. W., In *Encyclopedic Handbook of Emulsion Technology*, Sjöblom, J., Ed. Marcel Dekker: New York, 2001.
23. Mohammed, R. A.; Bailey, A. I.; Luckham, P. F.; Taylor, S. E., *Colloids and Surfaces A: Physiochem. Eng. Aspects* **1994,** 91, 129-139.
24. Long, Y.; Dabros, T.; Hamza, H. A., *Fuel* **2002,** 81, 1945-1952.
25. Nadiv, C.; Semiat, R., *Industrial & engineering chemistry research* **1995,** 34, 2427-2435.
26. Hemmingsen, P. V.; Silset, A.; Hannisdal, A.; Sjöblom, J., *Journal of Dispersion Science and Technology* **2005,** 26, 615-627.
27. Opedal, N.; Sørland, G.; Sjöblom, J., *Energy & Fuels* **2010,** 24, 3628-3633.
28. Aske, N.; Kallevik, H.; Sjöblom, J., *Journal of Petroleum Science and Engineering* **2002,** 36, 1-17.
29. Opedal, N.; Sørland, G.; Sjöblom, J., *Diffusion Fundamentals* **2009,** 9, (7), 1-29.
30. Simon, S.; Pierrard, Z.; Sjöblom, J.; Sørland, G., *Journal of Colloid and interface Science* **2011,** 356, 352-361.
31. Esbensen, K. H., *Multivariate Data Analysis - In Practice*. CAMO: Esbjerg, 2002.
32. Martens, H.; Martens, M., *Multivariate Analysis of Quality. An Introduction*. Wiley: Chichester, 2001.
33. Urdahl, O.; Møvik, A. E.; Sjöblom, J., *Colloids and Surfaces A: Physiochem. Eng. Aspects* **1993,** 74, 293-302.
34. Kang, W.; Jing, G.; Zhang, H.; Li, M.; Wu, Z., *Colloids and Surfaces A: Physiochem. Eng. Aspects* **2005,** 272, 27-31.
35. Stokes, G. G., *Transactions of the Cambridge Philological Society* **1851,** 9:8.
36. Freer, E. M.; Wong, H.; Radke, C. J., *Journal of Colloid and interface Science* **2005,** 282, 128-132.
37. Hannisdal, A.; Orr, R.; Sjöblom, J., *Journal of Dispersion Science and Technology* **2007,** 28, 81-93.

Paper IV

Is not included due to copyright

Paper V

Is not included due to copyright

Paper VI

Probing Molecular Interactions of an Asphaltene Model Compound in Organic Solvents Using a Surface Forces Apparatus (SFA)

Jing Wang[1], Nils van der Tuuk Opedal[2], Qingye Lu[1],

Zhenghe Xu[1,*], Hongbo Zeng[1,*], Johan Sjöblom[2]

[1]Department of Chemical and Materials Engineering, University of Alberta, Edmonton, Alberta, T6G 2V4, Canada.

[2]Ugelstad Laboratory, Department of Chemical Engineering, Norwegian University of Science and Technology (NTNU), N-7491 Trondheim, Norway.

*Corresponding author: hongbo.zeng@ualberta.ca; phone: 780-492-1044; fax: 780-492-2881; or e-mail: zhenghe.xu@ualberta.ca; phone: 780-492-7667; fax: 780-492-2881.

Abstract

Studies on the molecular interaction mechanisms of asphaltenes in organic solvent have not reached a widely accepted conclusion, mainly due to poor definition of asphaltene molecules and lack of accurate information on molecular structure. In this study C5Pe of polyaromatic core with proper molecular weight and hetero atoms in its structure was used as a model compound of asphaltenes in an attempt to understand interaction mechanisms of molecular aggregation in organic solvents. A surface forces apparatus (SFA) was used to directly measure the molecular interactions of C5Pe in toluene and heptane. For the interactions between two model clay (mica) surfaces across a C5Pe-in-toluene solution, the repulsion observed between the adsorbed C5Pe molecules was shown to be of a steric origin. The force-distance profiles at short separation distances under high compression during approaching were well fitted with the Alexander-de Gennes (AdG) scaling theory. However, weaker repulsive forces measured over longer separation distances deviate from the AdG model applicable to mono-dispersed brushes. The lower compression regime can be also fitted with the AdG model using an independent set of fitting parameters, indicating the presence of possible secondary brush structures of the C5Pe molecules in toluene. For interactions of casted C5Pe films (C5Pe *vs.* mica, and C5Pe *vs.* C5Pe), no significant adhesion was detected in toluene while strong adhesion was measured in heptane. The comparison of the results between the model compound C5Pe and native asphaltenes shows that C5Pe behaves qualitatively similar to asphaltenes in terms of intermolecular forces, indicating that the polar components in real asphaltene molecules play an important role in determining their interfacial activities.

Introduction

The froth produced from the classical Clark Hot Water Extraction process of oil sands industry roughly contains roughly 60 wt% bitumen, 30 wt% water and 10 wt% solids. Further (froth) treatment is needed to remove the water and solids from the froth prior to upgrading of bitumen. In froth treatment, bitumen froth is normally diluted with naphtha or paraffinic solvents before further separation by gravity settling and/or centrifugation to remove the coarse/fine solids and water droplets. Unfortunately, the diluted bitumen with naphtha after the above treatments still contains 2-3 wt% of water and 0.5 wt% of solids unless an excessive centrifugation is applied. The remaining water in diluted bitumen is usually in the form of fine droplets several μm in diameter, known as water in oil emulsions. These dispersed water droplets are extremely stable and contain a significant amount of chloride ions which can cause corrosion of downstream bitumen upgrading equipment. Therefore, the presence of residual water in bitumen is highly undesirable, leading to serious processing problems due to transportation difficulties and causing significant increase in maintenance cost of equipment. Moreover, the fine solids remained in water droplets or/and at oil-water interface can cause equipment fouling and reactor plugging. For these reasons, it is necessary to remove the entrained or emulsified water droplets from the continuous oil phase prior to downstream oil processing, which has attracted increasingly more attention during past decades in crude oil and oil sands production and processing.[1-2]

Several factors have been considered to determine the removal efficiency of emulsified water from W/O emulsions, including the size of emulsified water droplets, viscosity of continuous oil phase[3], density difference between the oil and aqueous phases[4], solids content at oil-water interfaces[5-6] and energy input[7-9]. It is commonly believed that asphaltenes play a critical

role in stabilizing the W/O emulsions in crude oil processing or bitumen production.[10-13] Asphaltenes are the fraction of crude oil or bitumen that are soluble in toluene while insoluble in alkanes, such as n-heptane or n–pentane.[14-15] Previous studies have shown that asphaltenes are complex organic molecules of fused polyaromatic rings linked together by aliphatic hydrocarbon chains. Asphaltene molecules also contain a varying amount of heteroatoms such as nitrogen, oxygen, sulphur and trace metals such as vanadium and nickel.[16] Up to date, the exact composition and molecular structure of asphaltenes remain unresolved. Controversial results have been reported on not only the asphaltene composition but also the mechanism of ashpaltene aggregation in various solvents. By considering the solubility of asphaltenes in various apolar solvents, Porte *et al.* [17] suggested that the forces responsible for asphaltene aggregation were strong specific molecular forces while asphaltene precipitation was determined by nonspecific dispersion forces. Wang[18-19] and some other researchers[20] reputed that asphaltene aggregation was mainly due to van der Waals attraction. Using an atomic force microscope (AFM) and a surface forces apparatus (SFA) respectively, Wang, *et al.*[18] and Natarajan *et al.*[21] determined molecular interaction forces of asphaltenes in various organic solvents. In their study attractive forces were detected in poor solvent such as heptane, indicating that the van der Waals interactions are crucial in driving the asphaltene aggregation.[18]

The inconsistent results are a result of largely unknown molecular structures and subtle differences in asphaltene molecules used in various studies. The definition of asphaltenes inherently indicates that asphaltenes are just a solubility class having undefined chemical composition and molecular structure, although largely unknown. This characteristic of asphaltenes implies that the molecular behaviour is highly sensitive to the method used for extracting asphaltene molecules and properties of organic media. It is clear that the controversial

results and mechanisms of asphlatene aggregation in even good solvent of toluene are unlikely to be resolved from studies using complex molecular mixtures of largely unknown molecular structures. Such a reality motivated researchers to study molecular aggregation using asphaltene model compounds of well defined chemical structures.[22-24] Sjöblom and his colleagues successfully synthesized several asphaltene model compounds and studied their interfacial properties at water-oil interfaces.[25-27] The model compounds were found to resemble the interfacial activities of asphaltenes, and it was also found that only the molecules with hydrophilic (polar) groups were capable of stabilizing W/O emulsion.[27] This finding is in line with the results, derived from a recent study using real asphaltene samples,[28-29] that only a small fraction of asphaltenes is responsible for the formation of stable interfacial films. Based on numerous studies using asphaltene model compounds in comparison with molecular behaviour of real asphaltene molecules, Gray *et al.*[30] proposed a supramolecular assembly model to account for variable molecular architectures formed from various types of cooperative bindings among complex asphaltene molecular mixtures.

In this study, C5Pe was selected as an asphaltene model compound. The chemical structure of C5Pe is shown in Figure 1. It consists of four aromatic rings fused together with three cyclic rings containing heteroatoms of O and N. A pentyl carboxylic acid is attached to one end of the fused rings through the nitrogen atom, while a hexyl-heptyl double chain is connected to the other end of the fused rings, also through the other nitrogen atom. The molecular weight (689 Da.) of C5Pe is within the molecular weight range of asphaltenes. The adsorption mechanism of C5Pe to clay surface (mica) and interactions between two C5Pe films in both toluene and heptane were measured using a surface forces apparatus (SFA). The results obtained

with C5Pe were compared with that obtained under similar experimental conditions using asphaltenes extracted from Athabasca bitumen (Alberta, Canada).

Materials and Experimental Methods

Materials. The solvents, e.g., toluene and heptane, used in this study were all of HPLC grade (> 99.9%, Fisher Scientific, Canada). The details on the synthesis of C5Pe used in this study has been reported elsewhere.[26] A given amount of C5Pe was first dissolved in toluene to obtain a 0.02 wt% C5Pe in toluene stock solution. To ensure that C5Pe was completely dissolved, the stock solution was sonicated for 30 minutes and then left to equilibrate for at least 24 hours. The prepared stock solution was then diluted by toluene to desired concentrations. All the solutions were filtered by a 0.2 μm PTFE filter prior to their use. Asphaltenes were precipitated from bitumen fed to vacuum distillation (Syncrude Canada Ltd., Alberta, Canada). The asphaltene precipitation was achieved at a 40:1 volume ratio of n-heptane to bitumen. The precipitates were washed with n-heptane repeatedly until the washing heptane became colorless. The more detailed descriptions of asphaltenes preparation were reported elsewhere.[31] The asphaltene solutions were prepared using similar procedure as used for C5Pe by dissolving a given amount of asphaltenes in toluene.

Preparation of C5Pe films and thickness measurement. The C5Pe film on mica was prepared by adsorption method. Briefly, several drops of C5Pe in toluene solution were placed on a molecularly smooth mica surface glued on a silica disk of radius R=2 cm. The C5Pe was allowed to adsorb/deposit on mica for 5~10 min in a sealed chamber saturated with liquid toluene vapour. The mica surface was then washed with pure toluene before being loaded in the SFA chamber. The C5Pe films adsorbed/deposited as such on mica surfaces were then used to

measure the interaction forces by SFA and obtain topographic image by AFM. The C5Pe films were also deposited on clean silicon wafers by the same adsorption method for film thickness measurement using ellipsometer. Prior to film preparation, silicon wafers were cleaned by following a standard procedure.[32] Briefly, silicon wafers were first soaked in a Piranha solution, a mixture of sulphuric acid (96%) and hydrogen peroxide (50%) in a volume ratio of 3:1, for two days. The cleaned silicon wafers were then washed 15-20 times with ultrapure water. After cleaning, silicon wafer surfaces were highly hydrophilic and stored in ultrapure water for future use. The C5Pe film thickness was measured using a Gaertner multiangle Ellipsometer (Acree Technologies, Concord, CA, USA). The thickness of multiple samples prepared using identical procedures was measured on at least six different positions for each sample. The accuracy of thickness measurement by the ellipsometer used in this study is ±0.1 nm.

Force measurement by SFA. An SFA (SurForce LLC, Santa Barbara, CA, USA) was used to measure the molecular forces of adsorbed C5Pe films in organic solvents. Due to its unique ability to simultaneously measure the force, F, as a function of the absolute surface separation, D, and the local geometry of two interacting surfaces (the local radius R or contact area) with a force sensitivity of ~10 nN and an absolute distance resolution of 0.1 nm, SFA has been extensively used to determine *in situ* and in real time the molecular interactions in many biological and non-biological systems.[33-39] Detailed setup for SFA experiments has been reported elsewhere.[36-37,40-44] Basically, a thin mica sheet (1-5 μm thick) was first glued onto a cylindrical silica disk (radius R=2 cm). Two prepared silica disks with or without C5Pe films on mica were then mounted into the SFA chamber in a cross-cylinder geometry which was locally equivalent to a sphere of radius R interacting with a flat surface or two spheres of radius 2R when the separation of the two surfaces was much smaller than R. The separation distance D was obtained

by an optical technique called multiple beam interferometry (MBI) using interference fringes of equal chromatic order (FECO). In each set of measurements, the reference distance ($D = 0$) was determined at the adhesive contact between the two bare mica surfaces in air. The force between the two cylindrical surfaces $F(D)$ was determined as a function of the separation distance D based the deflection of the supporting spring. When $\partial F(D)/\partial D$ is greater than the spring stiffness, there is a mechanical instability that causes the lower surface to jump either towards or away from the upper surface during the approaching or separation process, respectively. Using the Derjaguin approximation: $F(D) = 2\pi RW(D)$, the measured force $F(D)$ can be converted to interaction energy per unit area between two flat surfaces $W(D)$.[45] In this study, the molecular forces of C5Pe in organic solvents of interest were measured by SFA in three different configurations as shown in Figure 2.

Langmuir-Blodgett (LB) Trough Isotherm and Film Deposition. Interfacial pressure-area isotherm of C5Pe was recorded using a Langmuir interfacial trough (KSV Instruments, Finland) with an effective film area of 17010 mm^2. Prior to each experiment, the trough and barriers were thoroughly cleaned with toluene and acetone, followed by ultrapure water of 18.2 MΩ•cm resistivity. The C5Pe film was prepared by first spreading 50 µl of 0.02wt% C5Pe solution on ultrapure water subphase followed by careful pouring of 100 ml optima toluene (top phase) on the aqueous phase after 10 min incubation time. After 30 mins of equilibrium, compression and expansion of interfacial film were carried out at a barrier speed of 5 mm/min. The compression-expansion cycle was repeated for 3 times continuously one after another.

AFM Imaging and Contact Angle Measurement. Morphology and surface roughness of C5Pe films deposited on mica sheets were characterized by a multimode atomic force

microscope (AFM) (Veeco, Santa Barbara, CA, USA). The contact angle of water on C5Pe surface was determined by a Krüss drop shape analysis system (DSA 10-MK2, Germany) using a sessile drop method. During the measurement, an ultrapure water sessile drop of ~2 μL was placed on the sample surface. Microscope images of sessile drop were captured and the contact angle was determined by fitting the shape of the sessile drop sitting on the sample surface. All the measurements were done at room temperature (~20□). The average of measurements using more than 10 samples at three different positions on each sample was reported.

Results and Discussions

Characterization of C5Pe films. The AFM images of a bare mica surface and an adsorbed C5Pe film are shown in Figure 3. As expected, freshly cleaved mica was a flat, featureless surface with a root-mean-square (RMS) roughness of 0.2 nm (Figure 3a). The deposited C5Pe film on mica in Figure 3b appeared to be not uniform, with elongated holes distributed evenly across the film plane, which had a RMS roughness of ~0.3 nm. Previous studies have shown that a layer of asphaltene film strongly attached to hydrophilic substrates (e.g., mica or silica) even after rinsing with toluene.[19,46] Considering the adsorbed film of C5Pe on mica being thoroughly washed with toluene, the results here indicate a similar binding of C5Pe as asphaltenes to mica. Both AFM images (Figure 3b) and SFA measurement (discussed later) confirmed the successful deposition of a layer of C5Pe on mica by the adsorption method.

To further test the film stability, the deposited C5Pe film on mica was soaked in fresh toluene for half an hour. The film was then dried and imaged by AFM in air. Unlike asphaltene films we studied recently[21], there was no obvious conformational rearrangement or "molecular swelling" when C5Pe film was soaked in toluene for ~30 min, as shown by AFM image in Figure 3c. The AFM images before and after soaking in toluene showed similar surface features

and roughness of ~0.3 nm. The film thickness measurement by ellipsometry showed a film thickness of 5.8 and 5.5 nm for unsoaked and soaked C5Pe films, respectively. The above results indicate that the C5Pe molecules could stay firmly on mica surface even after re-exposing to organic solvents such as toluene.

The contact angle of water on the deposited C5Pe surface was measured to be 35 ± 3°. In comparison to the contact angle values above 80^{o} of deposited asphaltene films[18], the contact angle on C5Pe indicates that the C5Pe molecules were not uniformly adsorbed and packed as a highly ordered monolayer on mica with a substantial fraction of polar carboxylic terminal groups facing away from the mica to lead to much less hydrophobic film surfaces. Recent molecular dynamics simulations[47] confirmed molecular stacking or aggregation of C5Pe in toluene at these concentrations. This configuration was also confirmed at the oil-water interface by means of the Langmuir-Blodgett (LB) technique. Figure 4a shows the typical interfacial pressure-area isotherms of C5Pe at toluene-water interfaces. For comparison an interfacial isotherm of asphaltene at toluene-water interface was also shown in the insert of Figure 4a. The results indicate that C5Pe did not form as stable films as asphaltenes at the water-toluene interface, as evidenced by a low interfacial pressure of 22 mN/m in comparison to 30 mN/m for asphaltenes .[48]

It is important to note that the interfacial pressure of the C5Pe film in the second compression became lower at the same mean area per C5Pe molecule than the first compression, while for asphaltenes there was very little hysteresis between the first two compressions, evidencing again C5Pe can not form stable films like asphaltenes. Interestingly, there was no hysteresis between the second and third interfacial isotherms of C5Pe. These results collectively indicate the formation of C5Pe aggregates during the first compression shown by a significant

hysteresis between the first and second interfacial isotherms, and the molecular aggregation was irreversible as shown by a negligible hysteresis between the second and third isotherms obtained with a time interval of 3 hours. The aggregates were directly visualized by AFM on the LB-deposited C5Pe film as shown in Figure 4b. In this case, the C5Pe film was deposited by LB technique at a constant interfacial pressure of 5 mN/m with a pulling speed of 1 mm/min during the first compression. It is evident that C5Pe did not form a uniform monolayer at the toluene-water interface. Instead, small aggregates (domains) of ~50 nm diameter were seen to be evenly distributed throughout the film.

Adsorption kinetics. The 0.002 wt% and 0.02 wt% C5Pe in toluene solutions were injected between two closely placed mica surfaces in the SFA chamber saturated with toluene vapour to study the adsorption of C5Pe on a model clay surface (mica). For a typical force measurement, the normal force-distance (F vs. D) profile was obtained by an initial approach of two surfaces to a "hard wall" distance followed by separation of the two surfaces. Note that the "hard wall" distance in this study is defined as the mica-mica separation distance or thickness of confined C5Pe films, which shows a negligible change with increasing the normal load or pressure.[44,49] The approach and separation force-distance profiles for two mica surfaces interacting in 0.02 wt% C5Pe in toluene solutions are shown in Figure 5. Figure 5a shows quite similar interaction force-distance profiles during the approaching of two mica surfaces in 0.02 wt% C5Pe solution for the first four hours of adsorption. The hard wall distances shift slightly from 15 to 19 nm, which translates to a thickness of C5Pe film absorbed on each mica surface to be around 7.5-9.5 nm. This thickness value is slightly larger than the film thickness of 5.8 nm measured for adsorbed C5Pe films by ellipsometry, indicating a limited swelling or protrusion of the C5Pe molecules adsorbed. As the adsorption time increases to 20 hours, the hard wall

distance shifts to ~38 nm, while the range of repulsive force during approaching also increases from ~5 to ~10 nm. The great shift of hard wall distance to 38 nm indicates a slow build-up of C5Pe on mica surfaces to form nanoaggregates. Interestingly, this hard wall distance translates to C5Pe layer thickness of 19 nm on each mica surfaces which is in excellent agreement with film thickness of 18.2 nm measured by ellipsmetry on C5Pe films formed by adsorption on silicon wafer in C5Pe solution of the same concentration for overnight. The force-distance profiles during the separation processes in Figure 5b show weak adhesions (F_{ad}/R~-1 mN/m) for adsorption time below 4 hours. It is interesting to note that the adsorbed C5Pe layers were stretched for about 3-4 nm before the two surfaces jumped apart, indicating a limited interdigitation of C5Pe molecules/aggregates from two interacting surfaces upon compression.

The repulsive forces during the approach of the two mica surfaces mainly came from the steric repulsive interactions between the adsorbed C5Pe molecules. The polyaromatic rings with aliphatic hydrocarbon chains of adsorbed C5Pe molecules/nano-aggregates tended to be extended in toluene and repel each other. The aggregation and adsorption of C5Pe molecules were found to be similar to asphaltenes. The Alexander-de Gennes (AdG) scaling theory[40,46,50] for the steric repulsion between two interacting brush layers, given by Equation 1, is applied here to fit the force-distance profiles in Figure 5a.

$$\frac{F(D)}{R} = \frac{16\pi kTL}{35s^3}\left[7\left(\frac{2L}{D}\right)^{5/4} + 5\left(\frac{D}{2L}\right)^{7/4} - 12\right] \quad \text{for } D < 2L, \tag{1}$$

where T is the temperature and k is Boltzmann constant, s is the mean distance between anchoring (or grafting) sites on the surface, L is the absorbed layer thickness, R is the radius of local curvature in the SFA measurements.

The fitted values of L and s are summarized in Table 1. The good fitness of the measured force profiles with the AdG theory indicates that although C5Pe is not a polymer, the absorbed C5Pe layers on mica surfaces do bare some similarities to polymer brushes in terms of surface interactions. The fitted curve gives a film thickness L of 24 nm for C5Pe films adsorbed after overnight soaking. From the hard wall of the force curve, the film thickness is ~19 nm, while the ellipsometry measurement gives a value of 18.2 nm for the films adsorbed on silicon wafer overnight from C5Pe solutions of the same concentration as the above SFA measurement. The thickness values obtained by ellipsometry and SFA as summarized in Table 2 are in excellent agreement with each other. The fitted mean distances s between grafting sites are very close to each other in Table 2, which are also close to the s values obtained for asphaltenes under similar experimental condition[21], indicating a similar adsorption pattern of C5Pe and asphaltenes from toluene on mica.

It is noted from Figure 5a that the AdG scaling theory fits the force-distance profiles well at short distances under high compression. However, at longer distances under lower compression, a significant deviation is observed. It appears that there is a weaker repulsive force over longer separation distance which might be due to protrusion of flexible chains on C5Pe aggregates in the films, as schematically shown in the inset of Figure 6. Such model is not considered in the AdG theory which is applicable to mono-dispersed brushes. Nevertheless, the lower compression regime can also be fitted with the AdG model using an independent set of fitting parameters as shown by the dash line in Figure 6. The measured force-distance profiles between two adsorbed C5Pe films in toluene can therefore be explained as follows. The weak repulsion at large separation distances appears to be the result of steric repulsion between the secondary brushes of flexible aliphatic chains on C5Pe aggregate core, while the repulsion at

shorter separation distance under higher compression is the results of compressing the core of C5Pe molecular aggregates. The schematic of the proposed core-brush configuration is shown in the insert of Figure 6. The fitted parameters of *s* and *L* for the force-distance curve obtained for selected adsorption time are listed in Table 3.

Adhesion was detected during the separation processes for the first several hours adsorption as shown in Figure 5b. However, the adhesion disappeared after ~20 hours adsorption and only pure repulsive force was measured. It is suggested that the adhesion measured during the initial stage of adsorption was due to possible hydrogen bonding among the polar groups –COOH of C5Pe molecules as well as van der Waals interactions. The disappearance of the adhesion at longer adsorption times was attributed to the conformational rearrangement and aggregation of the C5Pe molecules, which was shown by AFM imaging in Figure 7 and increased contact angle from 35^{o} to 53 ± 5^{o}.

The adsorption behaviour of C5Pe on mica in a diluted (0.002 wt%) solution was also investigated. As shown in Figure 8a, there is no significant difference in both force profiles and the hard wall distances with adsorption time up to 20 hours. However the adhesion disappeared after overnight immersion as shown in Figure 8b. AFM imaging of C5Pe film adsorbed overnight on mica in Figure 7b revealed a similar surface morphology to the films formed at higher C5Pe concentrations as shown in Figure 7a, which was responsible for the disappearance of the adhesion forces although the hard wall thickness in these two cases were different. The observed differences indicate an important role of C5Pe concentration in toluene in determining the adsorption kinetics and molecular aggregation from C5Pe solutions.

For comparison, the force-distance profiles for two mica surfaces interacting in a 0.01 wt% asphaltene-toluene solution with different adsorption times are shown in Figure 9. The comparison of the results obtained with asphaltenes and C5Pe shows that the asphaltenes and C5Pe behave similarly in terms of adsorption behaviour to clay (mica) surfaces. Both the native asphaltenes and C5Pe model compound built up a layer on mica quickly (within 0.5 hour), and the layer then continued to grow slowly with time on the mica surface. The force-distance profiles on separation for both asphaltenes and C5Pe showed that the adhesion, observed during the initial stage of adsorption, decreased with increasing the adsorption time and eventually disappeared. Both C5Pe and asphaltenes were noted to have similar hard wall distance of 12-15 nm within the first half-hour adsorption. However, the C5Pe layer did not continue to grow significantly within the first few hours, while the asphaltene layer grew more quickly than C5Pe. After 2 hours of adsorption, the hard wall distance of the asphaltenes became much larger than that of C5Pe. After 20 hours adsorption, the hard wall distance for asphaltenes grew to ~60 nm in comparison to ~38 nm for C5Pe, suggesting a much stronger aggregation of asphaltene molecules than C5Pe, most probably due to more complex nature of asphaltene molecules.

Interaction forces of adsorbed C5Pe films in toluene and heptane: Figure 10a shows the interaction forces between a C5Pe film adsorbed on mica and a bare mica (asymmetric configuration) or between two C5Pe surfaces (symmetric configuration) in toluene. The hard wall distance of the asymmetric case was found to be about half of the symmetric case. Weak adhesion (F_{ad}/R ~ -0.5 mN/m) was measured during the separation for the asymmetric case, which was due to the affinity of C5Pe to the opposing mica surface. For both symmetric and asymmetric cases, there was a hysteresis between the approaching and separating force-distance profiles, even though there was no adhesion for the symmetrical case. The observed hysteresis

indicates an irreversible deformation of C5Pe films upon compression during the approaching. The absence of adhesion between two C5Pe films in symmetrical case indicates the absence of interdigitation or bridging of between C5Pe molecules across the two surfaces. These results on the interactions of C5Pe films in toluene were very similar to the results of asphaltenes reported recently.[21]

Heptane is a paraffinic and apolar solvent, which is considered as a poor solvent for the polyaromatic and polar C5Pe molecule. Previous study confirmed that the model compound C5Pe cannot be dissolved in heptane[51]. As shown in Figure 10(b), the hard wall distance of the asymmetric case was estimated to be about half of the symmetric configuration as anticipated. Strong adhesion forces were measured for both the asymmetric and symmetric configurations interacting in heptane, with F_{ad}/R ~ -32 and -30 mN/m, respectively. In our recent SFA study on asphaltenes, adhesion (F_{ad}/R ~ -3 mN/m) was measured between two asphaltene surfaces in heptane. The adhesion became slightly weaker after 30 min immersion. These findings indicate that some of the asphaltene components have limited swelling in heptane, leading to limited conformational rearrangement and aggregation of asphaltene molecules.[21] The adhesion forces measured for both C5Pe and asphaltenes in heptane were mainly attributed to van der Waals attraction between C5Pe or asphaltene surfaces across the poor solvent heptane, while the weaker adhesion forces measured between asphaltene films than C5Pe films were probably caused by more rigid and rougher asphaltene films than C5Pe films in heptane. The complex nature of asphaltenes have led to limited solubility and swelling of asphaltenes in heptane, which increases the steric effect and thus lowers the adhesion. Contrary to asphaltenes, C5Pe is completely insoluble in heptane, indicating the absence of swelling or molecular rearrangement even after longer time incubation. The measured smaller hard wall distance of ~4.6 nm in heptane than that

of ~6 nm in toluene for the asymmetric configuration supports non-swelling hypothesis of C5Pe in heptane. The direct AFM imaging of a C5Pe film shown in Figure 12 confirms a negligible change in morphology of C5Pe films after immersed in heptane for half an hour.

Conclusions

The adsorption of an asphaltene model compound, C5Pe onto a model clay (mica) and the interaction forces between the adsorbed C5Pe films in different organic solvents (toluene and heptane) were directly measured using an SFA. The results showed that organic solvents significantly affect the molecular interaction and aggregation behaviour of C5Pe model compound. For the interactions of two mica surfaces across C5Pe solutions, the repulsion measured showed a steric origin resulting from the adsorbed C5Pe molecules. The repulsive force-distance profiles measured during approaching were well fitted with the Alexander-de Gennes scaling theory over a short and long separation distance regimes using two independent sets of fitting parameters, indicating the core-brush configuration of C5Pe molecular aggregates. The direct force-distance measurement in this study provides an insight into mechanisms of molecular interaction and interfacial behaviour of asphaltene model compound C5Pe in different organic solvents.

For the interactions of C5Pe films (in asymmetric or symmetric configurations), no significant adhesion was detected in good solvent toluene, while strong adhesion was measured in heptane. The comparison of results between the asphaltene and model compound C5Pe shows that C5Pe behaves similarly as asphaltenes in terms of intermolecular forces in organic solvents, emphasizing the importance of the polar components in real asphaltenes for their interfacial activities and aggregation behaviour. However, there is a distinct difference quantitatively

between C5Pe and nature asphaltene molecules that C5Pe aggregates at a much slower rate and shows a negligible swelling in toluene as compared to asphaltnes. It is evident that using a single model compound is unlikely to mimic quantitatively the aggregation of asphaltenes in a given solvent. Nevertheless, a mixture of several well-designed asphaltene model compounds in combination with maltene molecules could probably provide a more accurate representation of real asphaltenes and hence successfully mimic the molecular aggregation of asphaltenes and their role in stabilizing water-in-oil emulsions.

Acknowledgement

The authors acknowledge an NSERC Discovery Grant Award and an NSERC RTI Grant Award (H. Zeng), NSERC Industrial Research Chair Program in Oil Sands Engineering (Z. Xu), and a grant from Statoil and financial support from JIP consortium (J. Sjöblom) for the support of the study.

References

(1) Dai, Q.; Chung, K. H. *Fuel* **1996**, *75*, 220-226.
(2) Liu, J.; Zhou, Z.; Xu, Z. *Industrial & Engineering Chemistry Research* **2002**, *41*, 52-57.
(3) Hemmingsen, P. V.; Silset, A.; Hannisdal, A.; Sjöblom, J. *Journal of Dispersion Science and Technology* **2005**, *26*, 615-627.
(4) Hiemenz, P. C.; Rajagopalan, R. *Principles of Colloid and Surface Chemistry*; CRC, 1997; Vol. 14.
(5) Chandra, W.; Dabros, T.; Hamza, H. A. *Energy & Fuels* **2007**, *21*, 912-919.
(6) Gu, G.; Zhou, Z.; Xu, Z.; Masliyah, J. H. *Colloids and Surfaces A: Physicochemical and Engineering Aspects* **2003**, *215*, 141-153.
(7) Liu, E. H.; McGrath, K. M. *Colloids and Surfaces A: Physicochemical and Engineering Aspects* **2005**, *262*, 101-112.
(8) McClements, D. J.; Decker, E. A.; Park, Y.; Weiss, J. *Critical Reviews in Food Science and Nutrition* **2009**, *49*, 577-606.
(9) Vankova, N.; Tcholakova, S.; Denkov, N. D.; Ivanov, I. B.; Vulchev, V. D.; Danner, T. *Journal of Colloid and Interface Science* **2007**, *312*, 363-380.
(10) Gafonova, O. V.; Yarranton, H. W. *Journal of Colloid and Interface Science* **2001**, *241*, 469-478.
(11) Schramm, L. L. *Emulsions:(fundamentals and applications in the petroleum industry)*; American Chemical Society, 1992.
(12) Yang, X.; Hamza, H.; Czarnecki, J. *Energy & Fuels* **2004**, *18*, 770-777.
(13) Yarranton, H. W.; Hussein, H.; Masliyah, J. H. *Journal of Colloid and Interface Science* **2000**, *228*, 52-63.
(14) Mitchell, D. L.; Speight, J. G. *Fuel* **1973**, *52*, 149-152.
(15) Yen, T. F.; Erdman, J. G.; Pollack, S. S. *Analytical Chemistry* **1961**, *33*, 1587-1594.
(16) Speight, J. G. *The Chemistry and Technology of Petroleum*; CRC, 2007; Vol. 114.
(17) Porte, G.; Zhou, H.; Lazzeri, V. *Langmuir* **2003**, *19*, 40-47.
(18) Wang, S.; Liu, J.; Zhang, L.; Masliyah, J.; Xu, Z. *Langmuir* **2009**, *26*, 183-190.
(19) Wang, S.; Liu, J.; Zhang, L.; Xu, Z.; Masliyah, J. *Energy & Fuels* **2008**, *23*, 862-869.
(20) Buckley, J.; Hirasaki, G.; Liu, Y.; Von Drasek, S.; Wang, J. X.; Gill, B. *Petroleum Science and Technology* **1998**, *16*, 251-286.
(21) Natarajan, A.; Xie, J.; Wang, S.; Liu, Q.; Masliyah, J.; Zeng, H.; Xu, Z. *The Journal of Physical Chemistry C* **2011.**
(22) Akbarzadeh, K.; Bressler, D. C.; Wang, J.; Gawrys, K. L.; Gray, M. R.; Kilpatrick, P. K.; Yarranton, H. W. *Energy & Fuels* **2005**, *19*, 1268-1271.
(23) López-Linares, F.; Carbognani, L.; González, M. F.; Sosa-Stull, C.; Figueras, M.; Pereira-Almao, P. *Energy & Fuels* **2006**, *20*, 2748-2750.
(24) Rakotondradany, F.; Fenniri, H.; Rahimi, P.; Gawrys, K. L.; Kilpatrick, P. K.; Gray, M. R. *Energy & Fuels* **2006**, *20*, 2439-2447.
(25) Nordgård, E. L.; Sørland, G.; Sjo blom, J. *Langmuir* **2009**, *26*, 2352-2360.
(26) Nordgard, E. L.; Sjoblom, J. *Journal of Dispersion Science and Technology* **2008**, *29*, 1114-1122.
(27) Nordgård, E. L.; Landsem, E.; Sjo blom, J. *Langmuir* **2008**, *24*, 8742-8751.
(28) Fossen, M.; Kallevik, H.; Knudsen, K. D.; Sjöblom, J. *Energy & Fuels* **2007**, *21*, 1030-1037.

(29) Fossen, M.; Sjoblom, J.; Kallevik, H.; Jakobsson, J. *Journal of Dispersion Science and Technology* **2007**, *28*, 193-197.
(30) Gray, M. R.; Tykwinski, R. R.; Stryker, J. M.; Tan, X. *Energy & Fuels* **2011**.
(31) Zhang, L. Y.; Lawrence, S.; Xu, Z.; Masliyah, J. H. *Journal of Colloid and Interface Science* **2003**, *264*, 128-140.
(32) http://engineering.tufts.edu/microfab/index_files/SOP/PiranhaClean_SOP.pdf.
(33) Zeng, H.; Zhao, B.; Israelachvili, J. N.; Tirrell, M. *Macromolecules* **2009**, *43*, 538-542.
(34) Zeng, H.; Pesika, N.; Tian, Y.; Zhao, B.; Chen, Y.; Tirrell, M.; Turner, K. L.; Israelachvili, J. N. *Langmuir* **2009**, *25*, 7486-7495.
(35) Teng, F.; Zeng, H.; Liu, Q. *The Journal of Physical Chemistry C* **2011**.
(36) Hwang, D. S.; Zeng, H.; Masic, A.; Harrington, M. J.; Israelachvili, J. N.; Waite, J. H. *J Biol Chem* **2010**, *285*, 25850-25858.
(37) Zeng, H.; Hwang, D. S.; Israelachvili, J. N.; Waite, J. H. *P Natl Acad Sci USA* **2010**, *107*, 12850-12853.
(38) Zeng, H.; Maeda, N.; Chen, N. H.; Tirrell, M.; Israelachvili, J. *Macromolecules* **2006**, *39*, 2350-2363.
(39) Zeng, H.; Tirrell, M.; Israelachvili, J. *J Adhesion* **2006**, *82*, 933-943.
(40) Israelachvili, J. N. *Intermolecular and Surface Forces*, 2011.
(41) Israelachvili, J.; Tabor, D. *Proceedings of the Royal Society of London. A. Mathematical and Physical Sciences* **1972**, *331*, 19.
(42) Israelachvili, J. N.; Adams, G. E. *J. Chem. Soc., Faraday Trans. 1* **1978**, *74*, 975-1001.
(43) Tabor, D.; Winterton, R. *Proceedings of the Royal Society of London. A. Mathematical and Physical Sciences* **1969**, *312*, 435.
(44) Zeng, H.; Tian, Y.; Anderson, T. H.; Tirrell, M.; Israelachvili, J. N. *Langmuir* **2008**, *24*, 1173-1182.
(45) Derjaguin, B.; Churaev, N. *Journal of Colloid and Interface Science* **1974**, *49*, 249-255.
(46) De Gennes, P. *Advances in Colloid and Interface Science* **1987**, *27*, 189-209.
(47) Teklebrhan, R. B. G., L.; Bhattacharjee, S.; Xu, Z.; Sjoblom, J. *in preparation* **2011**.
(48) Zhang, L. Y.; Lopetinsky, R.; Xu, Z.; Masliyah, J. H. *Energy & Fuels* **2005**, *19*, 1330-1336.
(49) Zhao, B.; Pesika, N.; Rosenberg, K.; Tian, Y.; Zeng, H.; McGuiggan, P.; Autumn, K.; Israelachvili, J. *Langmuir* **2008**, *24*, 1517-1524.
(50) Akbulut, M.; Alig, A. R. G.; Min, Y.; Belman, N.; Reynolds, M.; Golan, Y.; Israelachvili, J. *Langmuir* **2007**, *23*, 3961-3969.
(51) Nordgård, E. L. Model Compounds for Heavy Crude Oil Components and Tetrameric Acids. Characterization and Interfacial Behaviour. PhD thesis, 2009

Figures and figure legend

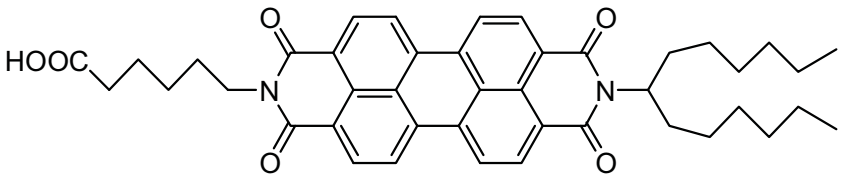

Figure 1. The structure of an asphaltene model compound C5Pe (MW=689) with nomenclature N-(1-hexylheptyl)-N'-(5-carboxylicpentyl) perylene-3,4,9,10-tetracarboxylic bisimide.

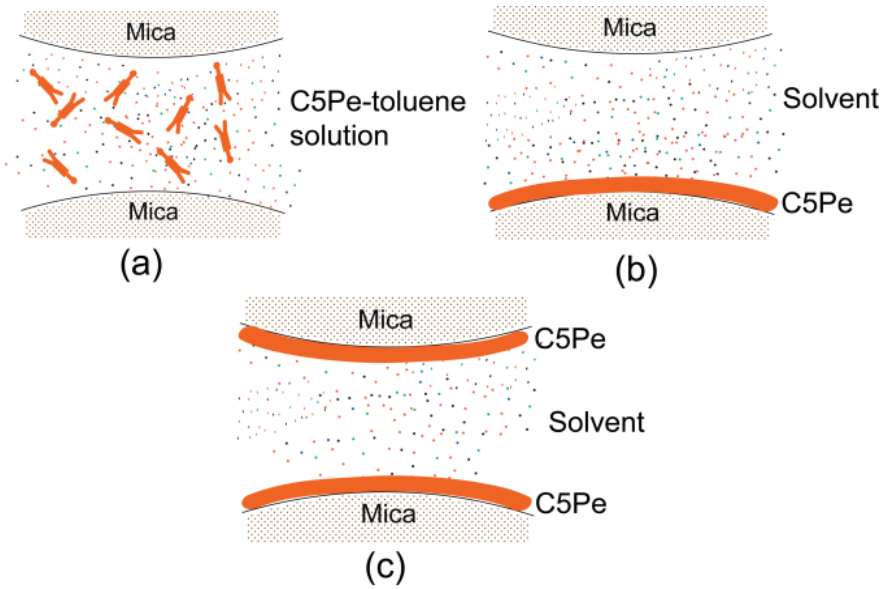

Figure 2. Experimental configurations of surface forces measurement using C5Pe in organic solvents: (a) C5Pe-toluene solution between two bare mica surfaces; (b) a C5Pe film deposited

on mica vs. a bare mica surface (asymmetric case); (c) two C5Pe films deposited on mica (symmetric case).

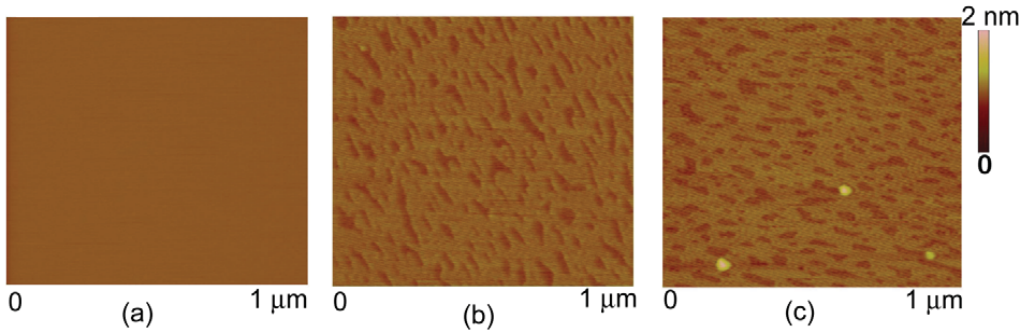

Figure 3. AFM images of (a) bare mica surface; (b) C5Pe adsorbed on mica surface; (c) C5Pe adsorbed on mica surface after immersion in toluene for 0.5 hour.

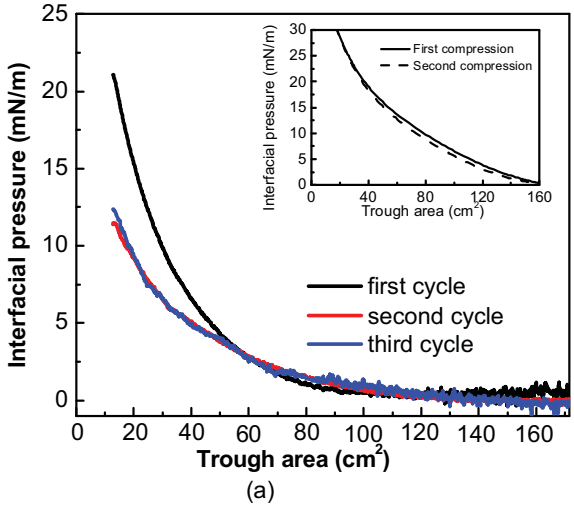

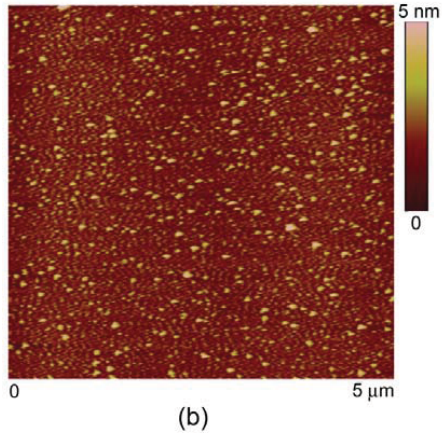

Figure 4. (a) Interfacial pressure-area isotherms of C5Pe film at toluene-water interface obtained with an interfacial Langmuir trough. The second cycle of the compression was carried out immediately after the first compression. The third cycle was carried out 3 hours after the second compression. Inset is the interfacial pressure-area isotherm of asphaltene film at toluene-water interface under similar experimental conditions from a previous work by Zhang *et al* [48] for comparison. In this case the second compression was carried out right after the first compression. (b) AFM image of the C5Pe film deposited with LB method at an interfacial pressure of 5 mN/m with a pulling speed of 1 mm/min during the first cycle with a transfer ratio of 1.15.

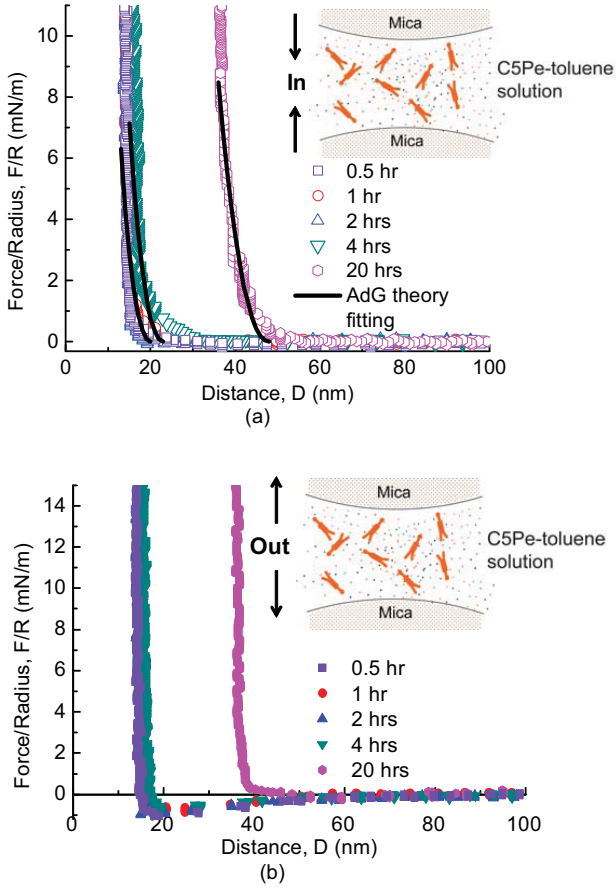

Figure 5. Force-distance profiles of two mica surfaces interacting in 0.02 wt% C5Pe-toluene solution at different time intervals: (a) approaching plots and fitting curves by Alexander-de Gennes (AdG) theory; (b) retracting plots following the approaching in (a) .

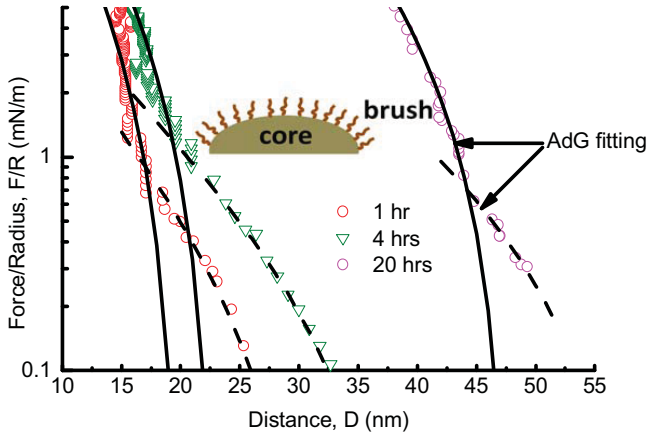

Figure 6. Experimentally measured repulsion forces and best fitted curves using the Alexander-de Gennes (AdG) theory. Open squares are the measured forces; solid lines are the fitting force curves at high compression regime and dash lines are the fitting force curves at low compression regime. Insert schematically shows a proposed core-brush configuration of the absorbed C5Pe aggregates.

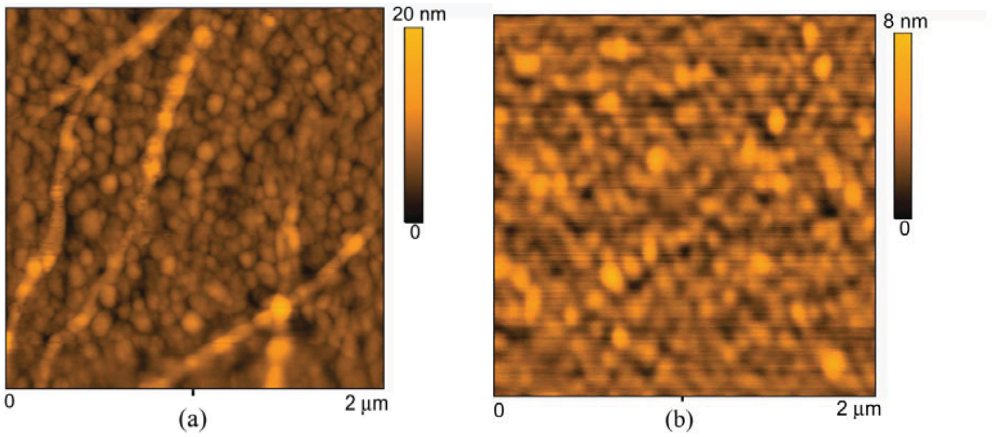

Figure 7. AFM images of C5Pe surfaces prepared by immersing the mica surface for 20 hours in a C5Pe-toluene solution of (a) 0.02 wt% and (b) 0.002 wt%.

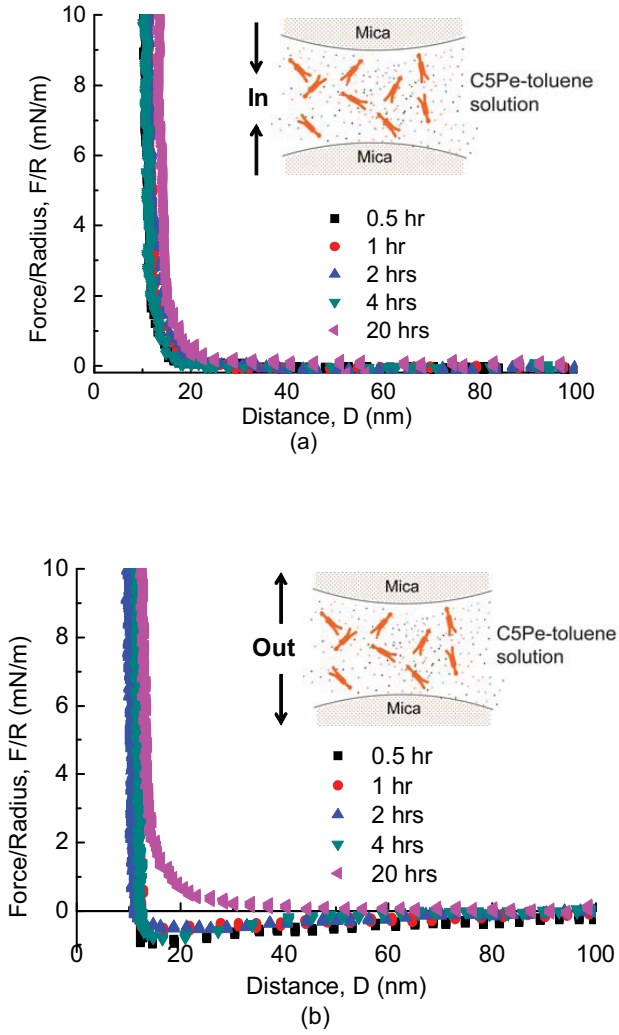

Figure 8. Force-distance profiles of two mica surfaces interacting in 0.002 wt% C5Pe-toluene solution at different time intervals during (a) approaching and (b) retracting following the approaching in (a).

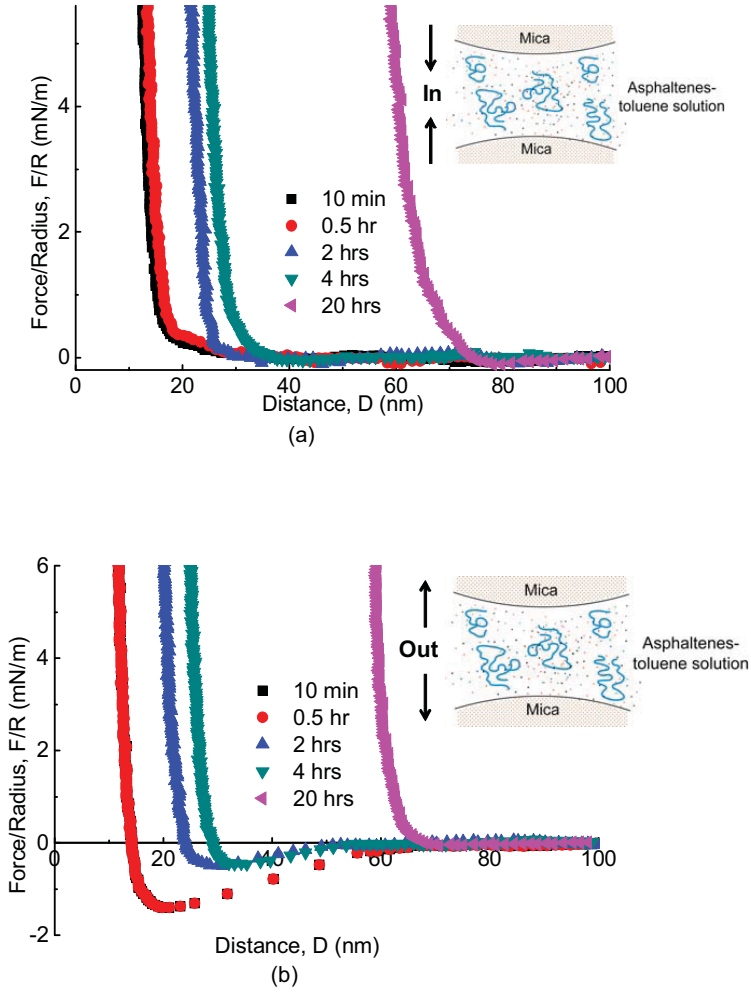

Figure 9. Force-distance profiles of two mica surfaces interacting in 0.01 wt% asphaltene-toluene solution at different time intervals during (a) approaching and (b) retracting following the approaching in (a).

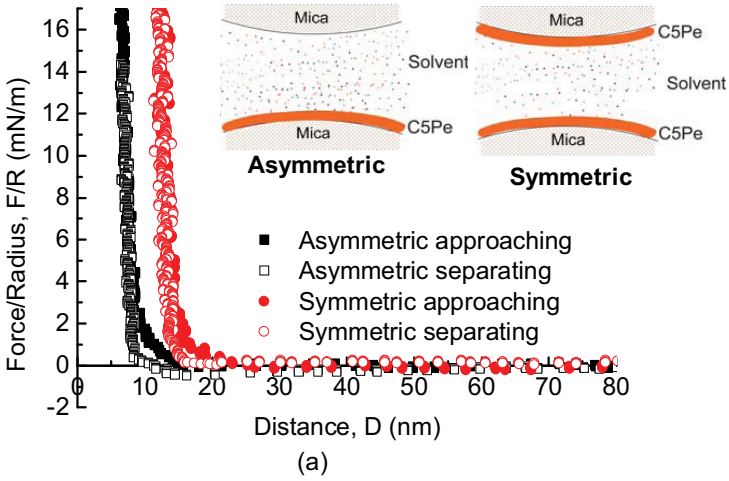

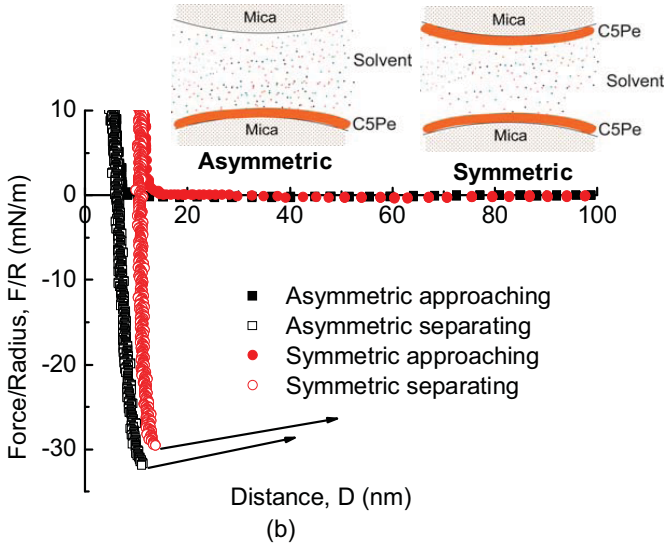

Figure 10. Force-distance profiles between two C5Pe films (symmetric configuration) and between a C5Pe film and a bare mica surface (asymmetric configuration) in (a) toluene and (b) heptane.

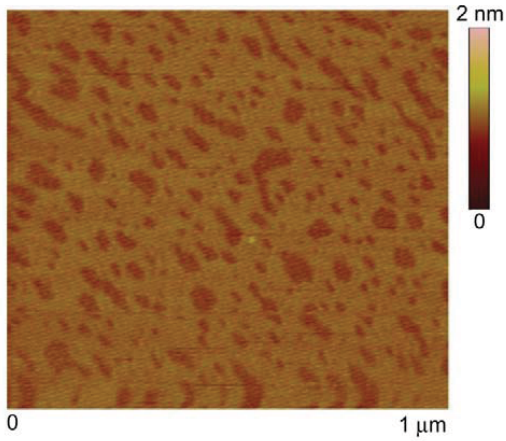

Figure 11. AFM image of deposited C5Pe film immersed in heptane for 0.5 hour.

Table 1. Fitting parameters using Alexander-de Gennes theory (corresponding to Figure 5a).

Adsorption time	≤2 hrs	4 hrs	20 hrs
L (nm)	10	11.5	24
s (nm)	2.8	2.8	2.6

Table 2. Film thickness (nm) obtained by different methods (corresponding to Figure 5).

Adsorption time	Ellipsomter measurement	Hard wall distance	Fitting value
≤ 4 hrs	5.8-5.5	7-11	10-12
20 hrs	18.2	19	24

Table 3. Fitting parameters using Alexander-de Gennes theory at high and low compression regimes (corresponding to Figure 6).

	1 hr of adsorption		4 hrs of adsorption		20 hrs of adsorption	
	high loading	low loading	high loading	low loading	high loading	low loading
L (nm)	10	16	11.5	20	24	30
s (nm)	2.8	8.1	2.8	8.7	2.6	6.7